EFFECTS OF CHAIN EXTENSION AND BRANCHING ON THE PROPERTIES OF RECYCLED POLY(ETHYLENE TEREPHTHALATE)-ORGANOCLAY NANOCOMPOSITES

A THESIS SUBMITTED TO
THE GRADUATE SCHOOL OF NATURAL AND APPLIED SCIENCES
OF
MIDDLE EAST TECHNICAL UNIVERSITY

BY

ALİ EMRAH KEYFOĞLU

IN PARTIAL FULFILLMENT OF THE REQUIREMENTS FOR THE DEGREE
OF
MASTER OF SCIENCE
IN CHEMICAL ENGINEERING

JUNE 2004

Approval of Graduate School of Natural and Applied Sciences

Prof. Dr. Canan Özgen
Director

I certify that this thesis satisfies all the requirements as a thesis for degree of Master of Science.

Prof. Dr. Timur Doğu
Head of the Department

This is to certify that we have read this thesis and that in our opinion it is fully adequate, in scope and quality, as a thesis for the degree of Master of Science.

Prof. Dr. Ülkü Yılmazer
Supervisor

Examining Committee Members

Prof. Dr. Hayrettin Yücel	(METU,CHEM.ENG.)	
Prof. Dr. Ülkü Yılmazer	(METU,CHEM)	
Prof. Dr. Erdal Bayramlı	(METU,CHEM)	
Prof. Dr. Ali Usanmaz	(METU,CHEM.ENG.)	
Assoc. Prof. Dr. Göknur Bayram	(METU,CHEM.ENG.)	

I hereby declare that all information in this document has been obtained and presented in accordance with acedemic rules and ethical conduct. I also declare that, as required by these rules and conduct, I have fully cited and referenced all material and results that are not original to this work.

Name, Lastname : Ali Emrah Keyfoğlu

Signature :

ABSTRACT

EFFECTS OF CHAIN EXTENSION AND BRANCHING ON THE PROPERTIES OF RECYCLED POLY(ETHYLENE TEREPHTHALATE)-ORGANOCLAY NANOCOMPOSITES

Keyfoğlu, Ali Emrah

M.S., Department of Chemical Engineering

Supervisor : Prof. Dr. Ülkü Yılmazer

June 2004, 136 pages

In this study, the effects of chain extension and branching on the properties of nanocomposites produced from recycled poly(ethylene terephthalate) and organically modified clay were investigated. As the chain extension/branching agent, maleic anhydride (MA) and pyromellitic dianhydride (PMDA) were used. The nanocomposites were prepared by twin-screw extrusion, followed by injection molding. Recycled poly(ethylene terephthalate), was mixed with 2, 3 and 4 weight % of organically modified montmorillonite. During the second extrusion step, 0.5, 0.75 or 1 weight % of MA or PMDA was added to the products of the first extrusion. As the second extrusion step is reactive extrusion, the anhydrides were added at three different screw speeds of 75, 150, 350 rpm, in order to observe the change of properties with the screw speed.

XRD analysis showed that, the interlayer spacing of Cloisite 25A expanded from 19.21 Å to about 28-34 Å after processing with polymer indicating an intercalated structure. PMDA, MA and organoclay content as well as the screw speed did not have a recognizable effect on interlayer distance. In the first extrusion step, nanocomposites containing 3% organoclay content gave significant increase in Young's modulus and decrease in elongation to break values indicating good interfacial adhesion. After the addition of chain extenders, it was observed that both MA and PMDA gave rise to improved mechanical properties of the nanocomposite owing to the branching and chain extending effects that increase the molecular weight. However, PMDA gave better mechanical properties at lower content which makes it a more effective chain extender. DSC analysis showed that MA was more effective in increasing the glass transition temperature and melting temperature in comparison to PMDA.

Key Words: Nanocomposite, Thermoplastic Nanocomposites, Recycled PET, Montmorillonite, Chain Extension/Branching

ÖZ

ZİNCİR UZAMASININ VE DALLANMASININ GERİ KAZANILMIŞ POLİ(ETİLEN TEREFTALAT)-ORGANOKİL NANOKOMPOZİTLERİNİN ÖZELLİKLERİNE ETKİLERİ

Keyfoğlu, Ali Emrah

Yüksek Lisans, Kimya Mühendisliği Bölümü

Tez Yöneticisi : Prof. Dr. Ülkü Yılmazer

Haziran 2004, 136 sayfa

Bu çalışmada zincir uzaması ve dallanmanın, geri kazanılmış PET ve organik olarak modifiye edilmiş kil ile hazırlanan nanokompozitlerin özellikleri üzerindeki etkisi incelenmiştir. Zincir uzatma ve dallandırma kimyasalı olarak maleik anhidrit (MA) ve piromellitik dianhidrit (PMDA) kullanılmıştır. Nanokompozit numuneleri çift vidalı ekstrüzyonu takiben, enjeksiyonla kalıplama yöntemiyle hazırlanmıştır. Geri kazanılmış PET, organik kil oranı ağırlıkça %2, %3 ve %4 olacak şekilde organik olarak modifiye edilmiş montmorillonitle karıştırılmıştır. İkinci ekstrüzyon basamağında ağırlıkça % 0.5, 0.75 ve 1 oranlarında MA veya PMDA ilk ekstrüzyondan elde edilen ürünlere eklenmiştir. Ikinci basamağın reaktif ekstrüzyon olmasından dolayı, anhidritler, vida hızının etkisini gözlemlemek için farklı vida hızlarında (75, 150 ve 350 devir/dakika) eklenmiştir.

XRD analizleri, kil tabakaları arasındaki mesafenin, polimerle işlendikten sonra yarı açılmış bir yapının elde edildiğini belirten bir şekilde 19.21 Å dan 28-34 Å'a çıktığını göstermiştir. PMDA, MA ve kil miktarıyla beraber vida hızının kil tabakaları arasındaki mesafeyi etkilemediği gözlenmiştir. İlk ekstrüzyon basamağında, ağırlıkça %3 kil içeren nanokompozitler ara yüzeyde iyi yapışmayı gösterecek şekilde Young modülünde önemli bir artış ve kopmadaki uzamada azalma sağlamıştır. Zincir uzatıcı ajanların eklenmesinden sonra, MA ve PMDA'nın molekül ağırlığında artış ve dallanmaya bağlı olarak mekanik özellikleri iyileştirdiği gözlenmiştir. Düşük oranlarda PMDA'nın daha etkili olduğu gözlenmiştir; buna bağlı olarak PMDA'nın daha etkili bir zincir uzatıcı olduğu söylenebilir. DSC analizi ile MA'nın camsı geçiş sıcaklığını ve erime sıcaklığını PMDA'ya göre daha çok arttırdığı gözlenmiştir.

Anahtar Kelimeler: Nanokompozit, Termoplastik Nanokompozitler, Atık PET, Montmorillonit, Zincir Uzaması/Dallanması

Dedicated to my family …

ACKNOWLEDGEMENTS

I express my sincere gratitude and thanks to my thesis supervisor Prof. Dr. Ülkü Yılmazer for his valuable guidance and support throughout this study. I appreciate his encouraging advice and discussions.

I wish to express my thanks to Göknur Bayram for her encouragement and help, Prof. Dr. Teoman Tincer from the Chemistry Department for providing the impact test machine and Prof. Dr. Erdal Bayramlı for providing the injection molding machine.

Special thanks go to Mihrican Açıkgöz from Chemical Engineering Department for the DSC analysis, Cengiz Tan from Metallurgical and Materials Engineering department for the SEM analysis and İnciser Girgin from General Directorate of Mineral Research and Exploration for the XRD analysis.

This thesis could not be written without the patience, support and understanding of Pınar Altun. I express my sincerest love and thanks to her for contributions in every single step of this study. The friendly and helpful contributions of the polymer group encouraged me during my studies. The polymer group including Gülsüm Özden, Elif Alyamaç, Güralp Özkoç, Pelin Toprak, Işıl Işık, Mert Kılınç, Çiğdem Başara, Cansu Altan, Özcan Köysüren, Aslı Tolga, Sertan Yeşil, Fatma Işık, İlknur Çakar and İbrahim Canlıoğlu deserve many thanks.

Finally, I want to thank my family Metin, Emel and Ebru Keyfoğlu and Meral Hünerlitürkoğlu for their support for the completion of my education and every part of my life. It would not have been possible without their love and support to complete this study.

TABLE OF CONTENTS

PLAGIARISM ……. iii
ABSTRACT……..... iv
ÖZ…… .. vi
DEDICATION viii
ACKNOWLEDGEMENTS ix
TABLE OF CONTENTS x
LIST OF TABLES xv
LIST OF FIGURES xvii

CHAPTER

1. INTRODUCTION..... 1

2. BACKGROUND INFORMATION..... 3

2.1 Composites..... 3
2.1.1 History of Composites…….... 3
2.1.2 Classification of Composites..... 4
2.1.2.1 Polymer Matrix Composites (PMC's)..... 4
2.1.2.2 Metal Matrix Composites (MMC's)…….....……. 4
2.1.2.3 Ceramic Matrix Composites (CMC's)…… 4
2.1.3 Basic Concepts of Composites..... 4
2.1.3.1 Wettability..... 5
2.1.3.2 Chemical Bonding..... 5
2.1.1.3 Mechanical Adhesion..... 5
2.1.4 Composite Properties..... 5
2.1.4.1 Advantages..... 6

2.1.4.2 Drawbacks of Composites..... 6

2.2 Polymer-Matrix Composites..... 6
2.2.1 Thermoplastics..... 7
2.2.2 Thermosets..... 7

2.3. Polymer Layered Silicate Nanocomposites..... 8
2.3.1 Clays..... 9
2.3.1.1 Morphology..... 9
2.3.1.2 Cation Exchange Process..... 10
3.2 Nanocomposite Synthesis Methods..... 11
2.3.2.1 In-Situ Polymerization..... 11
2.3.2.2 Melt Intercalation..... 12
2.3.2.3 Solution Method..... 13
2.3.3 Nanocomposite Structures..... 14

2.4 Extrusion..... 15
2.4.1 Extruder..... 15
2.4.1.1 Components of An Extruder..... 16
2.4.1.2 Types of Extruders..... 17
2.4.1.2.1 Single Screw Extruder..... 17
2.4.1.2.2 Twin Screw Extruder..... 17
2.4.2 Reactive Extrusion..... 18
2.4.3 Extrusion Parameters..... 18

2.5 Poly(Ethylene Terephthalate) (PET)..... 19
2.5.1 PET Recycling..... 20
2.5.1.1 Degradation of PET During Recycling... 20
2.5.2 Chain Extenders..... 21
2.5.2.1 Pyromellitic Dianhydride (PMDA)..... 22
2.5.2.2 Maleic Anhydride (MA)..... 23

2.6 Characterization of Polymer/Clay Nanocomposites..... 23
2.6.1 Mechanical Tests..... 23
2.6.1.1 Tensile Tests (ASTM D 638-91A)..... 24
2.6.1.2 Flexural Tests (ASTM D790m)..... 26
2.6.1.3 Impact Tests (ASTM D 256)..... 27
2.6.2 Differential Scanning Calorimeter (DSC) Analysis..... 27
2.6.3 X-Ray Diffraction (XRD) Analysis..... 28
2.6.4 Scanning Electron Microscopy (SEM)..... 29
2.6.5 Melt Flow Index (MFI) Test..... 29

2.7 Previous Studies..... 30

3. EXPERIMENTAL..... 33

3.1 Materials..... 33
3.1.1 Chain Extenders (Anhydrides)..... 33
3.1.2 Organoclay..... 33
3.1.3 Recycled PET Resin (R-PET)..... 35

3.2 Experimental Procedure..... 35
3.2.1 Extrusion of R-PET, Organoclay and Chain Extenders..... 35
3.2.2 Sample Preparation..... 36

3.3 Characterization of Specimens..... 39
3.3.1 Morphological Analysis..... 39
3.3.1.1 Scanning Electron Microscopy (SEM) Analysis..... 39
3.3.1.2 X-Ray Analysis..... 39
3.3.2 Mechanical Tests..... 39
3.3.2.1 Tensile Tests..... 40
3.3.2.2 Impact Tests..... 40
3.3.2.3 Flexural Tests..... 41
3.3.3 Differential Scanning Calorimeter (DSC) Analysis..... 41

3.3.4 Melt Flow Index (MFI) Test…….. 41
4. RESULTS AND DISCUSSION…….42

4.1 Morphological Analysis……. 42
4.1.1 X-RAY Analysis…… 42
4.1.2 Scanning Electron Microscopy (SEM) Analysis…… 45
4.2 Mechanical Analysis…….. 51
4.2.1 Effect of Extrusion Cycle on the Mechanical Properties of Recycled PET……. 51
4.2.2 Effect of Clay Content on the Mechanical Properties of the Nanocomposites……57
4.2.3 Effect of Order of Addition on the Mechanical Properties of the Nanocomposites……63
4.2.4 Effect of Extrusion Cycle on the Mechanical Properties of the Nanocomposites……....67
4.2.5 Effect of MA or PMDA Content on the Mechanical Properties of the Nanocomposites……71
4.2.6 Effect of Screw Speed on the Mechanical Properties of the Nanocomposites…….. .78

4.3 Differential Scanning Calorimeter (DSC) Analysis…….. 85

4.4 Melt Flow Index (MFI) Test…….. 87

5. CONCLUSIONS……... 89

6. REFERENCES.....91

7.APPENDIX A..... 95

A.1 Stress-Strain Data for all Compositions.....95
A.2 Tensile Data for all Compositions..... 99
A.3 Flexural Data for all Compositions..... 102

A.4 Impact Strength Data..... 105

8. APPENDIX B - DIFFERENTIAL SCANNING
CALORIMETER ANALYSIS..... 106

9. APPENDIX C - X-RAY ANALYSIS.....119

10. APPENDIX D – THERMO GRAVIMETRIC ANALYSIS (TGA)..... 136

LIST OF TABLES

TABLE

3.1 Physical Properties of Maleic Anhydride…… 33
3.2 Physical Properties of Pyromellitic Dianhydride. 33
3.3 Properties of Cloisite 25A……..... 34
3.4 Properties of PET Resin…. 35
3.5 Tensile test specimen dimensions…… 40
4.1 XRD results of Cloisite 25A and polymer-Cloisite25A nanocomposites…… 44
4.2 Thermal transition temperatures of recycled PET nanocomposites……. 86
4.3 Melt Flow Index values of recycled PET nanocomposites…….. 88
A.1.1 The data of tensile stress-strain curves of recycled PET…….. 95
A.1.2 The data of tensile stress-strain curves of nanocomposites containing only Cloisite 25A…… 95
A.1.3 The data of tensile stress-strain curves of nanocomposites containing PMDA and 3 weight percent Cloisite 25A…..... 96
A.1.4 The data of tensile stress-strain curves of nanocomposites containing MA and 3 weight percent Cloisite 25A……..... 96
A.1.5 The data of flexural stress-strain curves of recycled PET…..... 97
A.1.6 The data of flexural stress-strain curves of nanocomposites containing only Cloisite 25A….. 97
A.1.7 The data of flexural stress-strain curves of nanocomposites containing PMDA and 3 weight percent Cloisite 25A..... 98
A.1.8. The data of flexural stress-strain curves of nanocomposites containing MA and 3 weight percent Cloisite 25A…..... 98
A.2.1 Young's modulus data for all compositions…..... 99
A.2.2 Tensile strength data for all compositions..... 100
A.2.3 Tensile strain at break (%) data for all compositions……..... 101

A.3.1 Flexural modulus data for all compositions…… ..... …… 102
A.3.2 Flexural strength data for all compositions. ..... …… 103
A.3.3 Flexural strain at break (%) data for all compositions. 104
A.4.1 Impact strength data for all compositions. 105

LIST OF FIGURES

FIGURE

2.1 Idealized structure of 2:1 layered silicate showing two tetrahedral-site sheets fused to an octahedral-site sheet..... 10
2.2 The cation-exchange process between alkylammonium ions and cations initially intercalated between the clay layers. 11
2.3 Schematic representation of PLS obtained by in situ polymerization. 12
2.4 Schematic representation of PLS obtained by polymer melt intercalation process..... 13
2.5 Schematic representation of the intercalation of the polymer by the "solution" approach. 13
2.6 Schematic illustrations of A a conventional; B an intercalated; C an ordered exfoliated; and D a disordered exfoliated polymer–clay nanocomposite. 15
2.7 Hydrocarbon backbone of PET..... 19
2.8 Hydrolytic chain scission of PET caused by the retained moisture. 21
2.9 Thermal degradation of PET that occurs between 290°-310°C..... 21
2.10 Chain extension/branching reaction of PMDA with PET..... 22
2.11 Chain extension reaction of MA with PET (Formed carboxyl groups further reacts with hydroxyl end groups of PET)..... 23
2.12 Tension test specimen..... 24
2.13 The stresses on the sample during flexural testing..... 26
2.14 Principle of X-Ray Diffraction..... 28
3.1 Chemical structure of alkyl ammonium cation..... 34
3.2 Chemical structure of methyl sulfate anion..... 34
3.3 Schematic representation of the injection molding machine..... 37
3.4 Flowchart of composite specimen preparation, and characterization

methods used……..…… 38
3.5 Tensile Test Specimen (Type M-I)……..…… 40
4.1 Fracture surfaces of amorphous PET in the form of unprocessed pellets (a) extruded R-PET (b) and double extruded 3% Cloisite25A containing nanocomposite at 350 rpm (c)…… .....…… 47
4.2 Fracture surfaces of R-PET containing 2, 3 and 4 weight percents of Cloisite 25A, a, b, and c, respectively, at 350 rpm.....……. 48
4.3 Fracture surfaces of 0.5, 0.75 and 1 weight percent PMDA added 3 % Cloisite 25A containing nanocomposites, a, b, and c, respectively, at 350 rpm.....……49
4.4 Fracture surfaces of 0.5, 0.75 and 1 weight percent MA added 3 % Cloisite 25A containing nanocomposites, a, b, and c, respectively, at 350 rpm.....……50
4.5 Effect of repeated extrusion cycles on tensile stress-strain behavior of pure R-PET. .....……51
4.6 Effect of repeated extrusion cycles on Young's modulus of pure R-PET…… 52
4.7 Effect of repeated extrusion cycles on tensile strength of pure R-PET…… 52
4.8 Effect of repeated extrusion cycles on tensile strain at break of pure R-PET... 53
4.9 Effect of repeated extrusion cycles on flexural stress-strain behavior of pure R-PET…….. .....……53
4.10 Effect of repeated extrusion cycles on flexural modulus of pure R-PET…… 54
4.11 Effect of repeated extrusion cycles on flexural strength of pure R-PET…… 54
4.12 Effect of repeated extrusion cycles on impact strength of pure R-PET……. 55
4.13 Effect of organoclay content on tensile stress-strain behavior of nanocomposites…… .....……57
4.14 Effect of organoclay content on Young's modulus of nanocomposites……58
4.15 Effect of organoclay content on tensile strength of nanocomposites……..58
4.16 Effect of organoclay content on tensile strain at break of nanocomposites….59
4.17 Effect of organoclay content on flexural stress-strain behavior of nanocomposites…… .....…… 59
4.18 Effect of organoclay content on flexural modulus of nanocomposites……60
4.19 Effect of organoclay content on flexural strength of nanocomposites…… 60

4.20 Effect of organoclay content on flexural strain at break of nanocomposites.. 61
4.21 Effect of organoclay content on impact strength of nanocomposites…….61
4.22 Effect of order of addition of chain extenders and organoclay on
tensile stress-strain behavior of nanocomposites……..…… 64
4.23 Effect of order of addition of chain extenders and organoclay on
f lexural stress-strain behavior of nanocomposites. .....……. 64
4.24 Effect of order of addition of chain extenders and organoclay on
Young's and flexural modulus of nanocomposites.....……65
4.25 Effect of order of addition of chain extenders and organoclay on
tensile, flexural and impact strength of nanocomposites. .....……65
4.26 Effect of order of addition of chain extenders and organoclay on
tensile and flexural strain at break of nanocomposites. .....……66
4.27 Effect of repeated extrusion cycles on tensile stress-strain
behavior of nanocomposites.....……67
4.28 Effect of repeated extrusion cycles on flexural stress-strain
behavior of nanocomposites.....……68
4.29 Effect of repeated extrusion cycles on Young's and flexural
modulus of nanocomposites…….....……68
4.30 Effect of repeated extrusion cycles on tensile, flexural and
impact strength of nanocomposites…….....……69
4.31 Effect of repeated extrusion cycles on tensile and flexural
strain of nanocomposites…….....……69
4.32 Effect of PMDA content on tensile stress-strain behavior
of 3 weight % Cloisite25A containing nanocomposites, at 350 rpm.…….71
4.33 Effect of MA content on tensile stress-strain behavior
of 3 weight % Cloisite25A containing nanocomposites, at 350 rpm.…….72
4.34 Effect of MA or PMDA content on Young's modulus
of 3 weight % Cloisite25A containing nanocomposites, at 350 rpm.…….72
4.35 Effect of MA or PMDA content on tensile strength
of 3 weight % Cloisite25A containing nanocomposites, at 350 rpm… ……73
4.36 Effect of MA or PMDA content on tensile strain at break
of 3 weight % Cloisite25A containing nanocomposites, at 350 rpm……. 73

4.37 Effect of PMDA content on flexural stress-strain behavior
of 3 weight % Cloisite25A containing nanocomposites, at 350 rpm…….. 74
4.38 Effect of MA content on flexural stress-strain behavior
of 3 weight % Cloisite25A containing nanocomposites, at 350 rpm… ……74
4.39 Effect of MA or PMDA content on flexural modulus
of 3 weight % Cloisite25A containing nanocomposites, at 350 rpm.…….75
4.40 Effect of MA or PMDA content on flexural strength
of 3 weight % Cloisite25A containing nanocomposites, at 350 rpm.…….75
4.41 Effect of MA or PMDA content on flexural strain at break
of 3 weight % Cloisite25A containing nanocomposites, at 350 rpm.…….76
4.42 Effect of MA or PMDA content on impact strength
of 3 weight % Cloisite25A containing nanocomposites, at 350 rpm.…….76
4.43 Effect of screw speed (rpm) on tensile stress-strain behavior
of 3 weight % Cloisite25A - 1 weight %
PMDA containing nanocomposites. .....…….79
4.44 Effect of screw speed (rpm) on tensile stress-strain behavior
of 3 weight % Cloisite25A - 1 weight % MA containing nanocomposites….79
4.45 Effect of screw speed (rpm) on Young's modulus of 3 weight %
Cloisite25A - 1 weight % MA or PMDA containing nanocomposites. ……80
4.46 Effect of screw speed (rpm) on tensile strength of 3 weight %
Cloisite25A – 1 weight % MA or PMDA containing nanocomposites……...80
4.47 Effect of screw speed (rpm) on tensile strain at break of 3 weight %
Cloisite25A - 1 weight % MA or PMDA containing nanocomposites…….. .81
4.48 Effect of screw speed (rpm) on flexural stress-strain behavior of
3 weight % Cloisite25A - 1 weight % PMDA containing nanocomposites… 81
4.49 Effect of screw speed (rpm) on flexural stress-strain behavior of
3 weight % Cloisite25A - 1 weight % MA containing nanocomposites……..82
4.50 Effect of screw speed (rpm) on flexural modulus of 3 weight %
Cloisite25A – 1 weight % MA or PMDA containing nanocomposites……...82
4.51 Effect of screw speed (rpm) on flexural strength of 3 weight %
Cloisite25A - 1 weight % MA or PMDA containing nanocomposites……83

4.52 Effect of screw speed (rpm) on flexural strain at break of 3 weight % Cloisite25A - 1 weight % MA or PMDA containing nanocomposites…….83
4.53 Effect of screw speed (rpm) on impact strength of 3 weight % Cloisite25A – 1 weight % MA or PMDA containing nanocomposites……...84
B.1 DSC diagram of single extruded recycle PET.....……106
B.2 DSC diagram of the sample containing 3 weight % Cloisite25A at 350 rpm…….. .....……107
B.3 DSC diagram of the sample containing double extruded 3 weight % Cloisite25A at 350 rpm……. .....……108
B.4 DSC diagram of the sample containing 3 weight % Cloisite25A and 1 weight % PMDA at 350 rpm…..…….109
B.5 DSC diagram of the sample containing 3 weight % Cloisite25A and 1 weight % PMDA at 150 rpm…….....……110
B.6 DSC diagram of the sample containing 3 weight % Cloisite25A and 1 weight % PMDA at 75 rpm…….....……111
B.7 DSC diagram of the sample containing 3 weight % Cloisite25A and 0.75 weight % PMDA at 350 rpm…….....……112
B.8 DSC diagram of the sample containing 3 weight % Cloisite25A and 0.5 weight % PMDA at 350 rpm…….....……113
B.9 DSC diagram of the sample containing 3 weight % Cloisite25A and 1 weight % MA at 350 rpm…….....……114
B.10 DSC diagram of the sample containing 3 weight % Cloisite25A and 1 weight % MA at 150 rpm…….....……115
B.11 DSC diagram of the sample containing 3 weight % Cloisite25A and 1 weight % MA at 75 rpm…….....……116
B.12 DSC diagram of the sample containing 3 weight % Cloisite25A and 0.75 weight % MA at 350 rpm…….....……117
B.13 DSC diagram of the sample containing 3 weight % Cloisite25A and 0.5 weight % MA at 350 rpm…….....……118
C.1 XRD pattern of Cloisite 25A…….....……119
C.2 XRD pattern of sample containing 2 weight % Cloisite 25A at 350 rpm…….120

C.3 XRD pattern of sample containing 3 weight % Cloisite 25A at 350 rpm……121
C.4 XRD pattern of sample containing 4 weight % Cloisite 25A at 350 rpm……122
C.5 XRD pattern of sample containing double extruded 3 weight % Cloisite 25A at 350 rpm……123
C.6 XRD pattern of sample containing 3 weight % Cloisite 25A and 1 weight % PMDA at 350 rpm……124
C.7 XRD pattern of sample containing 3 weight % Cloisite 25A and 1 weight % PMDA at 150 rpm……125
C.8 XRD pattern of sample containing 3 weight % Cloisite 25A and 1 weight % PMDA at 75 rpm……126
C.9 XRD pattern of sample containing 3 weight % Cloisite 25A and 0.75 weight % PMDA at 350 rpm……127
C.10 XRD pattern of sample containing 3 weight % Cloisite 25A and 0.5 weight % PMDA at 350 rpm……128
C.11 XRD pattern of sample containing 3 weight % Cloisite 25A and 1 weight % MA at 350 rpm……129
C.12 XRD pattern of sample containing 3 weight % Cloisite 25A and 1 weight % MA at 150 rpm……130
C.13 XRD pattern of sample containing 3 weight % Cloisite 25A and 1 weight % MA at 75 rpm……131
C.14 XRD pattern of sample containing 3 weight % Cloisite 25A and 0.75 weight % MA at 350 rpm……132
C.15 XRD pattern of sample containing 3 weight % Cloisite 25A and 0.5 weight % MA at 350 rpm……133
C.16 XRD pattern of sample containing 1 weight % MA and 3 weight % Cloisite 25A and at 350 rpm……134
C.17 XRD pattern of single extruded R-PET. ……135
D.1 TGA diagram of Cloisite 25A……136

CHAPTER I

INTRODUCTION

The field of nanocomposites originates from the definition of composite in which one of the constituents is dispersed in the other at nano-scale (10^{-9} m). Most widely studied nanocomposites are polymer based, including clays, especially montmorillonite as the nanofiller. Montmorillonite is a layered silicate which has a very high surface area of 750 m^2/g if it is completely exfoliated; i.e. if the layers are completely dispersed in the polymer matrix. The montmorillonite layers are one nanometer thick with high lateral dimensions leading to very high aspect ratios. In its natural form, montmorillonite is quite hydrophilic; in order to make it compatible with the organic polymers, it is organically modified [1].

In polymer layered silicate nanocomposites, the interaction between the clay with tremendous surface area and the polymer matrix facilitates stress transfer to the reinforcement phase, yielding to improvement in properties such as barrier mechanical and thermal properties [2]. Although the history of polymer layered silicate nanocomposites dates back to 1950's, it was the Toyota researchers who accelerated the development of these materials when they focused on polymerization of caprolactam in the presence of clay [3-7].

Melt intercalation in which a molten thermoplastic is blended with an organoclay is a convenient method for the production of polymer layered silicate nanocomposites. It has been very popular because of its great potential for application in industry, in recent years. [1]

In this study, it is aimed to investigate the effects of chain extension and branching on the properties of nanocomposites produced from recycled poly(ethylene

terephthalate) (R-PET) and organically modified clay by melt intercalation. The commercial name of the organoclay used is Cloisite 25A, deliberately chosen since the previous studies have revealed that it is the most appropriate type of clay for recycled PET. An intermeshing co-rotating twin screw extruder was used in the melt intercalation process as it is the most suitable one for high levels of exfoliation.

PET is a linear thermoplastic polyester that has widespread commercial use as a synthetic fiber as well as being a film and moulding material owing to its good physical and chemical properties such as high strength, good impact strength and transparency [8]. In addition, PET is one of the largest polymers by volume because of its suitability for practically all recycling methods [9].

One of the problems met in the reprocessing of recycled PET is degradation which causes a decrease in the molecular weight. In this study, maleic anhydride (MA) and pyromellitic dianhydride (PMDA) were used as chain extenders to overcome this problem.

Throughout the study, the selected parameters were the screw speed, sequence of addition of the organoclay and chain extender and the chain extender type and content.

For characterization of the samples, X Ray Diffraction (XRD) and Scaning Electron Microscopy (SEM) were utilized to observe the degree of exfoliation. Mechanical behavior of the prepared nanocomposites was observed by performing tensile, flexural and impact tests. Differential Scanning Calorimetry (DSC) was done for the thermal analysis and Melt Flow Index (MFI) measurements were done to examine the effects of the selected parameters on the viscosity of the samples.

CHAPTER II

BACKGROUND INFORMATION

2.1 Composites

A composite is a combined material created by the synthetic assembly of two or more components –a selected filler or reinforcing agent and a compatible matrix binder (i.e., a resin)- in order to obtain specific characteristics and properties [10].

The idea behind the composite concept is to attain properties that the individual components by themselves can not attain, i.e., the final properties of composite materials are better than constituent material properties.

2.1.1 History of Composites

The concept of composites was not invented by human beings, it was found in nature. An example is wood, which is a composite of cellulose fibers in a matrix of natural glue called lignin [11]. Throughout history, it was found that combinations of materials would produce properties in those materials that were superior to those of the separate components themselves for some uses. For instance; mud bricks reinforced with straw were used by ancient Israelites in Egypt. The first man-made composites based upon polymers appeared in about 5000 B.C. in the Middle East where pitch was used as a binder for reeds in boat-building. Although some ceramic composites existed in the 1920's, the first modern application of composites was in 1945 which was a glass-reinforced phenolic-nylon fishing pole [12]. The growth of World War 2 during 1940's accelerated the use of composites as to compensate the need for military and technological problems. During 1960's composites captured the attention of industries with the introduction of polymer based composites [11]. It has

been estimated that in 1979 eight billion pounds of composites were produced [10]. Today, the major composite markets are automotive, aerospace, construction military and electronic industries [12].

2.1.2 Classification of Composites

A composite can include metal, plastic ceramic or wood. The most common composites can be divided into three main groups according to the matrix material.

2.1.2.1 Polymer Matrix Composites (PMC's)

These composites find the most commercial applications. These materials use a polymer-based resin as the matrix, and a variety of fibres as the reinforcement.

2.1.2.2 Metal Matrix Composites (MMC's)

Increasingly found in the automotive industry, these materials use a metal matrix. These composites find the most commercial applications; these materials use a metal such as aluminum as the matrix, and reinforce it with fibres such as silicon carbide.

2.1.2.3 Ceramic Matrix Composites (CMC's)

Used in very high temperature environments, these materials use a ceramic as the matrix and reinforce it with short fibres, or whiskers such as those made from silicon carbide and boron nitride.

2.1.3 Basic Concepts of Composites

The unique properties of advanced composite materials depend not only upon the properties of both the fibrous reinforcement and the resin matrix but also upon the interface between the fiber and the matrix [13].

Interface is defined as the bidimesional region through which material properties such as concentration of an element, crystal structure, atomic registry, elastic modulus, density and coefficient of thermal expansion change from one side to another. The reason the interface in a composite is of great importance is that the internal surface area occupied by the interface is quite extensive. Thus, it becomes extremely important to understand what interactions occur at the interface [14].

2.1.3.1 Wettability

Wettability is the term used to describe the extent to which a liquid would spread on a solid surface. Wettability refers to the extent of intimate contact possible at the molecular level [14]. It is essential that the fibers be wetted by the matrix in order to form a successful composite [15].

2.1.3.2 Chemical Bonding

Chemical bonding between the matrix and the reinforcement is one of the most effective methods of increasing the interfacial bond strength [15]. Good bonding implies that atomic or molecular bonds are formed uniformly all along the interface.

2.1.1.3 Mechanical Adhesion

Bonding of the matrix to the irregularities of the fiber surface takes place through mechanical interlocking. Fiber surface roughening usually enhances this mechanical adhesion because surface craters and other defects can serve as sites for mechanical interlocking.

2.1.4 Composite Properties

Composites have been routinely designed and manufactured for applications in which high performance and light weight are needed. They offer several advantages over traditional engineering materials [14].

2.1.4.1 Advantages

Generally the attraction of composites primarily stamps from their ability to replace standard materials with a lighter weight/higher strength alternative [12]. Composites offer new design flexibilities, improved corrosion and wear resistance and increased fatigue life [12]. Additionally, composite materials offer high corrosion resistance. Some net shaped parts can be produced with composite materials by utilizing proper design and manufacturing techniques. This feature eliminates several machining operations and thus reduces process time and cost [11].

2.1.4.2 Drawbacks of Composites

The drawbacks of the composites are usually the drawbacks of either the matrix or the reinforcement in a particular application [12]. The selection of the appropriate constituent in a composite plays a crucial role on the final properties of the product. For instance, should the matrix be susceptible to solvent attack, it would be expected for the composite to reveal the same deficiency.

2.2 Polymer-Matrix Composites

In the last fifty years, following the chemical discoveries of nylon and polyethylene, the emphasis for new material research has progressively moved towards non-metallic materials and especially the family of polymeric materials known as plastics [16]. Polymers are mostly organic compounds based on carbon, hydrogen and other non-metallic elements. PMC are the most developed composite materials group and they find widespread applications [17].

Polymer matrix composites are much easier to fabricate than metal-matrix, carbon-matrix and ceramic-matrix composites. This is mainly because of the relatively low processing temperatures required for fabricating polymer-matrix composites [18]. The polymer matrix spreads the load applied to the composite and protects the reinforcement from damage caused by abrasion and impact. High strengths and

stiffnesses, ease of moulding complex shapes, high environmental resistance coupled with low densities make the resultant polymer matrix composite superior to metal-matrix composites for many applications. In polymer-matrix applications, thermosetting or thermoplastic polymers can be used as the matrix component.

2.2.1 Thermoplastics

Thermoplastics are heat softenable, heat meltable and reprocesseable polymers [17]. Thermoplastics matrix materials derive their properties from their long chain entangled molecules. The entanglement of the chains provides the matrix with strength and the chains have the ability to slip past one another when subjected to intense local stress. Thus, this ability confers the property of toughness on the composite [16].

The thermoplastic family of materials is particularly broad in respect of the services it can offer. There are wide ranges of resins: elastomeric materials such as polyurethanes, general purpose resins such as polypropylene, engineering plastics such as nylon and polycarbonate, and high performance polymers such as polysulphones and polyacetones [16]. It is generally recognized that the use of thermoplastics in composite production results in a decrease in manufacturing costs [17]. Thermoplastic resins effectively avoid many of the problems of thermosets, nevertheless some new problems are encountered. One of these problems is the high viscosity of the melted resin which complicates the wet-out of the reinforcement [15]. Being partially crystalline for most cases, the resulting polymer matrix may also suffer from a change in the level of crystallinity during the fabrication and processing of the composite [17].

2.2.2 Thermosets

Thermoset resins are the most frequently used matrix materials in polymer-based composites production. The most common thermoset resins are epoxy, polyester and vinylester [17]. The bonds between chains in thermoset resins are usually created by

chemical reactions called crosslinks; this process of forming the crosslinks is called curing [15]. During curing, usually performed in the presence of heat and pressure, thermoset resin hardens gradually owing to the completion of polymerization [18]. When curing is extensive, that is when many chains are crosslink together, the effect is to increase the molecular weight dramatically. This high molecular weight may result in excellent mechanical and thermal properties [15].

Thermosets have many advantages over thermoplastics. Before curing, the resins have a low viscosity which facilitates the wetting out of the fiber reinforcements, thus the voids and porosities are reduced [11]. Thermosets, however, have several inherent problems, because thermoset curing is a chemical reaction, at least two components need to be mixed to initiate the curing. This mixing requires attention to proper proportions and often has the added problem of vapor and dangerous chemicals control [15]. Thermoset composite processing requires a lengthy cure time and thus results in lower production rates than thermoplastics. Once cured and solidified, thermoset composite parts can not be reformed to obtain other shapes [11].

2.3. Polymer Layered Silicate Nanocomposites

Composites that exhibit a change in composition and structure over a nanometer length scale have been shown over the last ten years to afford remarkable property enhancements relative to conventionally-scaled composites [2].

Nanocomposites can be considered as solid structures with nanometer-scale dimensional repeat distances between the phases that constitute the structure [19]. This term is commonly used in distinct areas of materials science: ceramics, metals and polymers; but polymers have been the most intriguing and focused on subject in nonocomposite technology.

Classified by nanofiller dimensionality, there are a number of types of nanocomposites. Zero dimensional (nanoparticle), one dimensional (nanofiber), two

dimensional (nanolayer) and three-dimensional (interpenetrating network) systems can all be imagined [20].

Polymer layered silicate nanocomposites are two dimensional systems, consisting of silicate layers of nanometer thickness and high aspect ratio (30-10000) dispersed in a polymer matrix. Although the history of polymer layered silicate nanocomposites dates back to 1950's, it was not until Toyota researchers began a detailed examination of polymer layered silicate clay mineral composites that pioneered revival of these materials [21-22].

2.3.1 Clays

Clay is a hydrous aluminum silicate in which alkalies or alkaline earths are also present. Clay may be amorphous (allophone), crystalline (kaolinite, hollocite ,montmorillonite, vermiculite), mixed-layer type (chlorite) or chain structured (attapulgate). These minerals, which are widely distributed geographically throughout the world, are the natural decomposition products of feldspar, and include kaolins (kaolinite, dickite, nacrite) [23].

Many clays have a sheet like (layered structure), and consist of silicon SiO4 tetrahedra bonded to alumina AlO6 octahedra in a variety of ways. A 2:1 ratio of the tetrahedral to the octahedral results in smectite clays, the most common of which is montmorillonite obtained from a rock called bentonite [24].

2.3.1.1 Morphology

The montmorillonite crystal lattice consists of 1 nm thin layers, with a central octahedral sheet of alumina fused between two external silica tetrahedral sheets(in such a way, so that the oxygens from the octahedral sheet also belong to the silica tetrahedra) [21]. Isomorphous substitutions of Si4+ for Al3+ in the tetrahedral lattice and of Al3+ for Mg2+ in the octahedral sheet, cause an excess of negative charges within the montmorillonite layers. This excess charge is counterbalanced by alkali or

alkaline earth cations situated within the layers. Due to the high hdyrophilicity of the clay, water molecules are usually also present between the layers. Stacking of the layers leads to regular van der Waals gaps called interlayers or galleries. The sum of the single layer thickness (9.6 Å) and the interlayer is called d-spacing (basal spacing) [1].

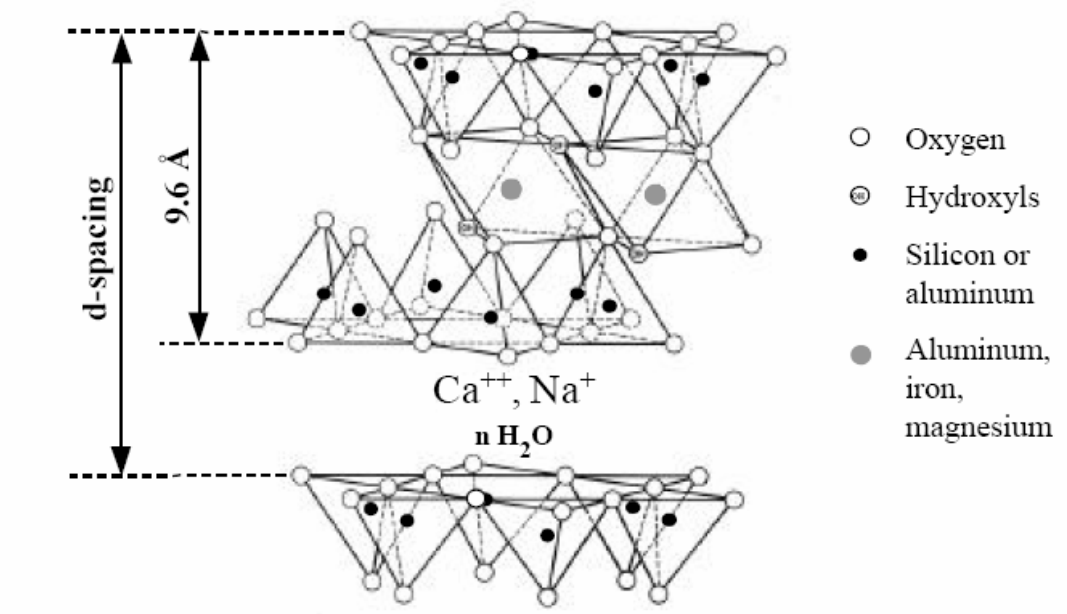

Figure 2.1 Idealized structure of 2:1 layered silicate showing two tetrahedral-site sheets fused to an octahedral-site sheet [1].

Montmorillonite has very high surface area: about 750 m2/g, a large aspect ratio: greater than 50, a platelet thickness of 10 Å (1 nm) [22].

2.3.1.2 Cation Exchange Process

Montmorillonite is characterized by a moderate negative surface charge (known as cation exchange capacity, CEC and expressed in meq/100g). The charge of the layer is not locally constant as it varies from layer to layer and must rather be considered as an average value over the whole crystals. Montmorillonite layers sorb certain cations and keep them in an exchangeable state. These exchangeable cations are usually Na^{+}, Ca^{+}, Mg^{++}, H^{+}, K^{+} and $NH4^{+}$ [1]. One important consequence of the

charged nature of clays is that they are generally highly hydrophilic species and therefore naturally incompatible with a wide range of polymer types [24]. In order to render these hydrophilic phyllosilicates organophilic, hydrated cations of the interlayer can be exchanged with cationic surfactants such as alkylammonium or alkylphosphonium (onium). The modified clay (or organoclay) being organophilic, its surface energy is lowered and is more compatible with organic polymers [25].

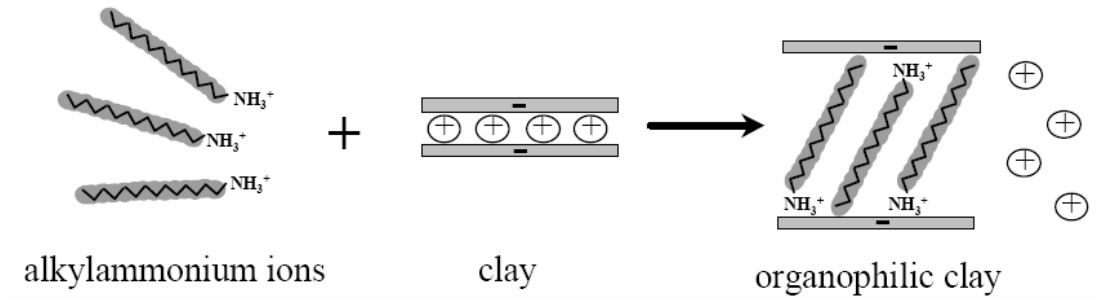

Figure 2.2 The cation-exchange process between alkylammonium ions and cations initially intercalated between the clay layers [1].

Alkylammonium ions have a general formula CH_3-$(CH_2)_n$-NH_3^+ where n is between 1 and 18. The length of the ammonium ions has a strong impact on the resulting structure of a nanocomposite [1].

2.3.2 Nanocomposite Synthesis Methods

Several strategies can be used to prepare polymer layered silicate nanocomposites. Three methods are mainly used.

2.3.2.1 In-Situ Polymerization

In-situ polymerization was the first method used to synthesize polymer-clay nanocomposites based on polyamide 6. Nowadays it is the conventional process used to synthesize thermoset-clay nanocomposites [1]. The modified layered silicate is

swollen by a liquid monomer or a monomer solution. The monomer migrates into the galleries of the layered silicate, so that the polymerization can occur within the intercalated sheets [26]. The polymerization reaction leads to the delamination of the clay [1]. The polymerization reaction can be carried out by heat, radiation or a suitable initiator.

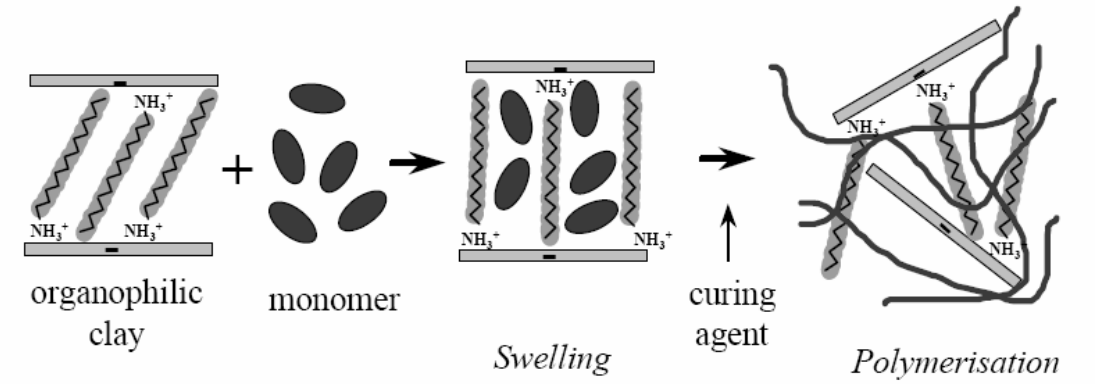

Figure 2.3 Schematic representation of PLS obtained by in situ polymerization [1].

2.3.2.2 Melt Intercalation

The layered silicate is mixed with the polymer matrix in the molten state. Under these conditions, if the layer surfaces are sufficiently compatible with the chosen polymer, the polymer can crawl into the interlayer surface to form either an intercalated or an exfoliated nanocomposite. In this technique, no solvent is required [25]. Owing to its great potential in industrial applications, the melt intercalation process has become increasingly popular.

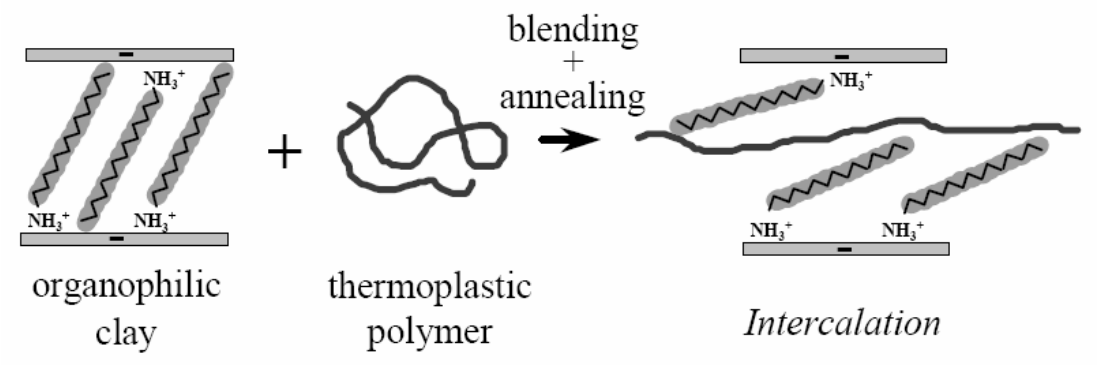

Figure 2.4 Schematic representation of PLS obtained by polymer melt intercalation process [1].

2.3.2.3 Solution Method

It is well known that such layered silicates, owing to the weak forces that stack the layers together can be easily dispersed in an adequate solvent [25]. Then the polymer dissolved in the solvent, is added to the solution and intercalates between the clay layers. The last step consists in removing the solvent by evaporation under vacuum. Nanocomposites, based on untreated clays can also be synthesized using this approach [1].

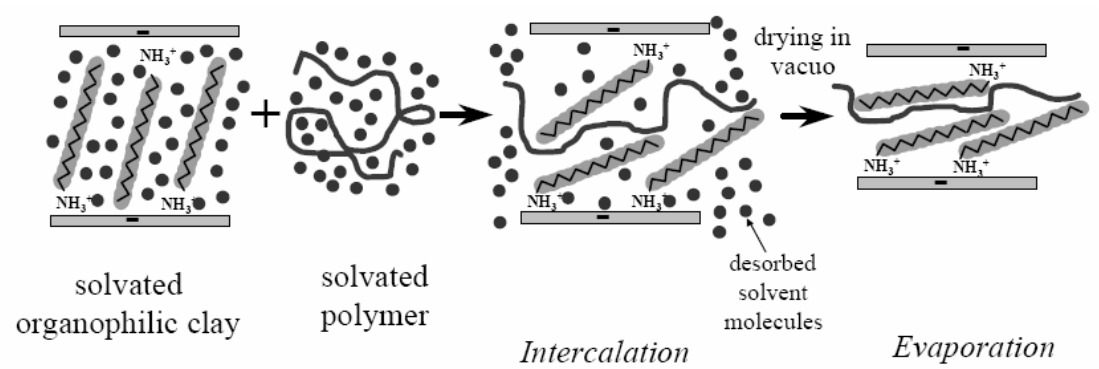

Figure 2.5 Schematic representation of the intercalation of the polymer by the "solution" approach [1].

2.3.3 Nanocomposite Structures

The essence of nanotechnology is the ability to work at the molecular level to create large structures with fundamentally new molecular organization [20]. The small size provides that the particles do not create large stress concentrations and leads to an exceptionally large interfacial area [19].

Three main types of composites can be obtained when a layered silicate is dispersed in a polymer matrix. This dominantly depends on the nature of the components used including polymer matrix, layered silicate, and organic cation [26]. The choice of method for making a nanocomposite depends on the final form of the hybrid.

Conventional

If the clay particles are dispersed as tactoids in the polymer matrix; i.e. if the clay layers are not separated a microcomposite structure is obtained. The clay acts as conventional filler in this case. [1]

Intercalated

In an intercalated system, the polymer swells the galleries of the silicate layers but preserves the stacking of layers [27]. The resulting structure is a multilayered system built up with alternating polymeric and inorganic layers [25].

Exfoliated (delaminated)

Exfoliated or delaminated structures are obtained when the silicates are completely and uniformly dispersed in the continuous polymer matrix. This structure is of particular interest because it maximizes the polymer-clay interaction surface area [26].

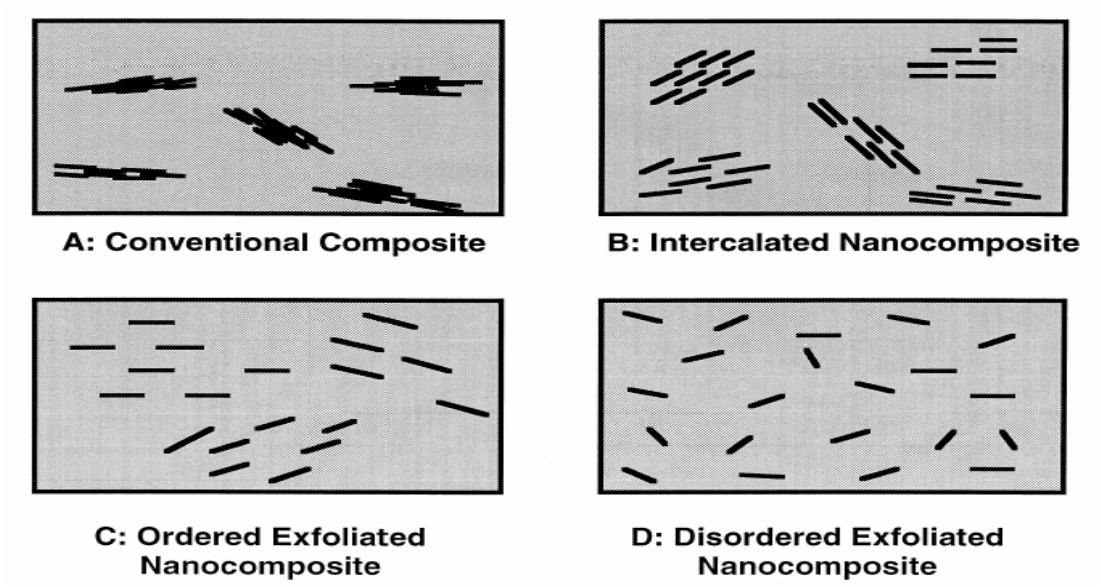

Figure 2.6 Schematic illustrations of A a conventional; B an intercalated; C an ordered exfoliated; and D a disordered exfoliated polymer–clay nanocomposite [2].

2.4 Extrusion

The commercial process of extrusion is the conversion of a raw material usually in the form of a powder or pellet, into a finished product or part, by forcing it through an opening. The first extruders were developed for food and building materials industry. During extrusion, a polymer is pumped through a shaping die into the final form via heat and pressure [28].

2.4.1 Extruder

The main function of an extruder is to develop sufficient pressure in the material to force the material through the die [29.]. The first extruders were ram-type extruders and they were built in 1797 to extrude seamless head pipes.

2.4.1.1 Components of an Extruder

Control Panel

The control panel consists of different indicators to stabilize and control the extrusion. Feeding rate, screw speed and temperature can be adjusted. Pressure and temperature as well as torque can be monitored.

Feeder

Feeding sections consists of the feed hooper and the feed throat. The feed throat is connected to the barrel; it contains the opening through which plastic material is introduced to the extruder [29]. The feeding rate can be adjusted from the control panel and determines the product output.

Screw

Screw is the dominating part of the extruder affecting the performance of the machine. The screw rotates in a cylinder that fits closely around it [29]. The screw has the following tasks;

- Feeding of raw material from the feeder to the die
- Melting of the material
- Homogenization of the material
- Pressurizing the material [30]

Barrel

The extruder barrel is a cylinder that houses the screw. It provides the bearing surface where shear is imparted to the plastic granules. The barrel consists of cast or fabricated steel sections and a smooth inner liner often made of a wear resistant material [29].

Die

The form of the final product is mainly determined by the extrusion die. The extruder die has an opening with the shape of the cross-section of the product. The die has to be able to withstand the high temperatures and pressures exerted on it. The pressure built up, called die head pressure, depends upon the properties of the polymer, temperature of the polymer, the shape of the die and the flow rate through the die [31].

2.4.1.2 Types of Extruders

Single and twin screw extruders are the extruders that are used for continuous reactive extrusion processes.

2.4.1.2.1 Single Screw Extruder

In all extruders, the melt is dragged along the barrel by the rotation of screw(s). Mixing is poor in single screw extruders with respect to twin screw extruders. Some mixing enhancers are used to modify mixing.

2.4.1.2.2 Twin Screw Extruder

An extruder with two screws is called a twin screw extruder. Twin screw extruders are preferred for plastics and reactive extrusion operations because of superior mixing resulting from the interaction of one screw with the other one.

If both screws rotate in the same direction, the extruder is called a co-rotating twin screw extruder [29]. If the screws of a twin screw extruder rotate in opposite directions it is called a counter-rotating twin screw extruder. Mostly, counter-rotating twin screw extruders are preferred because they have better conveying performance [29].

2.4.3 Reactive Extrusion

In addition to being used as plasticizing and compounding units, extruders are increasingly being employed to conduct polymer reactions as well. Reactive extrusion refers to the deliberate performance of chemical reactions during continuous extrusion of polymers and/or polymerizable monomers [32]. Continuous synthesis and modification of polymers can be accomplished by reactive extrusion in a single step process. It is very convenient for industrial applications, because it does not require any solvents in addition to high process flexibility. Energy savings can also be considered as an advantage in reactive extrusion and production of new materials are feasible by this method.

Some reactions that can be performed by reactive extrusions are:

- Bulk polymerization.
- Graft reactions.
- Chain extension and branching reactions.
- Controlled molecular weight degradation.
- Functionalization or functional group addition [32]

2.4.4 Extrusion Parameters

Some parameters have controlling effects in an extrusion process and they must be adjusted accurately in order to maximize the efficiency of the process and obtain the desired product properties.

Screw speed is a key factor of the process, an increase in the screw speed will increase the volumetric output yielding an increase in the shear rate as well [33]. The mean residence time decreases with increasing screw speed.

Temperature of the zones in an extruder can be closely controlled in most commercial extruders. In extrusion process, the melt temperature of the extruder

zones controls the flow properties i.e. viscosity, whereas excessively high temperatures may lead to degradation of the polymer.

Feed rate tuning is a factor that should not be ignored during extrusion. When the feed rates are increased, the specific energy requirement and motor torque are raised accordingly; and in the other case, if the machine is starve-fed the mass feed rates controls productivity [33].

2.5 Poly(Ethylene Terephthalate) (PET)

Polyesters are hydrocarbon backbones which contain ester linkages (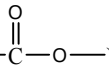) in long chains. PET is a linear thermoplastic polyester [8] which was first prepared in 1946 and was commercially introduced in 1953 as a textile fiber. Owing to the good properties of containers made from PET, it became a very important commercial plastic used in food packaging [34].

The ester groups in the polyester chain are polar with carboxyl oxygen atom having a negative charge and the carboxyl carbon atom having a positive charge. The positive and negative charges of different ester groups are attracted to each other. This allows the ester groups of nearby chains to line up with each other in crystal form. This is the cause of PET's high glass transition and melting temperature.

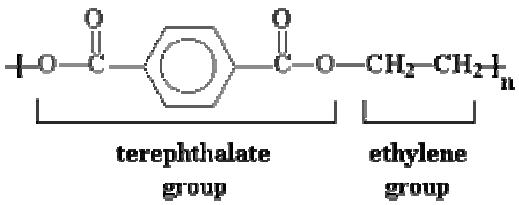

Figure 2.7 Hydrocarbon backbone of PET.

2.5.1 PET Recycling

In recent years, recycling of plastics has been one of the most focused subjects of interest. Recycling of plastics not only alleviates the environmental pollution but also favors the reduce of cost [35]. PET recycling represents one of the most successful and widespread examples of polymer recycling. In 1998, 10.4x104 tons of PET was recycled in Europe compared to 3.6x104 tons in 1995 and only 2.3x104 tons in 1993 [36] The main driving force responsible for the increased in recycling of PET is its widespread use, especially in the beverage industry.

2.5.1.1 Degradation of Pet during Recycling

It is known that primary recycling, which is also known as reprocessing can give rise to a deterioration of the most important properties of polymers due to the change of MW involved in repeated production cycles [37].

Hydrolysis catalysts are acids or bases promoting mechanism at elevated temperatures but below 205 °C. Degradation of the polymer chain leads to low molecular weight polymers with carboxylic acid end groups causing further hydrolysis. Once it occurs, the reaction, between ester bonds and the retained moisture, is autocatalytic [38]. Even if the most sophisticated techniques being used today cannot achieve a PVC content lower than 100ppm. Polyvinylchloride (PVC), easily degrades at normal processing temperatures, releasing hydrochloric acid (dechlorination) which occurs more rapidly in the presence of oxygen atmosphere [39].

During reprocessing, PET undergoes three different degradation phenomena namely: thermal, mechanical and hydrolytic chain scission. Hydrolytic chain scission is the fastest and the most dangerous process leading to a significant decrease in molecular weight and causes mechanical degradation especially when multiple step processes are applied as in recycling. A prerequisite to limit hydrolytic chain scission is the careful drying of PET before usage [17].

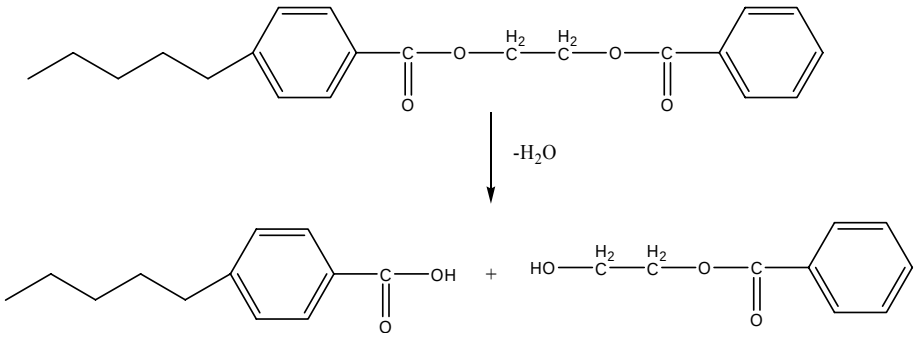

Figure 2.8 Hydrolytic chain scission of PET caused by the retained moisture [40].

Thermal degradation of PET occurs in the temperature range 290°-310°C. Degradation occurs randomly along the polymer chain, the main volatile products being terephthalic acid, acetaldehyde and carbon monoxide. At 900°C a multitude of hydrocarbons are produced, with carbon dioxide, carbon monoxide and methane as the main volatiles [17].

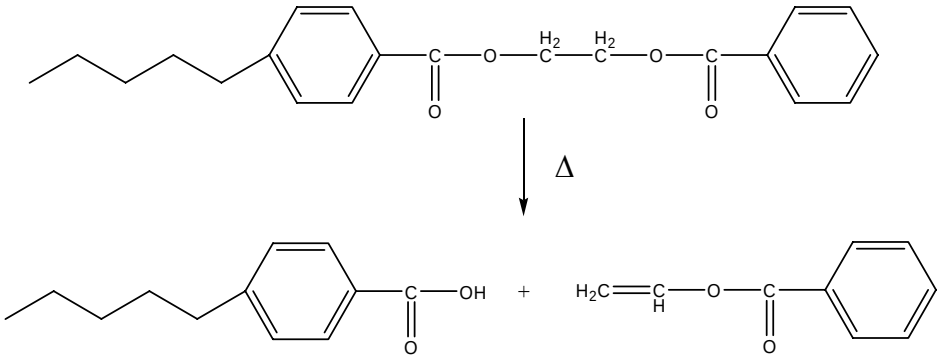

Figure 2.9 Thermal degradation of PET that occurs between 290°-310°C [40].

2.5.2 Chain Extenders

The negative effects of different types of hydrolytic and thermal degradation can be counterbalanced by the use of chain extenders. It is known that chain extenders are low molecular weight compounds that can be used to increase the MW of polymers [41]. These are polyfunctional compounds, thermally stable and capable of fast

reactions with the hydroxyl or carboxyl end groups of PET in nearly irreversible manner under normal process conditions.

2.5.2.1 Pyromellitic Dianhydride (PMDA)

Common polyester modifiers listed in the open and patent literature include polyanhydrides such as pyromellitic dianhydride (PMDA) [42]. PMDA is a tetrafunctional modifier with a melting point about 283°C close to that of PET and reacts within a few minutes in the ordinary PET processing conditions. A suggested reaction mechanism with PMDA involves as a first step linear extension through reaction of terminal polyester hydroxyl end groups with the anhydride functionalities and the formation of two carboxyl groups per incorporated moiety. Subsequent reactions may involve all functionalities of the PMDA molecule through esterification and transesterifications to yield branched or even crosslinked structures [42].

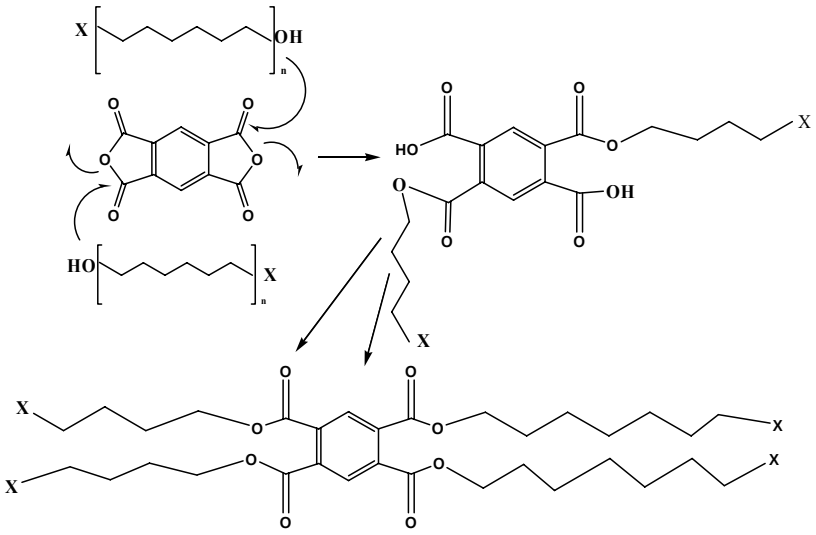

Figure 2.10 Chain extension/branching reaction of PMDA with PET.

2.5.2.2 Maleic Anhydride (MA)

Maleic anhydride (MA) is a rigid five membered ring with permanent dipole moment. It has a melting point about 55°C, and a vaporization point about 200°C being at the gaseous phase at the melting temperature of PET. During processing, the ring opening reaction takes place forming two carboxyl groups that can react with the hydroxyl end groups of PET. This suggested reaction mechanism of MA is similar to the reaction of PET and phthalic anhydride [40].

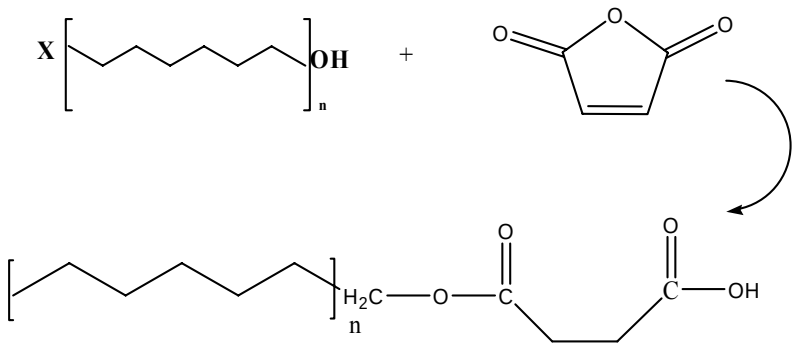

Figure 2.11 Chain extension reaction of MA with PET (Formed carboxyl groups further reacts with hydroxyl end groups of PET)

2.6 Characterization of Polymer/Clay Nanocomposites

Some standard testing methods are used in order to obtain the characteristic properties of the materials produced . The product specifications, such as mechanical properties (tensile, flexural, and impact) thermal properties (Tg, Td, Tm etc.) and morphological properties (homogeneity etc.), can be expressed using standard test methods defined by authorized foundations, like the American Society for Testing and Materials (ASTM).

2.6.1 Mechanical Tests

The mechanical properties are often the most important sources to make a decision about product specifications. The material selection for a variety of end-use

applications is mostly dependent on these properties, such as tensile strength, modulus, elongation at break and impact strength [43].

2.6.1.1 Tensile Tests (ASTM D 638-91a)

Tensile test in a broad sense is a measurement of the ability of a material to withstand forces that tend to pull it apart and to determine to what extent the material stretches before breaking [43]. The tensile strength test employs samples of a specified shape typically a dogbone.

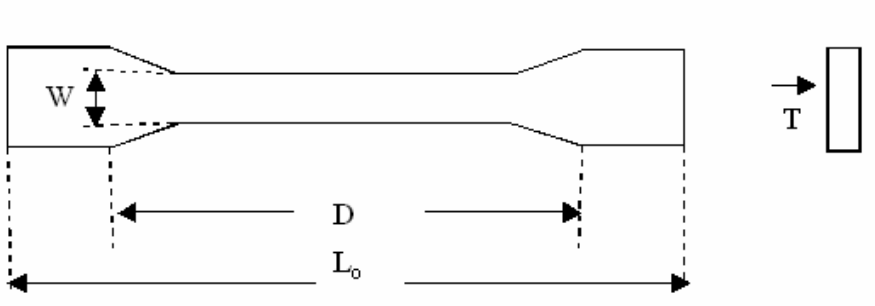

Figure 2.12 Tension test specimen

The sample is clamped at one end and pulled at a constant rate of elongation until the center of the specimen fails. Test specimen dimensions vary considerably depending on the requirements and are described in ASTM book of standards [44]. When performing tensile tests, some definitions are to be clearly comprehended.

As the specimen elongates, the resistance to the tension increases, and it is detected by a load cell. The tensile strength can be calculated by dividing the maximum load in newtons by the original minimum cross sectional area of the specimen in square millimeters, and the result can be explained in the term of mega Pascal (MPa) [43].

$$\text{Tensile Strength} = \frac{\text{Force (Load) (N)}}{\text{Cross Section Area (mm}^2\text{)}} \qquad (2.1)$$

When maximum stress occurs at the yield point it is designated as tensile strength at yield.

$$\text{Tensile Strength at Yield (MPa)} = \frac{\text{Max. Load Recorded (N)}}{\text{Cross Section Area (mm}^2\text{)}} \quad (2.2)$$

When maximum stress occurs at break it is designated as tensile strength at break.

$$\text{Tensile Strength at Break (MPa)} = \frac{\text{Load Recorded at Break}}{\text{Cross Section Area (mm}^2\text{)}} \quad (2.3)$$

Tensile modulus and elongation values are derived from the stress-strain curve. If the specimen gives a yield load larger than the load at break, percent elongation at yield is calculated; if not, percent elongation at break is calculated [44].

$$\text{Strain} = \frac{\text{Change in Length (elongation)}}{\text{Original Length (gauge length)}}$$

$$\varepsilon = \frac{\Delta L}{L} \quad (2.4)$$

$$\text{Elongation at yield} : \Delta L = \varepsilon \text{ (the value at the yield point on the x-axis)} * L \quad (2.5)$$

$$\text{Percent Elongation at yield} = \Delta L * 100 \quad (2.6)$$

In a tensile stress strain curve, values of tensile stress are plotted as ordinates against corresponding values of tensile strain as abscissas [44]. From this curve tensile modulus can be determined by extending the initial linear portion of the stress strain curve. Tensile modulus is defined as;

$$\text{Tensile Modulus} = \frac{\text{Difference in Stress}}{\text{Difference in Corresponding Strain}} \quad (2.7)$$

The result is expressed in mega Pascal [44].

2.6.1.2 Flexural Tests (ASTM D790M)

Flexural strength is the ability of the material to withstand bending forces applied perpendicular to its longiditual axis. Flexural properties are reported and calculated in terms of the maximum stress and strain that occur at the outside surface of the test bar. The machine used for tensile testing is also used for flexural testing. In a three point loading system, a bar of rectangular cross section rests on two supports and is loaded by means of a loading nose midway between the supports.

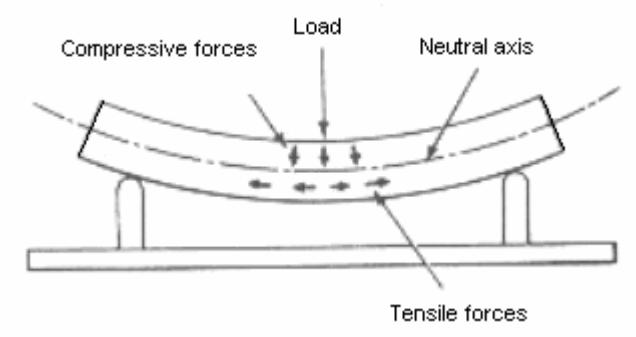

Figure 2.13 The stresses on the sample during flexural testing [43].

The maximum stress is related to the load and sample dimensions and is calculated using the following equation,

$$S = \frac{3PL}{2bd^2} \qquad (2.8)$$

where; S is the stress in the outer fibers at midspan (MPa), P is the load at a given point on the load-deflection curve (N), L is the support span (mm), b and d are the width and the depth of beam tested, respectively (mm).

The maximum strain in the outer fibers occurs at midspan is calculated as follows,

$$r = \frac{6Dd}{L^2} \qquad (2.9)$$

where; r is the maximum strain in the outer fibers (mm/mm), D is the maximum deflection of the center of the beam (mm), L is the support span (mm), and d is the depth of the sample (mm).

The modulus of elasticity is the ratio, within the elastic limit of stress to corresponding strain, and can be represented by the slope of the initial straight-line portion of the stress-strain curve, calculated as follows [45].

$$E_b = \frac{L^3 m}{4bd^3} \qquad (2.10)$$

where; Eb shows the modulus of elasticity in bending (MPa), L is the support span (mm), b and d are the width and the depth of beam tested, respectively (mm), and m is the slope of the tangent to the initial straight line portion of the load-deflection curve (N/mm).

2.6.1.3 Impact Tests (ASTM D 256)

The impact properties of polymers are related with the toughness of the material. Impact tests measure the energy required for failure when a standard specimen receives a rapid stress loading. The impact strength of a polymer can be measured by applying a number of techniques including the Izod and Charpy tests in which a weight is released, causing the specimens to be struck [47]. The energy to break values are determined from the loss in the kinetic energy of the weight [46].

One advantage of the Charpy test over an Izod test is that the specimen does not have to be clamped; therefore, it is free of variations in clamping pressures [43].

2.6.2 Differential Scanning Calorimeter (DSC) Analysis

Differential scanning calorimeter (DSC) is the most widely used thermal analysis technique. In DSC, the heat flow into or away from a reference is measured as a function of temperature or time. DSC equipment measures the heat flow by a thermal

balance between the maintaining reference and the sample by changing a current passing through the heaters under the two chambers [46]. The test procedure is simple. A small quantity of sample is weighed out into an inert capsule. The capsule is placed in the DSC sample holder. In DSC, at a transition point the sample requires either more or less energy depending on whether the change is endothermic or exothermic. For example, when the glass transition point is reached, the heat capacity increases. The midpoint is taken as the glass transition temperature [43].

2.6.3 X-Ray Diffraction (XRD) Analysis

X-Rays are electromagnetic radiation with typical photon energies in the range of 100eV-100keV. Because the wavelength of X-Rays is comparable to the size of atoms, they are ideally suited for probing the structural arrangement of atoms and molecules in a wide range of materials. The energetic X-Rays can penetrate deep into the materials and provide information about the molecular structure [1]. X-Rays are produced generally by X-Ray tubes. XRD relies on Bragg's Law,

$$n\lambda = 2d\sin\theta \qquad (2.11)$$

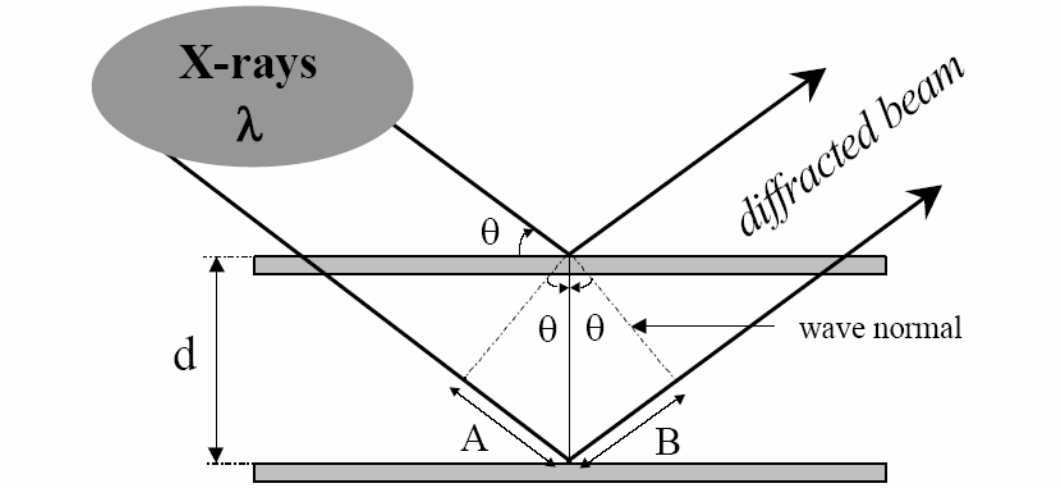

Figure 2.14 Principle of X-Ray Diffraction [1]

During XRD, the scattering angle theta is measured. The order of diffraction peak, "n", can be any positive integer. The "d" value is to be determined so the only

variable needed to be controlled is the wavelength of the X-Rays. Wavelength is controlled by the target used to create the beam. The peaks in a XRD pattern are directly related to the atomic distances. If the atoms are arranged in a periodic fashion, as in crystals, the diffracted waves will consist of sharp peaks with the same symmetry as in the distribution of atoms. When talking of nanocomposites, XRD results yield peaks only for intercalated structures. General to say, XRD is a quite versatile method as it does not damage the specimen and a small area of the sample is adequate for measurement. The results from XRD measurements provide direct information on the atomic-level spacing of crystal planes within the lattice of the sample [1].

2.6.4 Scanning Electron Microscopy (SEM)

The scanning electron microscope (SEM) is a microscope that uses electrons rather light to form an image. The combination of higher magnification, larger depth of focus, greater resolution and ease of sample observation makes the SEM one of the most heavily used instruments in research areas today. By scanning and electron cascade across a specimen, high resolution 3D images of morphology with high magnifications can be obtained. In the case of nanocomposites, no peaks are observed in X-Ray analysis (XRD) in their disordered state due to lack in structural observation of the layers having large d-spacings. Thus in such cases, scanning electron microscopy (SEM) yields more accurate results than XRD analysis in characterization [48]. Therefore, the use of XRD and SEM methods yield the best result for morphological properties in testing such structures.

2.6.5 Melt Flow Index (MFI) Test

The melt index is not an intrinsic or fundamental property of a polymer. It is rather a conventional property of a polymer for expressing important flow characteristics [49]. The melt index, also known as melt flow rate, test measures the rate of extrusion of a thermoplastic material through an orifice of standard diameter under prescribed conditions of temperature and load [43]. The weight of the material

extruded during the specified time is the melt index expressed in grams per ten minutes.

2.7 Previous Studies

Pegoretti et al. [50] prepared nanocomposites of recycled PET with various amounts of Cloisite 25A and non-modified natural montmorillonite by melt intercalation. Cloisite 25A dispersed better in PET compared to Cloisite Na+. Both clays increased the young's modulus of R-PET composites; Cloisite 25A however is more effective in the improvement of mechanical properties. Also both clays have improvement on the dimensional stability of the composites in contrast to the neat R-PET.

Solis et al. [51] mixed PET with clay by an extrusion process. MA and pentaerythrytol were added to provide compatibility between clay and the matrix. Thermal, mechanical and rheological properties of the nanocomposites were evaluated. The nanocomposites with additives revealed improved mechanical strength, also viscoelastic properties decreased with rising particle concentration. The novel materials possess convenience in processing and performance improvements.

Incarnato et al. [41] studied the effect of PMDA on the molecular structure (molecular weight and molecular weight distribution) and on the rheological and thermal properties of PET industrial scraps coming from a PET processing plant. They observed that PMDA is an effective chain extender in the reactive extrusion of PET and by selecting the appropriate processing conditions and controlling the PMDA amount, structural changes can occur to obtain polyester with predetermined properties. The GPC, rheological and thermal results revealed that with an amount of PMDA included between 0.5 and 0.75 weight %, the chain extension reaction produces an increase of molecular weight and broadening of molecular weight distribution and branching phenomena.

Ke et al. [52] investigated the crystallization process and crystal morphology of PET-clay nanoscale composites prepared by intercalation, followed by in-situ polymerization. The materials were characterized by scanning electron microscopy (SEM), transmission electronic microscopy (TEM), dynamic scanning calorimetry (DSC), and X-Ray techniques, together with mechanical methods. They observed exfoliated clay particles play a nucleating role and have strong interactions with PET molecular chains. The nano-PET properties were enhanced a lot compared with the neat resin.

Yılmazer et al. [42] studied the effects of PMDA and a diepoxide with terminal epoxy end groups on the melt flow, die swell and viscoelastic properties using an intensive batch mixer. Chain extended/branched PET's were characterized by their low MFI, high die swell, high viscosity, high shear sensitivity, pronounced non-newtonian behavior and high storage modulus. The modified resins were more elastic making them more conducive to low density foaming.

Paci et al. [35] investigated the behavior of R-PET when treated in a melt mixer, in order to better understand the processing conditions that can reduce or avoid the hydrolytic chain scission. They observed that PET processed in humid conditions and air undergoes dramatic degradation. It sis understood that the extent to which degradation takes place might be limited by carefully pre-drying the material before processing.

Spinace et al. [34] studied the effects of repeated extrusion cycles on the properties of commercial PET, used in the production of soft drink bottles, in five processing cycles. PET pellets were reprocessed in a single screw extruder and cut into pellets. The rheological, mechanical and thermal properties were investigated for characterization. A significant change in mechanical properties and crystallinity degree was observed after three processing cycles. After two extrusion cycles an increase in mechanical properties was observed and the material could be used again for applications where virgin PET is usually employed. In addition, after five cycles

the samples were thermally stable, however mechanochemical degradation was observed after five cycles.

Torres et al. [36] focused on the effects of diisocyanates, bisoxazolines and diepoxides on the molecular weight, intrinsic viscosity and mechanical properties of recycled PET. Diisocyanates showed to be more reactive toward the end groups of virgin PET. PET reacted with diisocyanates have high molecular weight and intrinsic viscosity compared to that of virgin PET. Also, by the addition of isocyanates, they observed that elongation at break increased dramatically.

CHAPTER III

EXPERIMENTAL

3.1 Materials

3.1.1 Chain Extenders (Anhydrides)

Maleic Anhydride (MA) and Pyromellitic Dianhydride (PMDA) chain extenders were purchased from Sigma-Aldrich Co. Ltd. in the powder form. Some relevant properties of MA and PMDA are listed in Table 3.1 and Table 3.2 respectively.

Table 3.1 Physical Properties of Maleic Anhydride

Purity (%)	99
Melting Point (°C)	54-56
Boiling Point (°C)	200

Table 3.2 Physical Properties of Pyromellitic Dianhydride

Purity (%)	99
Melting Point (°C)	284-286

3.1.2 Organoclay

Experiments were carried out with organically modified montmorillonite (Cloisite 25A), produced by Southern Clay Products. The organic modifier is a quaternary alkyl ammonium salt. The thermo gravimetric behavior, TGA diagram, of Cloisite

25A can be seen in Appendix D. Some significant properties of Cloisite 25A, obtained from the manufacturer are shown in Table 3.3.

Table 3.3 Properties of Cloisite 25A

Organic Modifier *	2MHTL8
Cation Exchange Capacity (CEC)	95 meq/100g clay
% Moisture	< 2%
% Weight Loss on Ignition	34%
Density, g/cc	1.87

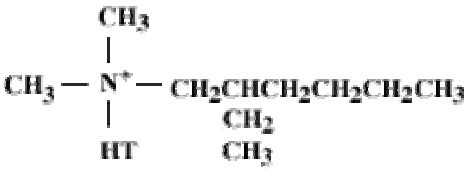

Figure 3.1 Chemical structure of alkyl ammonium cation
Where HT is Hydrogenated Tallow (~65% C18; ~30% C16; ~5% C14)

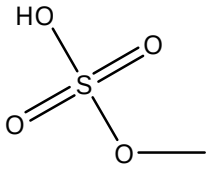

methyl sulfate

Figure 3.2 Chemical structure of methyl sulfate anion

* 2MHTL8: dimethyl, hydrogenated tallow, 2-ethylhexyl quaternary ammonium

Typical Dry Particle Sizes: (microns, by volume)

10% less than: 2μ; 50% less than: 6μ; 90% less than: 13μ

X Ray Results: d_{001} = 18.6Å

3.1.3 Recycled PET Resin (R-PET)

PET soft drink bottle regrind was purchased from DupontSA Company in the form of flakes. General physical properties of the used PET are as follows, as specified by DupontSA.

Table 3.4 Properties of PET Resin

Contaminants (ppm)	PVC	60
	Polyethylene	5
	Metal pieces	0
	Adhesive	10
	Paper pieces	3
Lighting Characteristics	Value L, Shining	66.1
	Value B, Yellowness	2.6
	Value A, Redness	-2.0
Material Properties	Intrinsic Viscosity, [η]	0.750 g/cm.s
	Glass Transition Temperature, T_g	60 ºC
	Melting Temperature, T_m	255 ºC – 260 ºC

3.2 Experimental Procedure

3.2.1 Extrusion of R-PET, Organoclay and Chain Extenders

The nanocomposites were prepared in two extrusion steps. In the first run, 3 % Cloisite25A and 97% R-PET containing nanocomposites were prepared by melt mixing in a co-rotating twin screw extruder (Thermoprism TSE 16 TC, L\D = 25). Prior to processing, R-PET resin was dried for 12 hours in a vacuum oven at 150 ^{o}C to prevent degradation by retained moisture. The organoclay, capable of absorbing moisture, was also dried for 4 hours at 120 ^{o}C. The R-PET pellets were fed from the

main-feeder, and Cloisite25A was fed from the side-feeder. The feed rate of R-PET was 25 g/min, and to obtain the desired composition, feed rate of the side feeder was calibrated. The ingredients were fed into the extruder barrel at a constant screw speed of 350 rpm, as the previous studies indicate better dispersion characteristics at this speed [53]. Throughout the study, barrel zone temperatures were kept constant at 285, 285, 285, 250 ^{o}C in melting, mixing, metering, and feeding sections, respectively. The die temperature was also kept constant at 290 ^{o}C in the extrusion process. Molten nanocomposite exiting from the die of the extruder was water cooled and pelletized.

In the second run, the chain extenders Maleic Anhydride and Pyromellitic Dianhydride were added to the nanocomposites prepared in the first extrusion process. Pellets of nanocomposites were dried for 12 hours in a vacuum oven at 150 ^{o}C to prevent degradation by retained moisture. Prior to processing, nanocomposites were ground to smaller particle size and mixed with the chain extender. The 0.5%, 0.75% and 1% (by weight) MA or PMDA containing batches were fed at a rate of 25 g/min through the secondary feeder to the twin-screw extruder. Three different screw speeds, 75, 150, 350 rpm, were chosen to see the effects of screw speed. Other process parameters were set as stated earlier. The prepared pellets of composites were injection molded to prepare specimens for characterization. Materials were vacuum dried for 4 hours at 120 ^{o}C before the injection molding process to avoid the effects of moisture.

3.2.2 Sample Preparation

Injection Molding

The specimens for mechanical characterization experiments were molded by using a laboratory scale injection-molding machine (Microinjector, Daca Instruments). Figure 3.3 is the schematic view of the injection molding machine. The composites were injection molded at the injection nozzle temperature of 280 ^{o}C and at the mold temperature of 18 ^{o}C. The preparation of each specimen lasted about 3.5 minutes

including 30 sec for filling the barrel and 3 min for melting. During the process, the injection pressure was kept at 8 bars. Parameters of injection molding process (barrel temperature, mold temperature, injection pressure) were kept constant throughout the experiments.

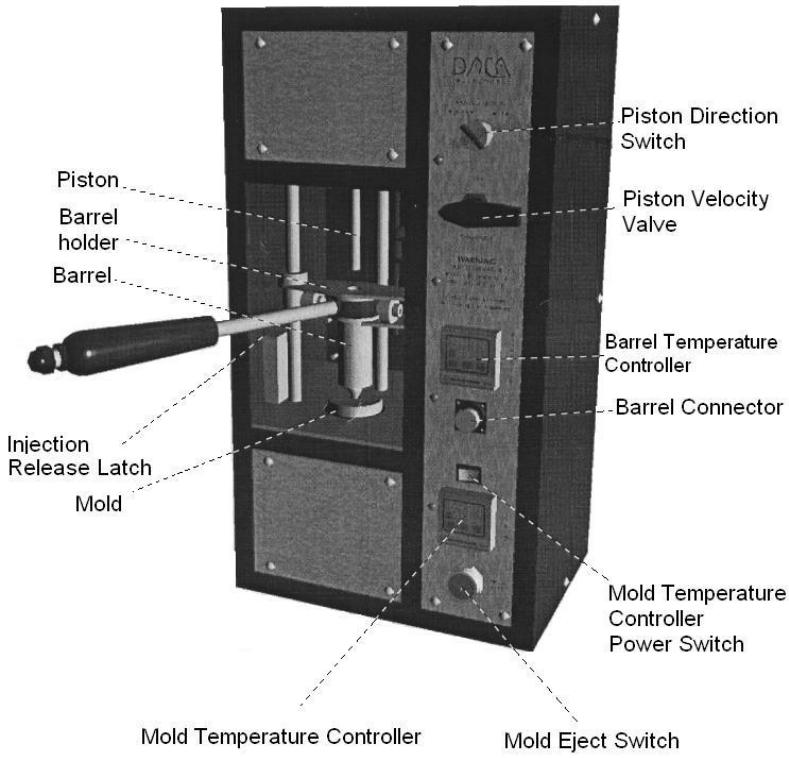

Figure 3.3 Schematic representation of the injection molding machine

In the preparation of the composite materials, the following steps shown in Figure 3.4 were carried out.

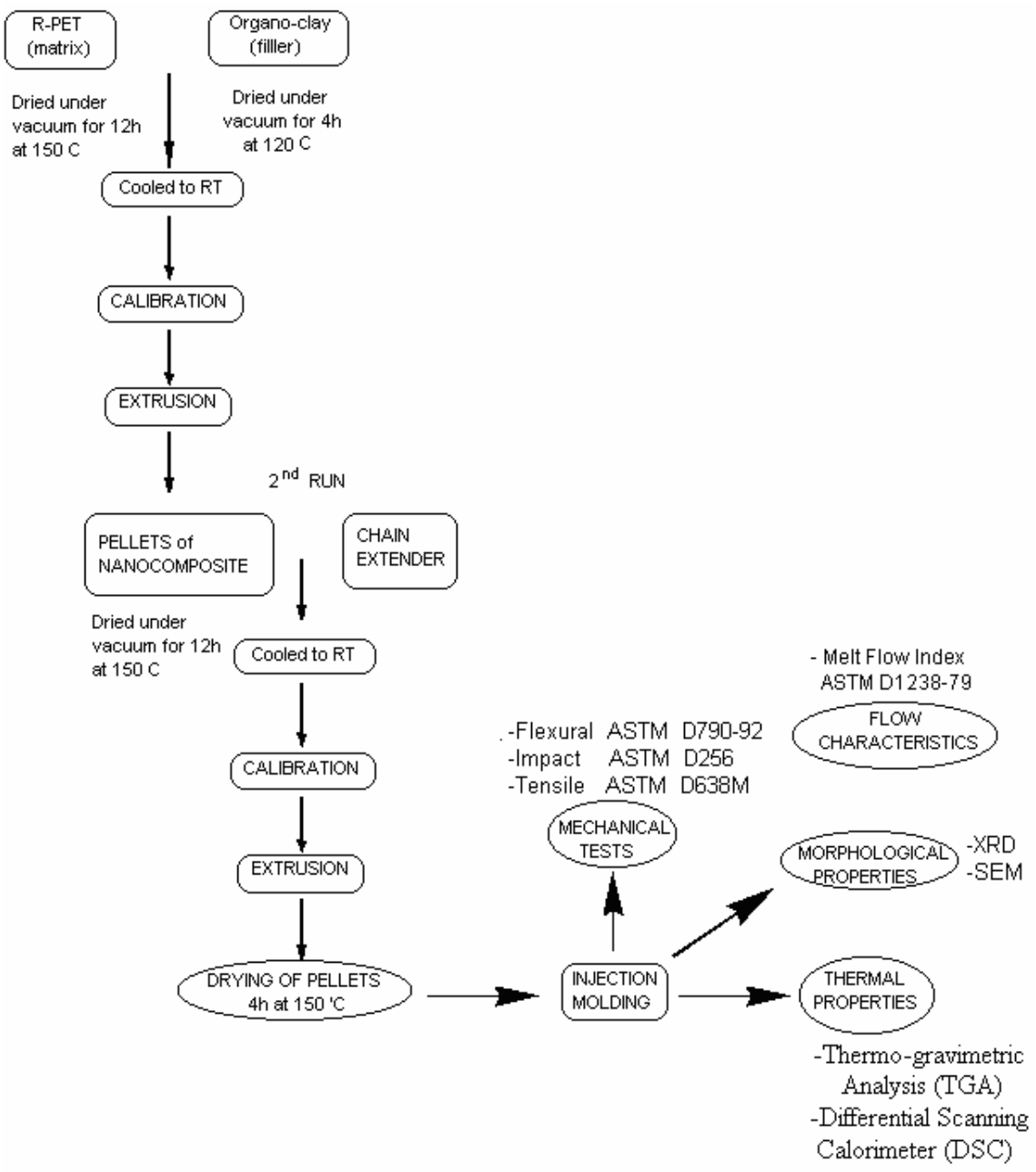

Figure 3.4 Flowchart of composite specimen preparation, and characterization methods used

3.3 Characterization of Specimens

In order to observe the effects of chain extenders, organoclay contents and screw speed on the final properties of the composites morphological, mechanical and thermal properties of the samples were characterized.

3.3.1 Morphological Analysis

3.3.1.1 Scanning Electron Microscopy (SEM) Analysis

A low voltage SEM (JEOL JSM-6400) was used to analyze the impact fracture surfaces of the composites to observe the effects of organoclay content, chain extender content and processing conditions on the morphology of the composites. The fracture surfaces of impact samples were coated with a thin layer of gold before SEM to provide conductive surfaces. The SEM photographs were taken at x250 and x3500 magnifications.

3.3.1.2 X-Ray Analysis

The nanocomposites were analyzed by using a Philips PW3710 based X-Ray diffractometer. Diffractometer, equipped with Cu anode radiation source operated at a generator tension of 40 kV and a generator current of 55 mA. The diffraction patterns were collected at a diffraction angle 2θ from 1° to 10° at a scanning rate and step size of 3°/min and 0.02°, respectively.

3.3.2 Mechanical Tests

All mechanical tests were performed at room temperature. At least seven samples were tested and the average results with the standard deviations are reported for each type of composite.

3.3.2.1 Tensile Tests

Tensile tests were performed according to ASTM 638-M 91a (Standard Test Method for Tensile Properties of Plastics) by using a Lloyd 30K Universal Testing Machine. The shape and dimensions conformed to Type M-I. The shape and dimensions of the specimens are given in Figure 3.5 and Table 3.5. The crosshead speed of 8mm/min giving a strain rate of 0.1 min^{-1} was calculated by using the corresponding dimensions from the method given in the ASTM. Tensile strength, Young's modulus, and strain at break values were calculated.

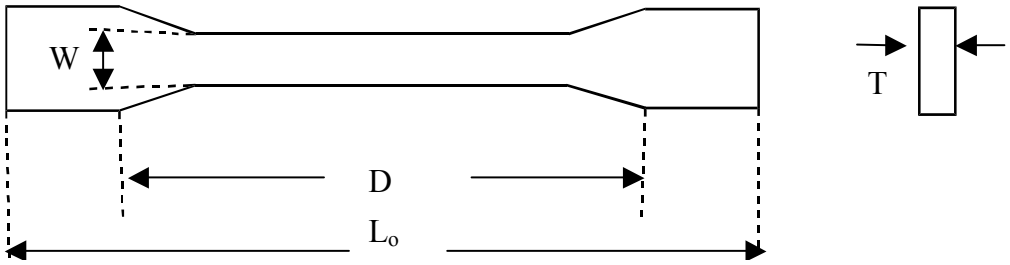

Figure 3.5 Tensile Test Specimen (Type M-I)

Table 3.5 Tensile test specimen dimensions

Symbol, Term	Dimensions (mm)
D- Distance between Grips	80
L_o - Length Overall	112
W- Width of Narrow Section	7.50
T- Thickness	2.00

3.3.2.2 Impact Tests

Charpy impact test was performed by using a Pendulum Impact Tester of Coesfeld Material Test; according to the test Method-I Procedure A in ASTM D256-91a (Standard Test Method for Impact Resistance of Plastics). Unnotched samples had dimensions of 50x7.50x2.00 mm, respectively.

3.3.2.3 Flexural Tests

Three-point bending tests were applied according to Test Method-I Procedure A of ASTM D790M-92 (Standard Test Methods for Flexural Properties of Unreinforced and Reinforced Plastics and Electrical Insulating Materials) on rectangular specimens. Dimensions were 80x7.50x2.00 mm as given in Table 3.5. Three point bending was conducted. The support span and the rate of crosshead motion were 50 mm, and 2.08 mm/min, respectively. This corresponds to a strain rate of 0.01 min^{-1}. Strength, strain at break, and modulus properties were studied.

3.3.3 Differential Scanning Calorimeter (DSC) Analysis

Differential scanning calorimeter (DSC) analyses were performed on the fractured pieces of the samples using a General V4.1.C DuPont 2000. Measurements were carried out in the temperature range of 20-280 ^{o}C with 20 ^{o}C/min heating rate under nitrogen atmosphere. Changes in T_g and T_m values were observed.

3.3.4 Melt Flow Index (MFI) Test

Melt flow index (MFI) test was performed according to ASTM Standards, ASTM D 1238-79, Condition type T, with pellets of the samples using a Omega Melt Flow Indexer. Measurements were carried out with a load of 2.16 kg at 250 ^{o}C, for both the barrel and the die. The method was based on determining the weight, in grams, of the sample that passes through a die in 10 min. Changes in melt flow index values were evaluated for each composition and screw speed.

CHAPTER IV

RESULTS AND DISCUSSION

4.1 Morphological Analysis

4.1.1 X-RAY Analysis

XRD analysis is a convenient method for examining the crystal structure of the nanocomposites. Table 4.1 shows the basal spacings observed in the nanocomposites prepared. The X-Ray figures are given in Appendix C.

During the analysis, the starting angle is set to 2θ = 1° to see the d-spacings greater than 40 Å, which occurs below 2θ = 2°. If the starting was used as 2θ = 2° in the analysis, the d-spacing greater than 35 Å would not appear in the diffraction pattern and a false conclusion implying complete exfoliation may be drawn.

The interaction between clay and PET matrix can be demonstrated by the enlargement of the interlamellar distance. Generally, the greater the interlamellar distance, the greater the interaction of R-PET chains with clay layers. However, the amount of clay particles intercalated can not be determined from the XRD patterns.

Organically modified montmorillonite, Cloisite 25A, showed a strong peak with a characteristic interlayer spacing of about 19.2 Å (Figure C.1 in Appendix C). After processing with the polymer, however, the interlayer spacing increased to about 28.8-34.41 Å, indicating intercalation of the clay. Also, there is another peak seen around 2θ = 5.5° with a basal spacing around 15.5 Å. This peak belongs to the unintercalated organoclay. The basal spacing collapsed from 19.21 Å to 15.5 Å due to the high temperature of the processing. This is an expected result. The alkyl chains

in the interlayer rearrange in such a way that the interlayer distance decreases due to the breakup of electrostatic interaction between modifier ammonium and negative charge of silicate surface [54].

Organoclay content did not change the interlamellar distance. In repeated cycles, the d-spacing did not change; nevertheless the amount of intercalated organoclay may have changed.

The parameters PMDA and MA content, as well as the screw speed did not change the interlamellar distance. Supported by the given results, it can be concluded that the d-spacing of the nanocomposites is mainly dependent on the compatibility of the matrix and the clay surface. The obtained results, however are not sufficient to make statement about the intercalated amount of clay.

Table 4.1 XRD results of Cloisite 25A and polymer-Cloisite25A nanocomposites

Specifications	2 theta	d-spacing
Cloisite 25A	4.59	19.21
R-PET-2%25Asingleextr	2.57	34.34
	5.69	15.50
R-PET-3%25Asingleextr	2.70	32.69
	5.69	15.51
R-PET-4%25Asingleextr	2.56	34.41
	5.36	16.47
R-PET-3%25Adoubleextr	2.77	31.86
	5.79	15.23
R-PET3%25A-1%PMDA350	2.87	30.70
	5.44	16.21
R-PET-3%25A-1%PMDA150	2.66	33.18
	5.52	15.98
R-PET-3%25A-1%PMDA75	3.06	28.80
	5.90	14.96
R-PET-3%25A-0.75%PMDA350	2.74	32.15
	5.59	15.79
R-PET-3%25A-0.5%PMDA350	2.81	31.36
	5.64	15.65
R-PET-3%25A-1%MA350	2.86	30.86
	5.67	15.57
R-PET-3%25A-1%MA150	2.88	30.59
	5.68	15.53
R-PET-3%25A-1%MA75	2.74	32.21
	5.77	15.30
R-PET-3%25A-0.75%MA350	2.78	31.69
	5.68	15.53
R-PET-3%25A-0.5%MA350	2.84	31.08
	5.50	16.04
R-PET-1%MA-3%25A350	2.59	34.01
	5.91	14.92

4.1.2 Scanning Electron Microscopy (SEM) Analysis

In order to examine the relationship between the morphological structure and the fracture mechanism, impact fracture surfaces of various anhydride modified nanocomposites were analyzed using a Scanning Electron Microscopy (SEM).

Figure 4.1 shows the fracture surfaces of the pellets of amorphous unprocessed PET (APET), single extruded recycled PET and 3 weight percent Cloisite 25A containing nanocomposite. These are the samples used as reference materials for comparison to the other nanocomposites. The surface of unprocessed amorphous PET is very smooth and the crack propagation lines can easily be seen on the micrograph (a). In micrograph (b), the effect of extrusion on the fracture mechanism of R-PET can be seen. The difference may be due to the heterogeneous nature of the structure. The crack propagation lines are closer and shorter with respect to APET that may lead to higher impact resistance. In micrograph (c) the effect of organoclay on the fracture mechanism of R-PET can be seen. The surface roughness indicates that the cracks propagate along a more tortuous pathway that prevents easy crack propagation [1].

Figure 4.2 shows the fracture surfaces of R-PET containing 2, 3 and 4 weight percents of Cloisite 25A, a, b, and c, respectively, at 350 rpm. At x250 magnification, micrographs of 2 and 3 weight % organoclay containing nanocomposites look similar. However at x3500 magnification, the crack propagation lines of 2 weight % organoclay containing nanocomposite can clearly be seen, whereas 3 weight % organoclay containing nanocomposite has more tortuous structure. At x250 magnification, micrograph of 4 weight % organoclay containing nanocomposite looks more tortuous than the others. However, at 4 weight %, unintercalated clay particles form agglomerates due to high loading. The agglomerates can clearly be seen on the micrograph (c). These agglomerates act as stress concentrator in the structure that decreases impact strength. At 3 weight % organoclay content, optimized structure may be accomplished with better dispersion of organoclay that leads to an effective interaction area.

Figure 4.3 shows the effect of PMDA content on the fracture surfaces of 3 weight % Cloisite25A containing nanocomposites, at 350 rpm. The effect of increasing molecular weight and branching should be considered to analyze the micrographs. The molecular weight has two different effects; primarily the diffusion of smaller chains into the sheets of the organoclay is easier than diffusion of larger chains. However, high molecular weight systems, owing to higher melt viscosities, transfer more stress or energy to achieve separation of platelets [55]. Since the organoclay is added to the R-PET in first extrusion and PMDA is added after the diffusion mechanism, higher molecular weights attained should lead to better dispersion. At x3500 magnification, micrographs of 0.5, 075 and 1 weight % PMDA containing nanocomposites look similar however at x250 magnification micrograph of 0.5 weight % PMDA containing nanocomposite shows more tortuous path with smaller distances between crack propagation lines leading to higher stress absorbance, possibly due to the highly branched structure or higher molecular weight attained.

Figure 4.4 shows the effect of MA content on the fracture surfaces of 3 weight % Cloisite25A containing nanocomposites, at 350 rpm. At 0.5 % MA content, micrographs of x250 and x3500 magnifications show a smoother surface than the other compositions indicating lower impact strength. At x250 magnification, micrographs of 0.75 and 1 weight % MA containing nanocomposites look similar. However at x3500 magnification, the crack propagation lines of 0.75 weight % organoclay containing nanocomposite can clearly be seen, whereas 1 weight % organoclay containing nanocomposite has more tortuous structure.

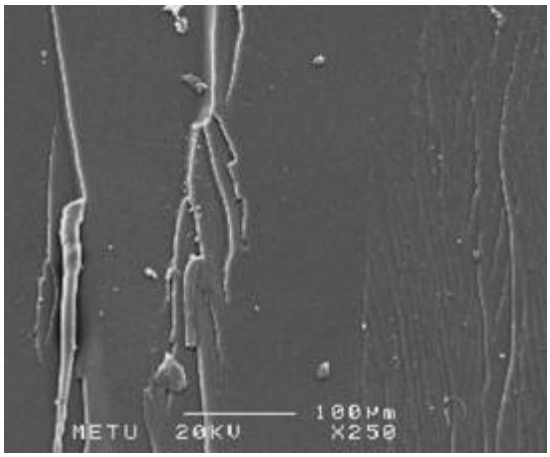

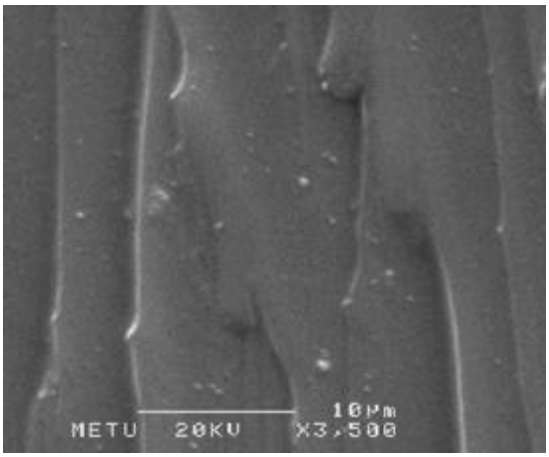

APETp-250 APETp-3500 (a)

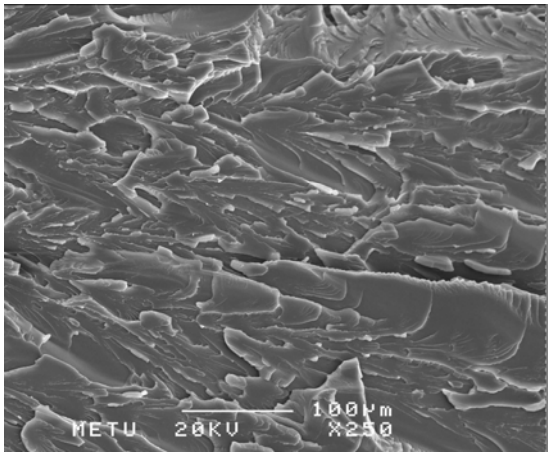

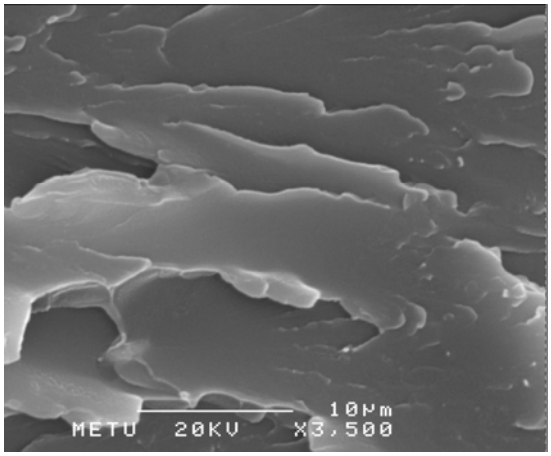

R-PETsingleextr-250 R-PETsingleextr-3500 (b)

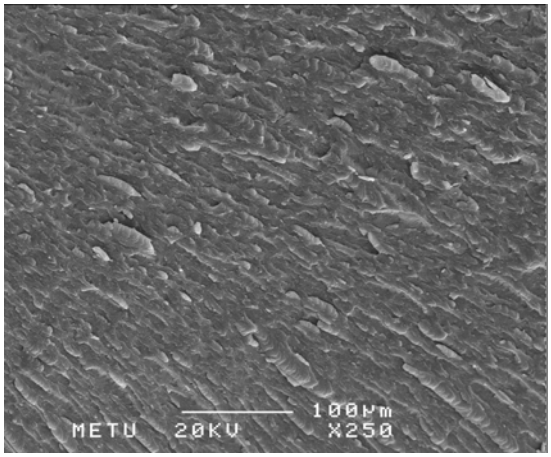

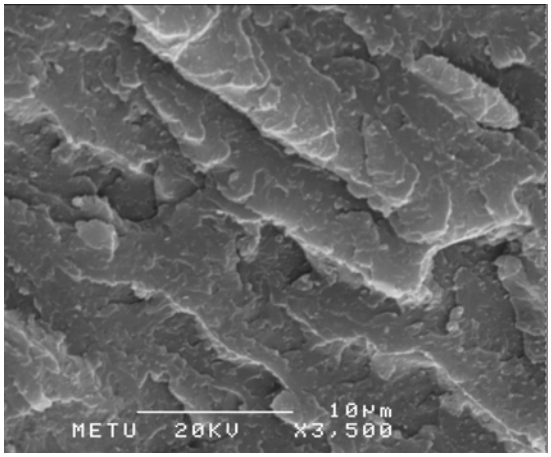

R-PET-3%25Adoubleextr350-250 R-PET-3%25Adoubleextr350-3500 (c)

Figure 4.1 Fracture surfaces of amorphous PET (a) in the form of unprocessed pellets, single extruded R-PET (b) and double extruded 3% Cloisite25A containing nanocomposite at 350 rpm (c).

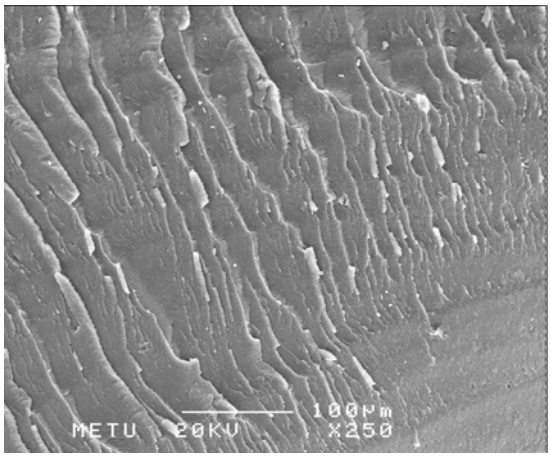

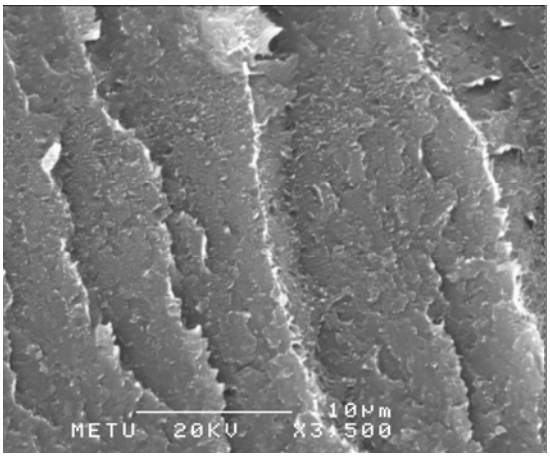

R-PET-2%25A350-250 R-PET-2%25A350-3500 (a)

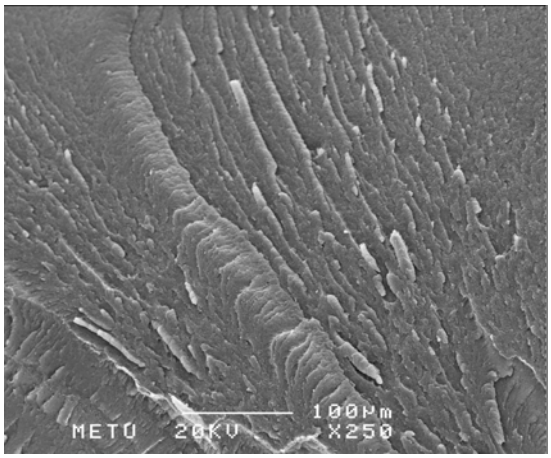

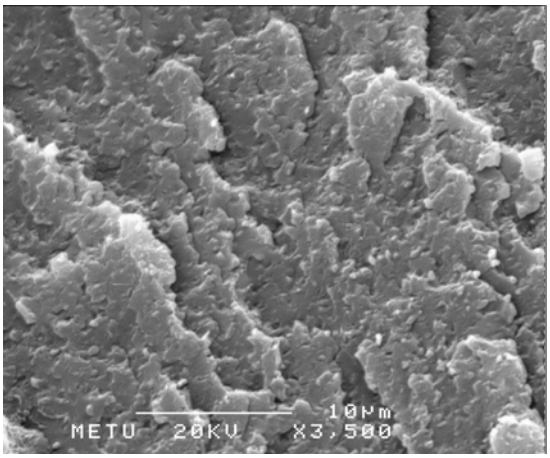

R-PET-3%25A350-250 R-PET-3%25A350-3500 (b)

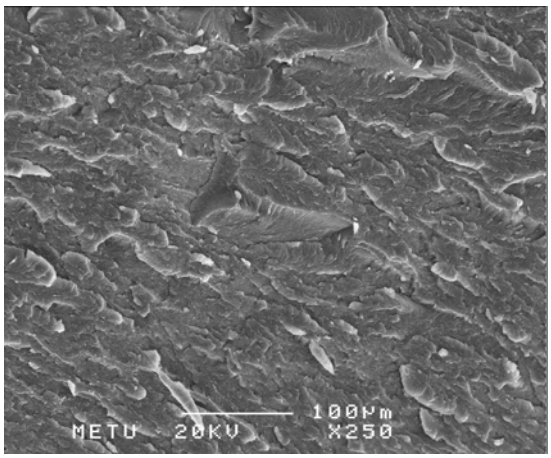

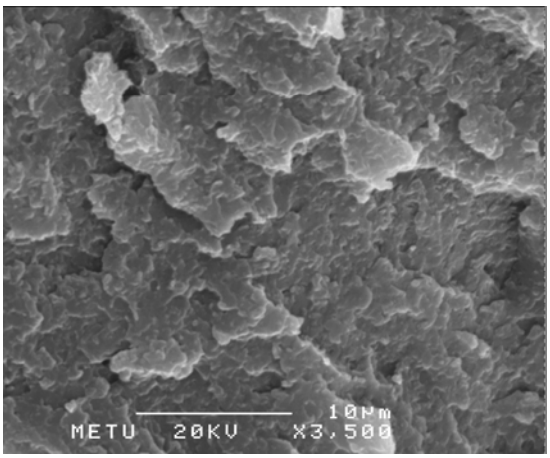

R-PET-4%25A350-250 R-PET-4%25A350-3500 (c)

Figure 4.2 Fracture surfaces of R-PET containing 2, 3 and 4 weight percent of Cloisite 25A, a, b, and c, respectively, at 350 rpm.

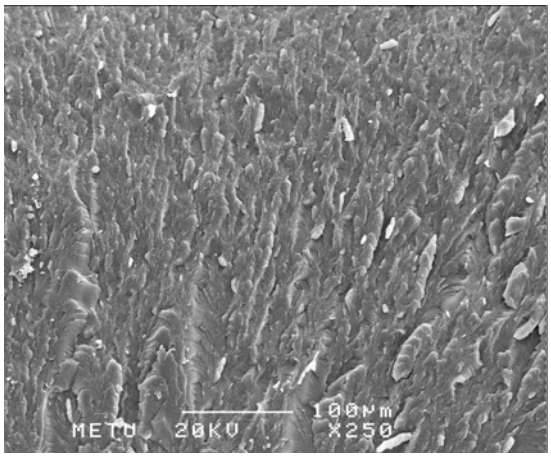

R-PET3%25A-0.5%PMDA350-250

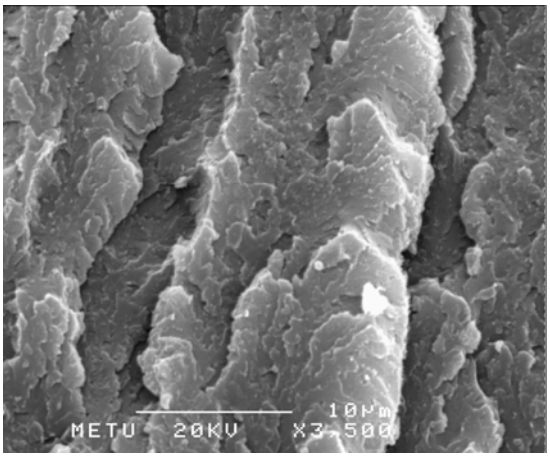

R-PET3%25A-0.5%PMDA350-3500 (a)

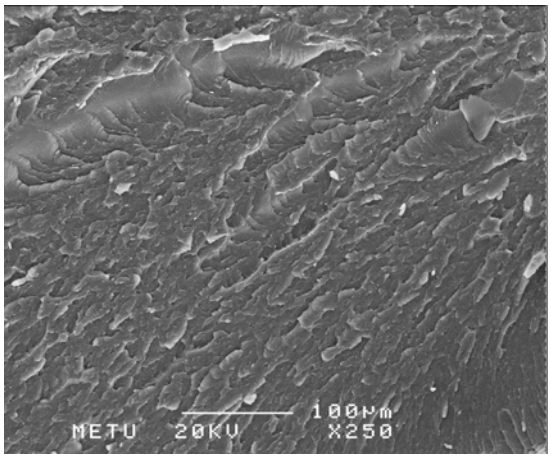

R-PET3%25A-0.75%PMDA350-250

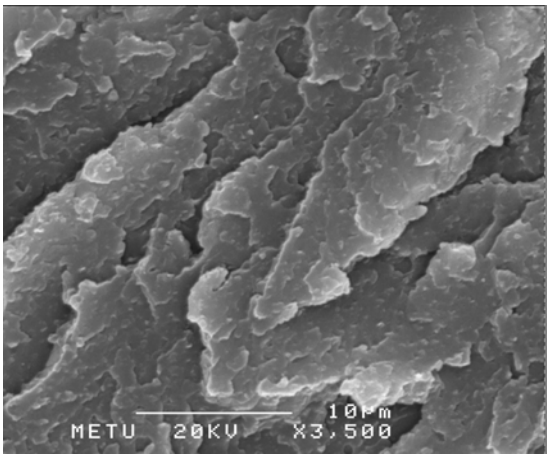

R-PET3%25A-0.75%PMDA350-3500 (b)

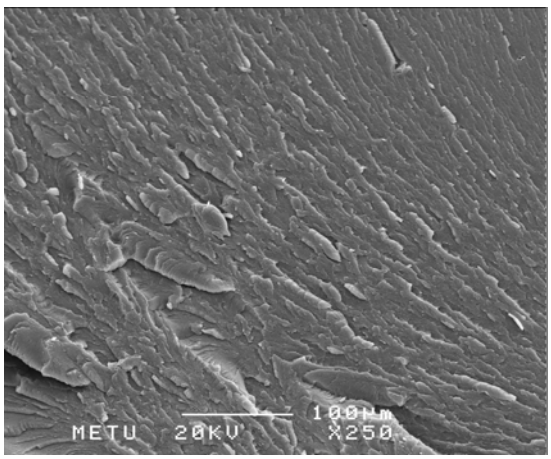

R-PET3%25A-1%PMDA350-250

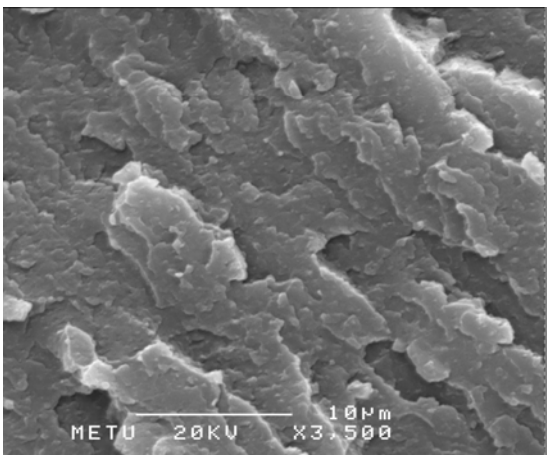

R-PET3%25A-1%PMDA350-3500 (c)

Figure 4.3 Fracture surfaces of 0.5, 0.75 and 1 weight percent MA added 3 % Cloisite 25A containing nanocomposites, a, b, and c, respectively, at 350 rpm.

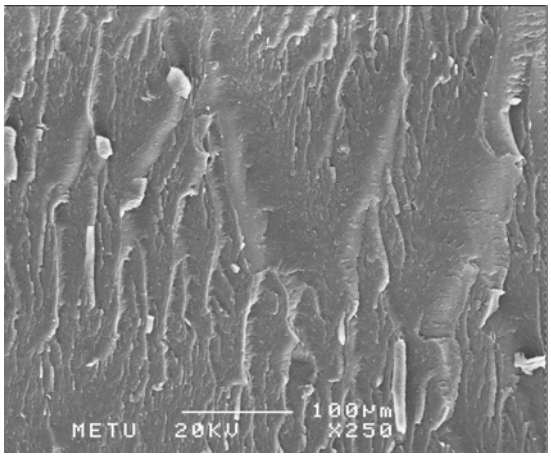

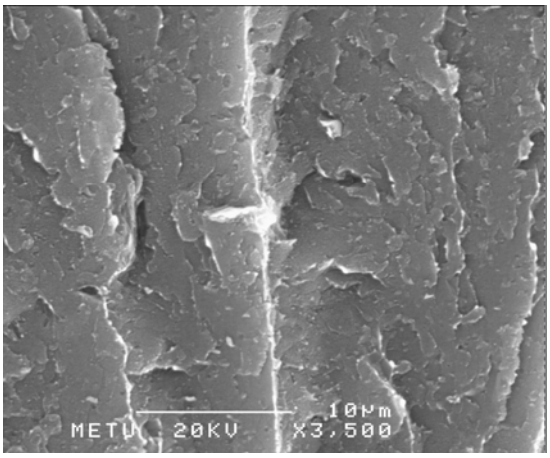

R-PET3%25A-0.5%MA350-250 R-PET3%25A-0.5%MA350-3500 (a)

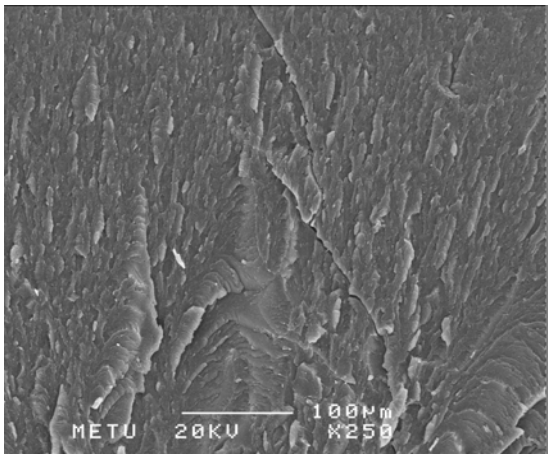

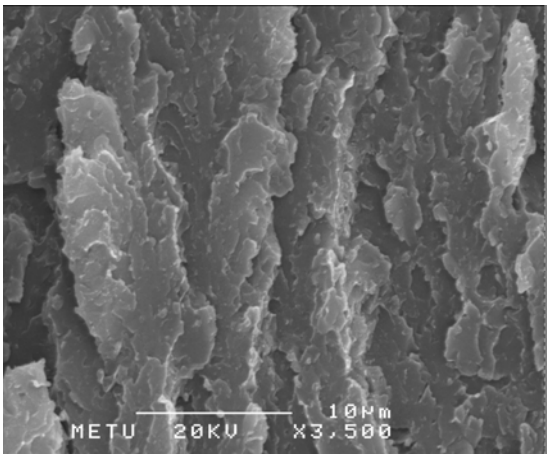

R-PET3%25A-0.75%MA350-250 R-PET3%25A-0.75%MA350-3500 (b)

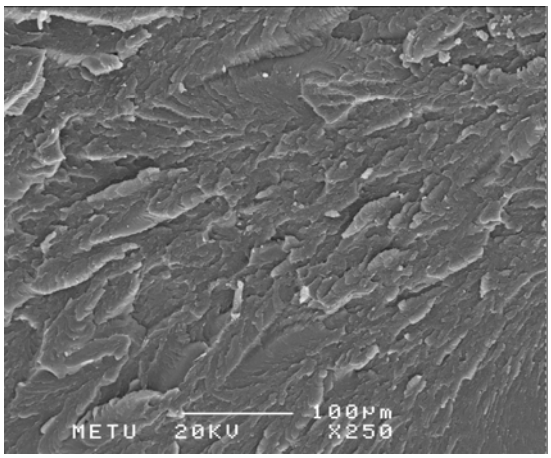

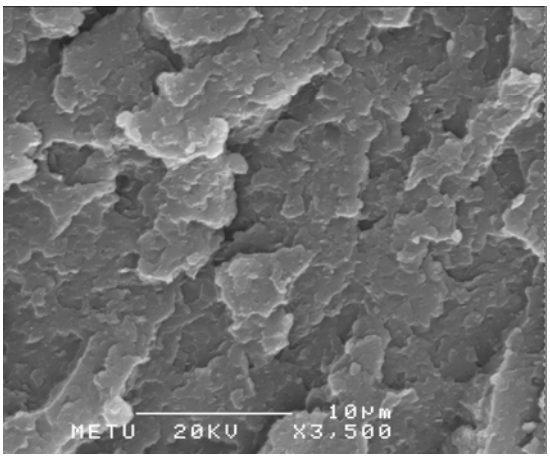

R-PET3%25A-1%MA350-250 R-PET3%25A-1%MA350-3500 (c)

Figure 4.4 Fracture surfaces of 0.5, 0.75 and 1 weight percent PMDA added 3 % Cloisite 25A containing nanocomposites, a, b, and c, respectively, at 350 rpm.

4.2 Mechanical Analysis

4.2.1 Effect of Extrusion Cycle on the Mechanical Properties of Recycled PET

In order to examine the effects of extrusion cycle on the mechanical properties of recycled PET, tensile, flexural and impact tests were performed. This feature is illustrated in Figures 4.5 through 4.12.

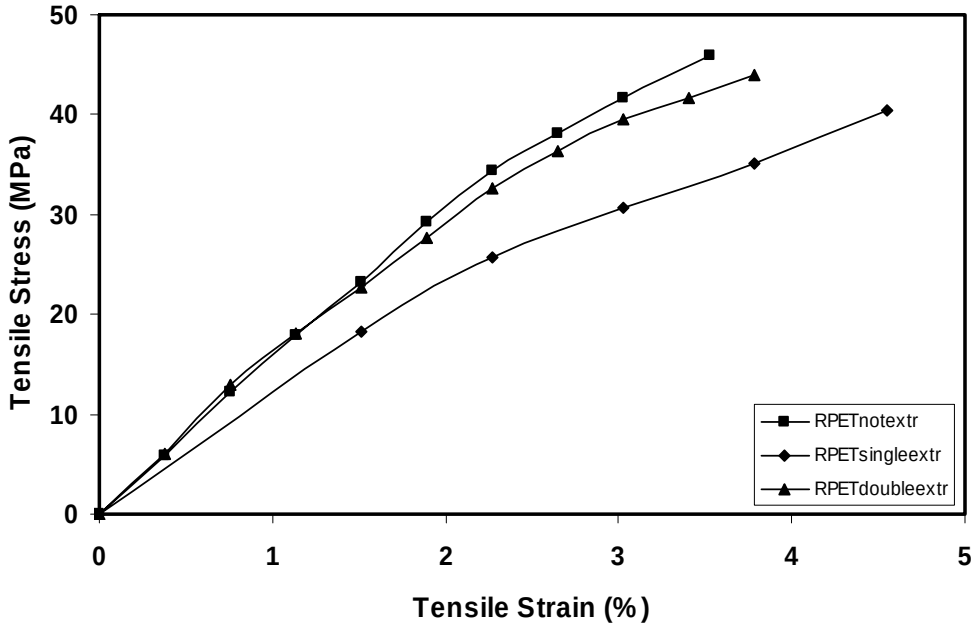

Figure 4.5 Effect of repeated extrusion cycles on tensile stress-strain behavior of pure R-PET

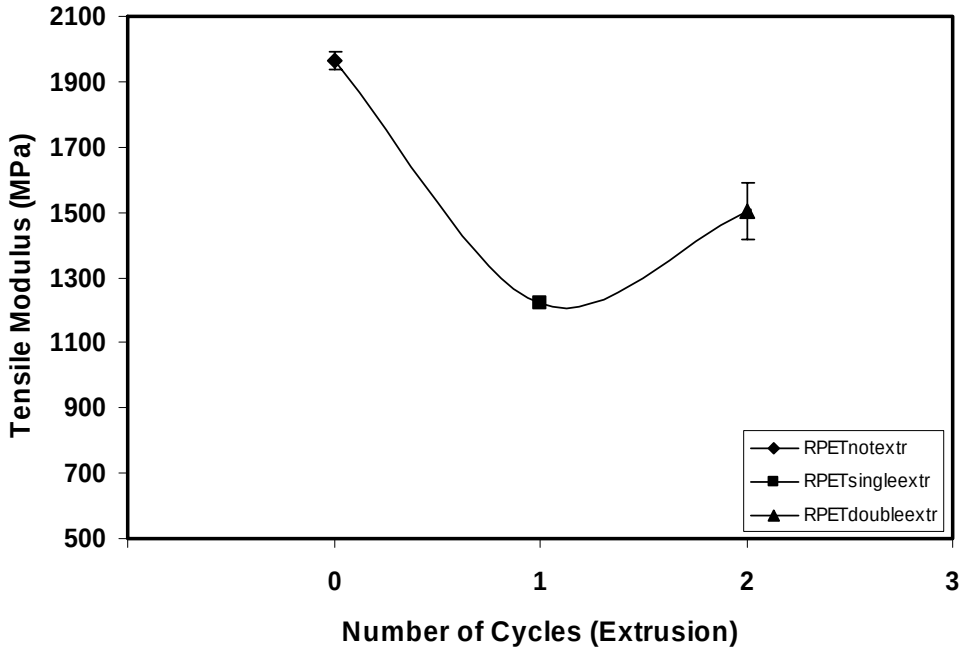

Figure 4.6 Effect of repeated extrusion cycles on Young's modulus of pure R-PET

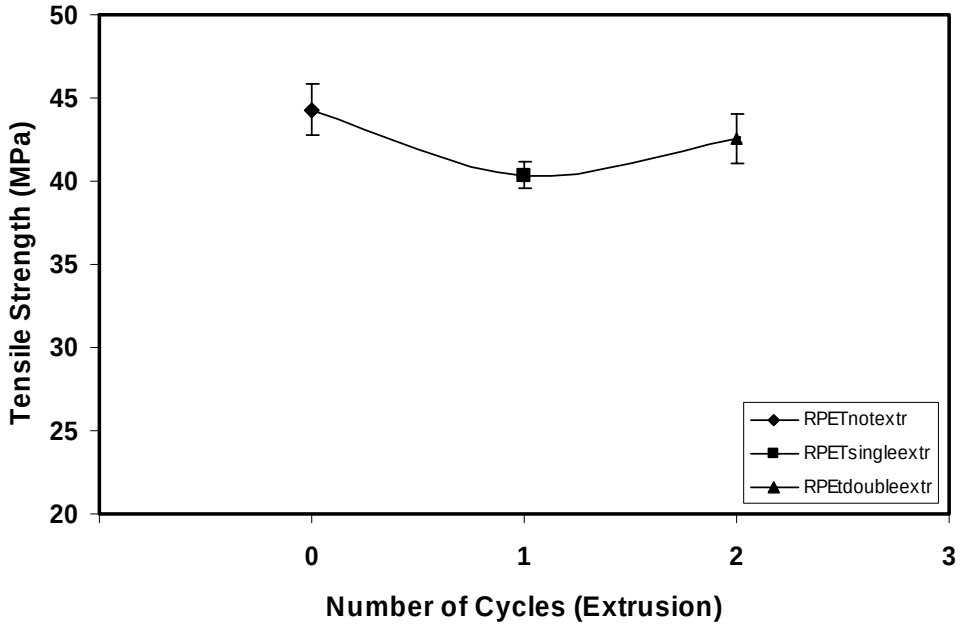

Figure 4.7 Effect of repeated extrusion cycles on tensile strength of pure R-PET

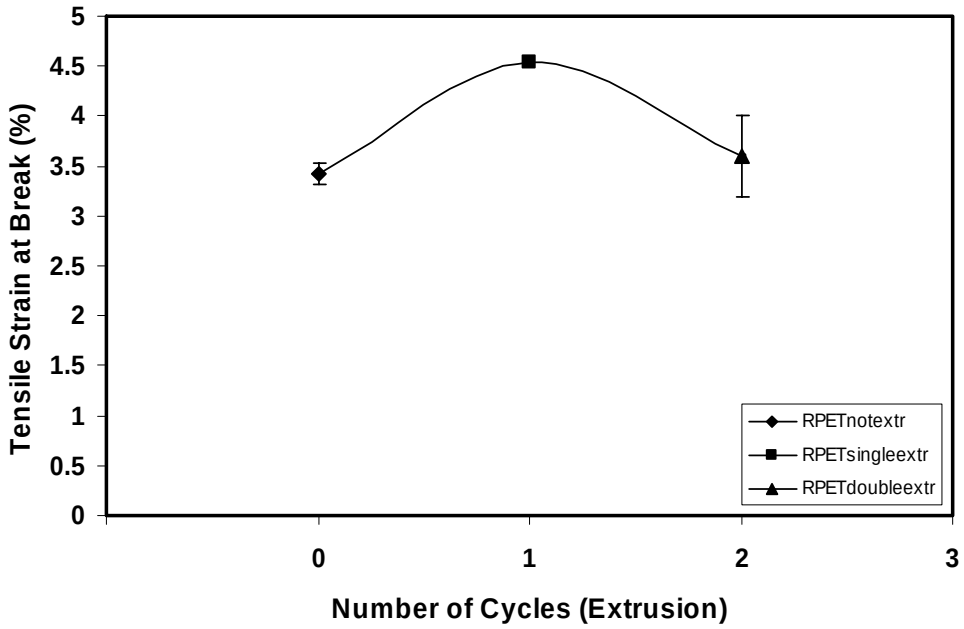

Figure 4.8 Effect of repeated extrusion cycles on tensile strain at break of pure R-PET

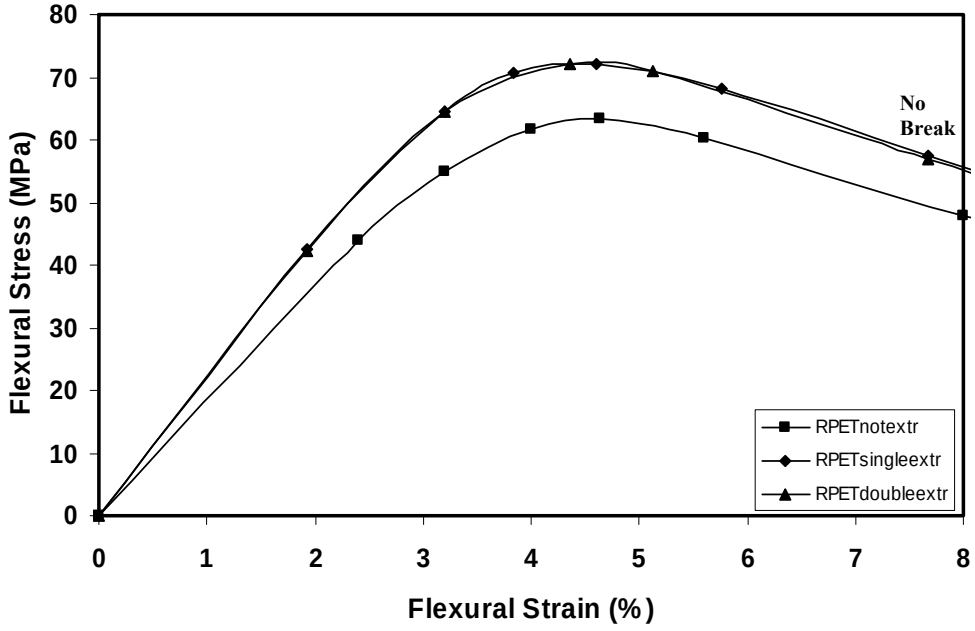

Figure 4.9 Effect of repeated extrusion cycles on flexural stress-strain behavior of pure R-PET

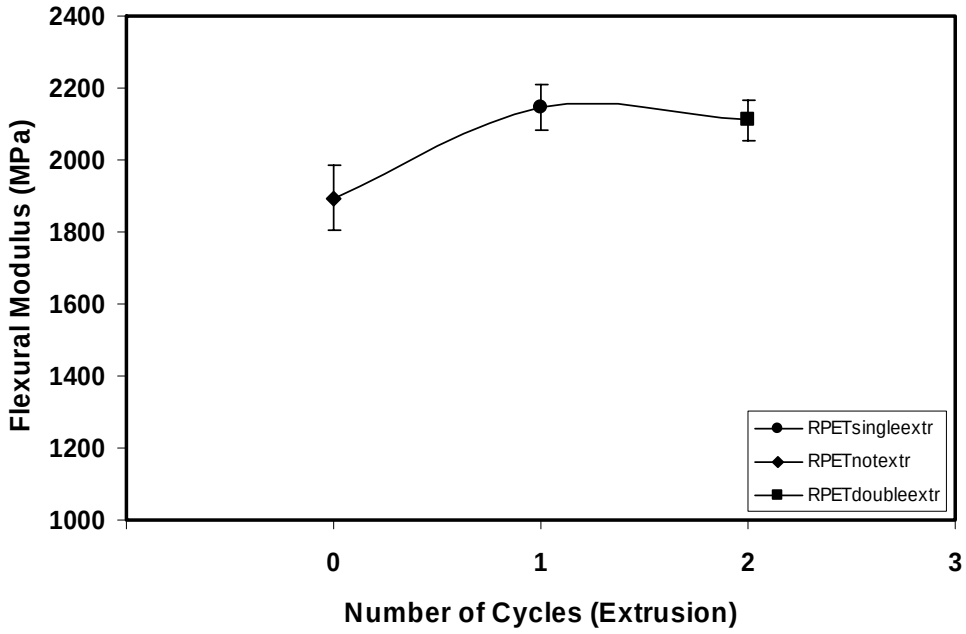

Figure 4.10 Effect of repeated extrusion cycles on flexural modulus of pure R-PET

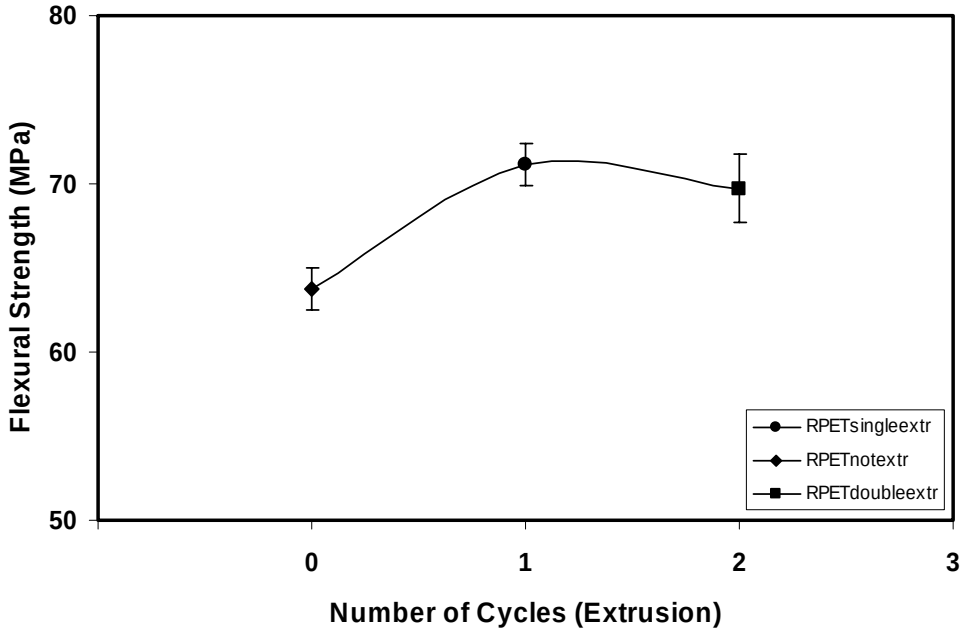

Figure 4.11 Effect of repeated extrusion cycles on flexural strength of pure R-PET

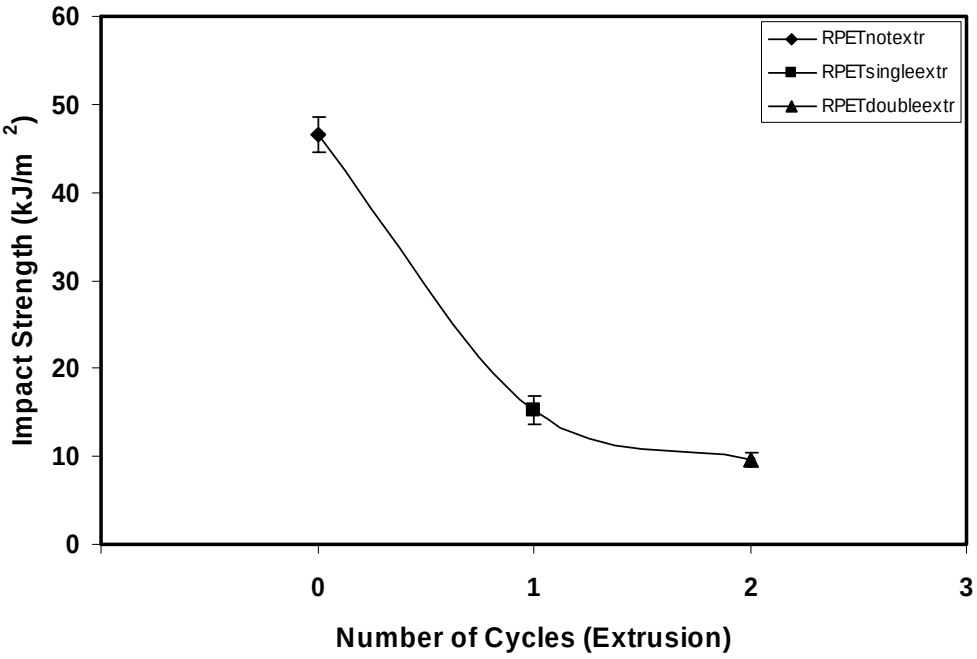

Figure 4.12 Effect of repeated extrusion cycles on impact strength of pure R-PET

Figure 4.5 displays the mentioned degradation behavior of R-PET in repeated extrusion cycles. After repeated extrusion higher strain at break, lower modulus and strength values are observed. This indicates that the molecular weight is lower after the extrusion due to the thermo-mechanical degradations. In general, a higher molecular weight increases modulus and strength due to the formation of more entanglements and secondary bonding. Higher molecular weight implies longer polymer chains and longer polymer chains imply more entanglements and secondary bonding that tend to keep the molecular chains associated together [56]. There is a slight increase in the properties after the first cycle owing to the possible completion of uncompleted polycondensation reactions at high temperatures leading to an increase in molecular weight.

Effect of repeated extrusion cycles on Young's modulus of pure R-PET is seen in Figure 4.6. The modulus or stiffness of a polymer is a function of intermolecular forces. Since molecular weight directly affects the secondary forces, lower modulus is observed after repeated extrusion.

Figure 4.7 shows the effect of repeated extrusion cycles on the tensile strength of pure R-PET. Entanglement and other intermolecular attractions have a strong effect on tensile strength. After extrusion, lower molecular weight polymers having greater number of chain ends per unit volume are obtained. These chain ends act as imperfections in the structure which have adverse effect on strength properties [46].

As seen in Figure 4.8, tensile strain at break values tend to increase in repeated cycles. At higher molecular weights, secondary forces dominate over the primary intramolecular forces and also at higher molecular weights more entanglements are formed that resists sliding over each other. Thereby chain slippage is prevented at higher molecular weights, and that makes lower molecular weight polymers more extensible [56].

Figure 4.9 shows the effect of repeated cycles on the flexural stress-strain behavior of pure R-PET. Flexural strength shows similar trend to tensile strength, as explained earlier in Figure 4.7. However, owing to the nature of the flexural tests, strength values are greater than those of tensile samples. In flexural testing, the upper half of specimens is in compression while the lower half is in tension. Thus, cracks cannot easily propagate towards the compression side. The compressive stresses tend to close the cracks rather than opening them leading to ductile behavior and higher strength [56]. Therefore, higher flexural modulus, flexural strength is observed in flexural tests as seen in Figures 4.9 - 4.11. Also, the flexural specimens did not break in flexural tests.

Figure 4.12 shows the effect repeated cycles on the impact strength of pure R-PET. Impact toughness depends on the ability of the material to absorb energy through vibrating and minor movements rather than resisting input forces. If the material can not move, impact energy will be concentrated in one area and rupture will occur. Long chains, however, mean that the energy can be transmitted along the chain and shared over more atoms [49]. As expected, decreased impact strengths are observed after extrusion since the molecular weight is decreased. Also, the stress-strain curves

are an indication of the toughness of a material. The tendency of stress-strain curves and impact strength are related.

4.2.2 Effect of Clay Content on the Mechanical Properties of the Nanocomposites

In order to examine the effects of organoclay content on the mechanical properties of nanocomposites, tensile, flexural and impact tests were performed. This feature is illustrated in Figures 4.13 through 4.21.

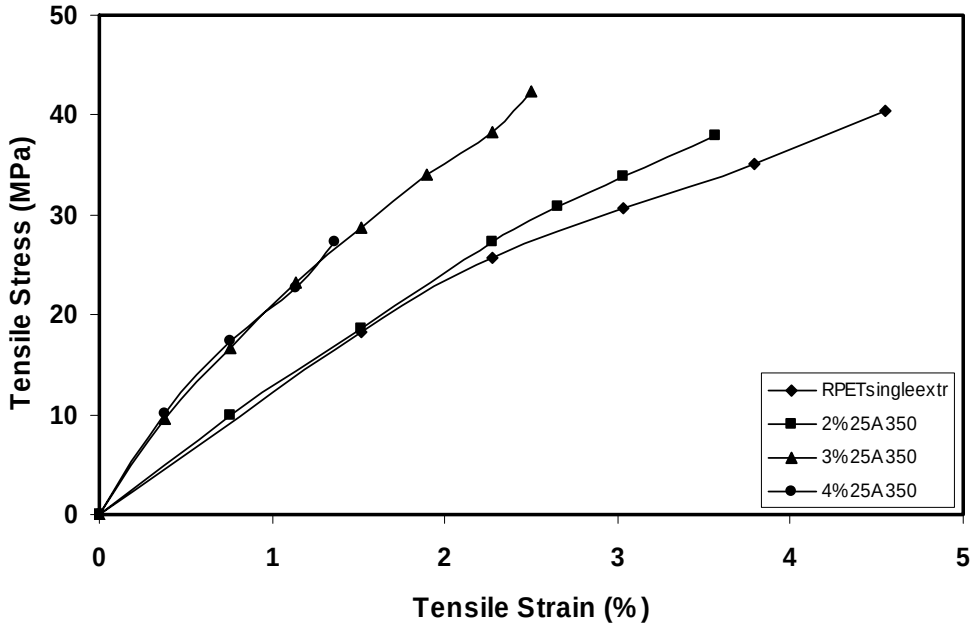

Figure 4.13 Effect of organoclay content on tensile stress-strain behavior of nanocomposites

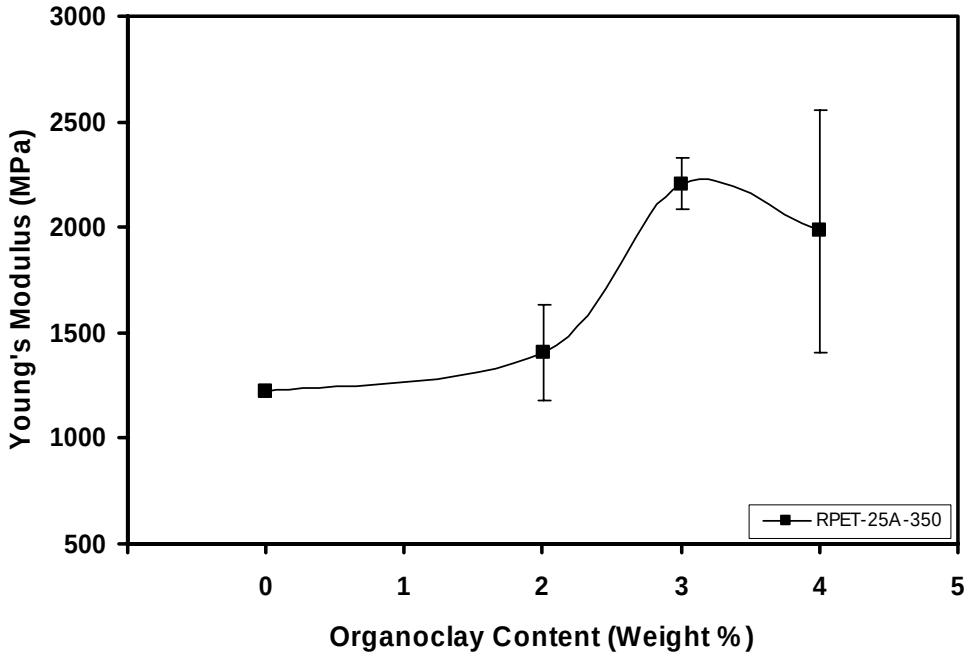

Figure 4.14 Effect of organoclay content on Young's modulus of nanocomposites

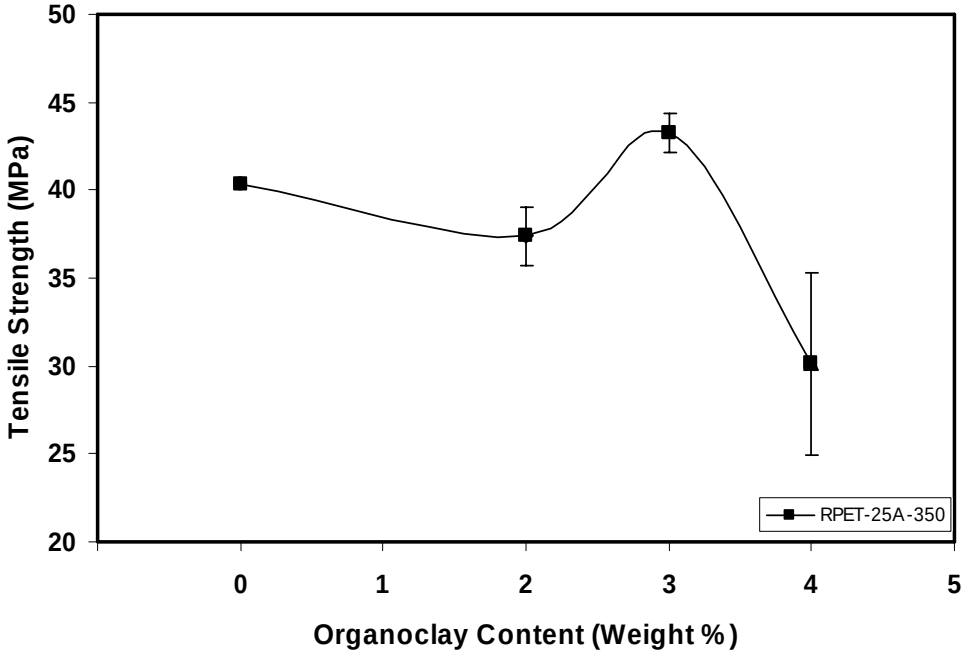

Figure 4.15 Effect of organoclay content on tensile strength of nanocomposites

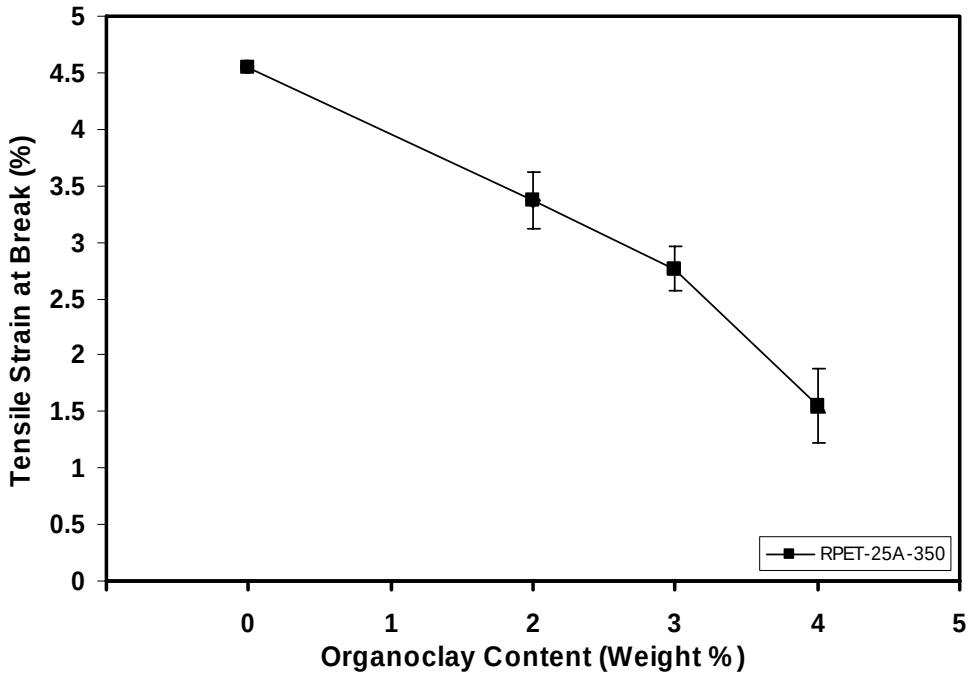

Figure 4.16 Effect of organoclay content on tensile strain at break of nanocomposites

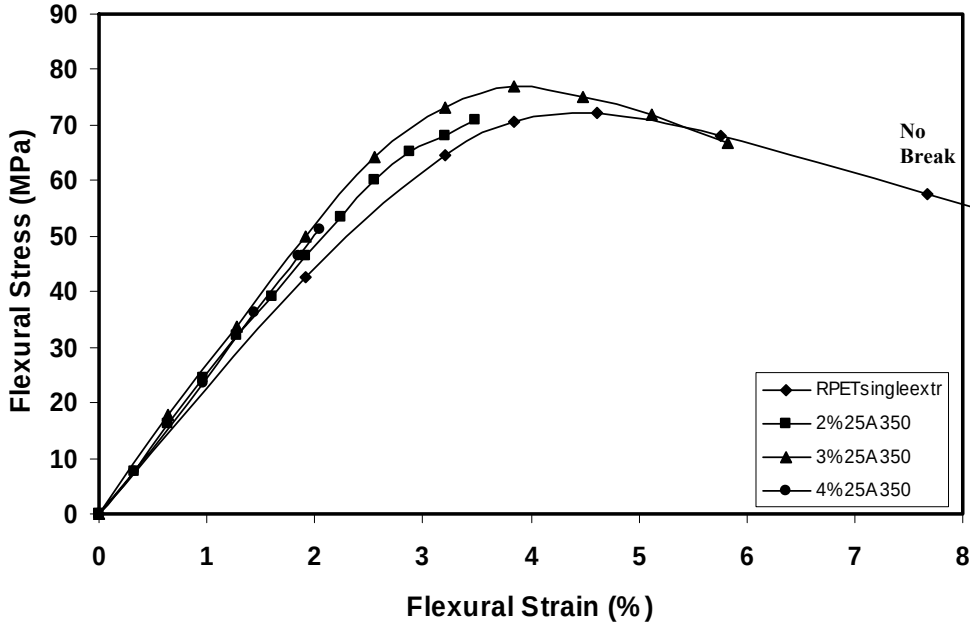

Figure 4.17 Effect of organoclay content on flexural stress-strain behavior of nanocomposites

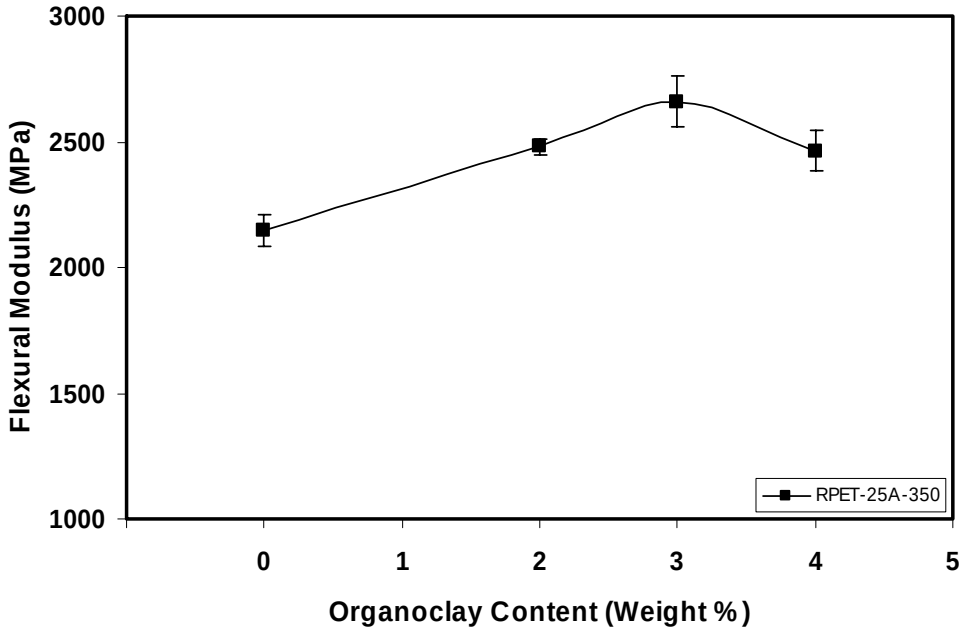

Figure 4.18 Effect of organoclay content on flexural modulus of nanocomposites

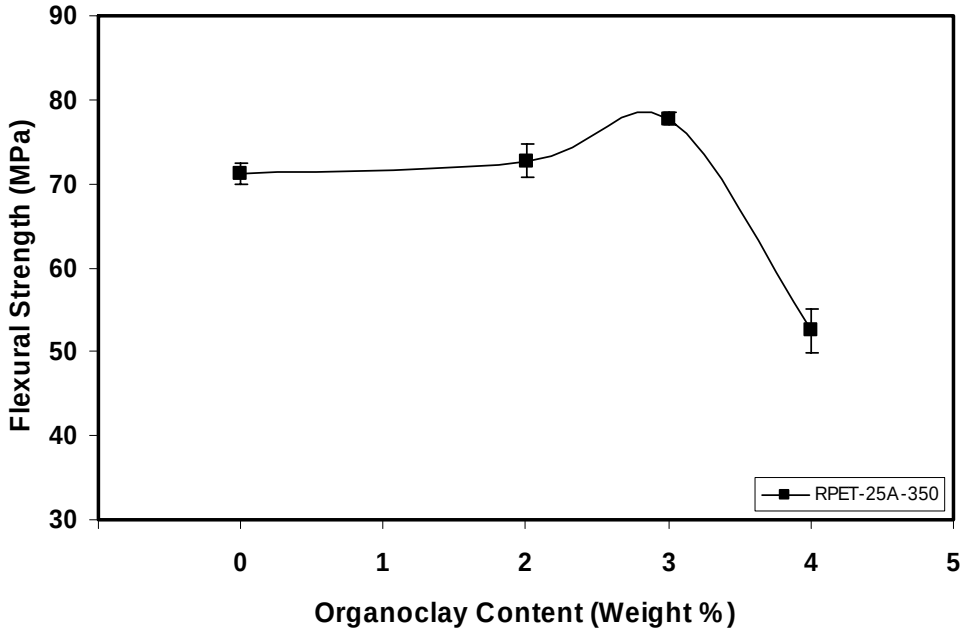

Figure 4.19 Effect of organoclay content on flexural strength of nanocomposites

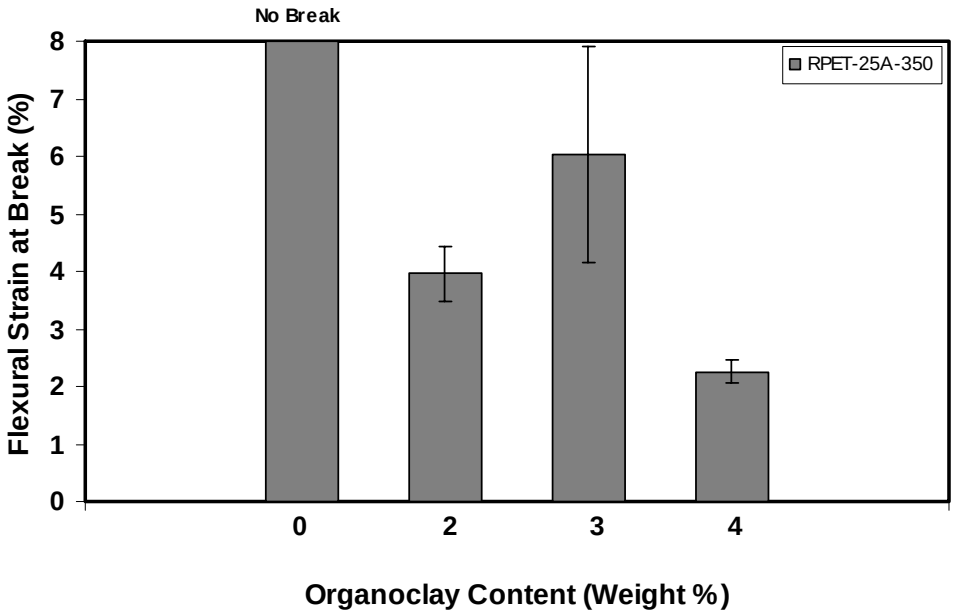

Figure 4.20 Effect of organoclay content on flexural strain at break of nanocomposites

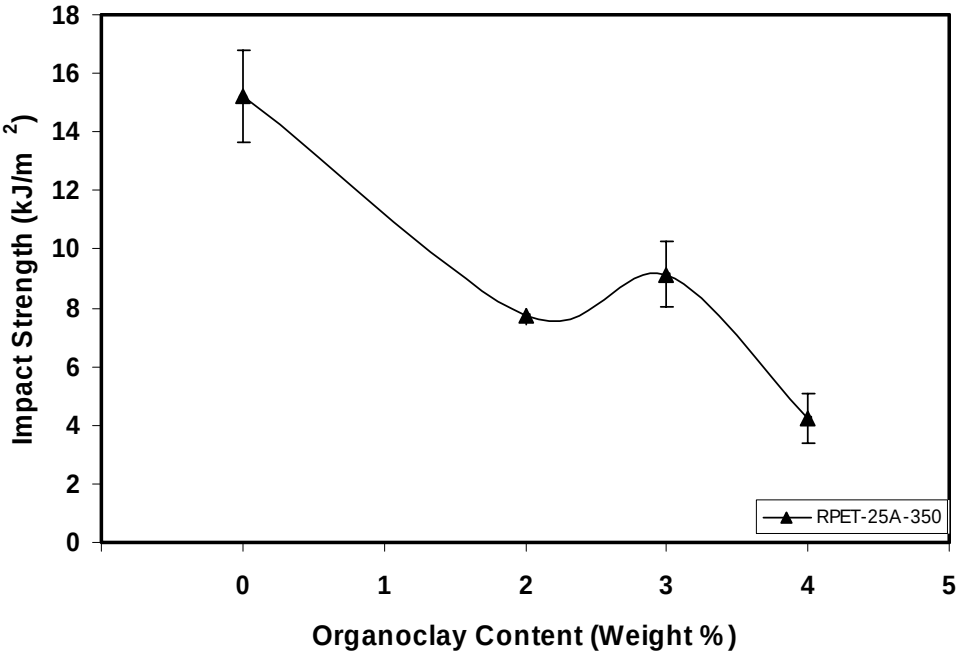

Figure 4.21 Effect of organoclay content on impact strength of nanocomposites

Figure 4.13 shows the effect of organoclay content on the stress-strain behavior of nanocomposites. In the case of good adhesion at the interface, rigid particulate fillers generally increase the modulus. However, these fillers generally cause a dramatic decrease in elongation at break and often decrease the tensile strength of a material. As seen from the figure, with addition of some amount of clay, nanocomposites show sharper increase in stress with increasing strain until sample failure. This behavior is an indication of approaching a more brittle structure compared to the neat resin.

The tensile modulus increases with increasing amount of organoclay as shown in Figure 4.14. The modulus of a composite depends on the ratio of filler modulus to matrix material modulus. Since organoclay has higher modulus, due to the more rigid structure, the tensile modulus increases with increasing amount of organoclay content. At 3 weight % organoclay content there is a significant increase in Young's modulus as 83% with respect to single extruded R-PET and 15 % with respect to non- extruded R-PET. At 3 weight % organoclay content, optimized structure may be accomplished with an effective filler-matrix interaction area, with sufficient organoclay content to accommodate polymer chains without agglomeration of the clay particles. At 4 weight %, unintercalated clay particles tend to form agglomerates which may be strong enough to increase the initial modulus.

The tensile strength results for the materials prepared with varying concentrations of organoclay are shown in Figure 4.15. Rigid particulate fillers often decrease the tensile strength of a material, unless good adhesion at the interface is attained since dewetting and crazing phenomena largely determine tensile strength [56]. The stress is better distributed in the structure containing 3 weight % organoclay, owing to well-dispersed clay particles, which indicates good interfacial adhesion. At 4 weight % organoclay content, unintercalated organoclay particles tend to form agglomerates and organoclay-polymer surface interaction gets very low that reduces the tensile strength.

The tensile strain at break decreases with increasing amount of organoclay content as shown in Figure 4.16. Addition of rigid particulate fillers generally causes a dramatic

decrease in elongation at break. Since the organoclay particles have rigid structures, the actual elongation of the pure resin decreases as more clay is loaded to the matrix. At 4 weight % organoclay content, elongation at break decreases in a dramatic manner due to the tendency of the clay particles agglomerating in the structure, and these agglomerates act as stress concentrators that decrease elongation at break.

Effect of organoclay content on flexural properties of nanocomposites is illustrated from Figure 4.17 to Figure 4.20**.** The stress-strain curves of tensile and flexural tests show resemblance. However, flexural modulus, strength and strain at break values are greater than tensile properties. This may be due to the nature of the test, since flexural testing involves both tension and compression. As seen from Figures 4.17 through 4.20, flexural modulus, strength and strain at break show maxima at 3 weight % organoclay content. At 3 weight % organoclay content there is a significant increase in flexural modulus: 24% with respect to single extruded R-PET and 40% with respect to not extruded R-PET. Flexural strength and strain at break show similar trend to tensile properties, as explained before in Figures 4.15 and 4.16.

The effects of organoclay content on the impact properties of the nanocomposites are shown in Figure 4.21. It is not surprising that impact strength of brittle polymers decreases on the addition of rigid fillers since the impact strength should correlate with the area under the stress-strain curve. Both the tensile strength and elongation at break decreases on the addition of nanoparticle, but the differential decrease with pure PET is the least at 3 weight % organoclay content.

4.2.3 Effect of Order of Addition on the Mechanical Properties of the Nanocomposites

In order to examine the effects of sequence of addition of anhydride chain extenders and organoclay on the mechanical properties of nanocomposites, tensile, flexural and impact tests were performed. This feature is illustrated in Figures 4.22 through 4.26.

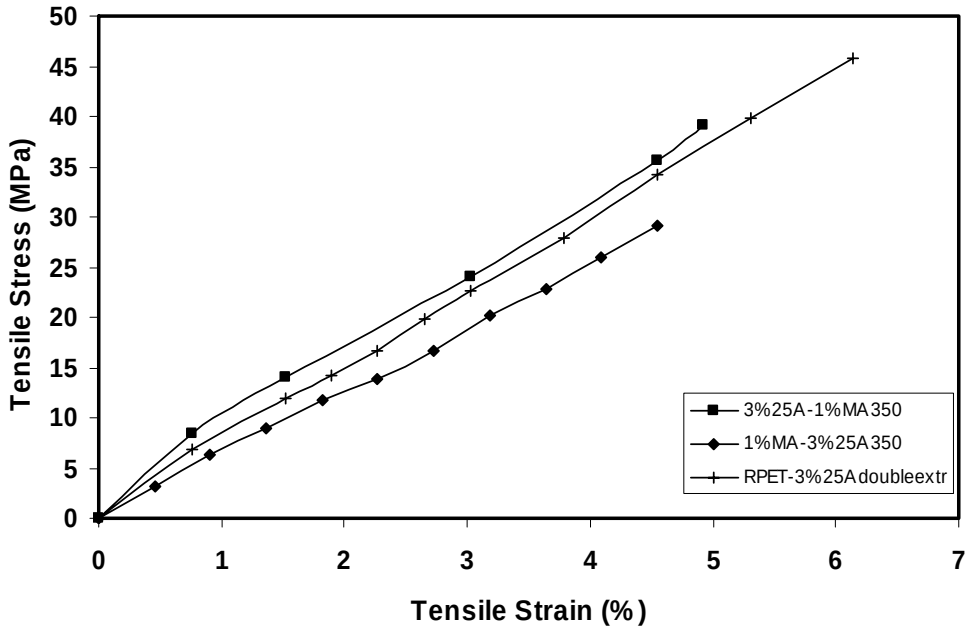

Figure 4.22 Effect of order of addition of chain extenders and organoclay on tensile stress-strain behavior of nanocomposites

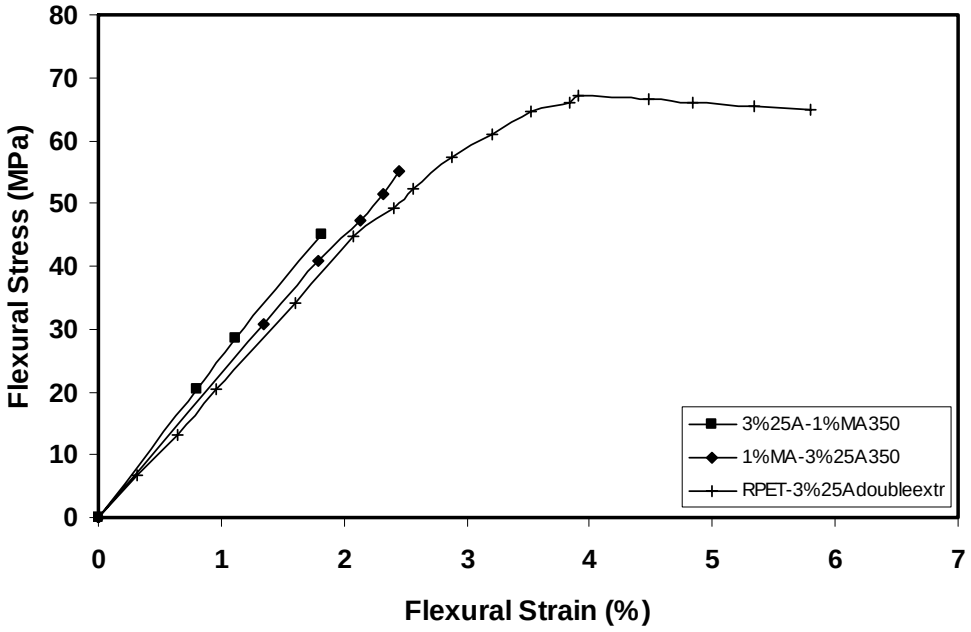

Figure 4.23 Effect of order of addition of chain extenders and organoclay on flexural stress-strain behavior of nanocomposites

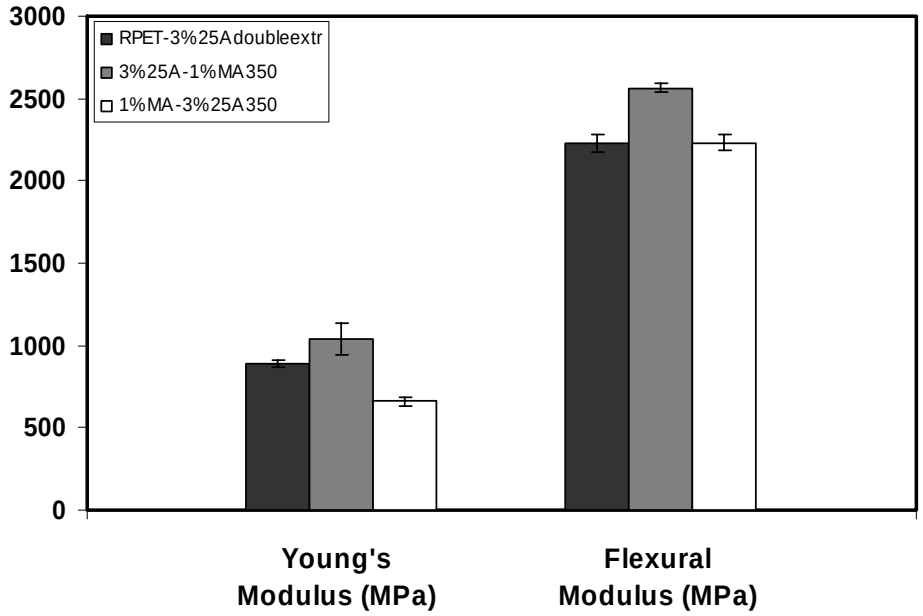

Figure 4.24 Effect of order of addition of chain extenders and organoclay on Young's and flexural modulus of nanocomposites

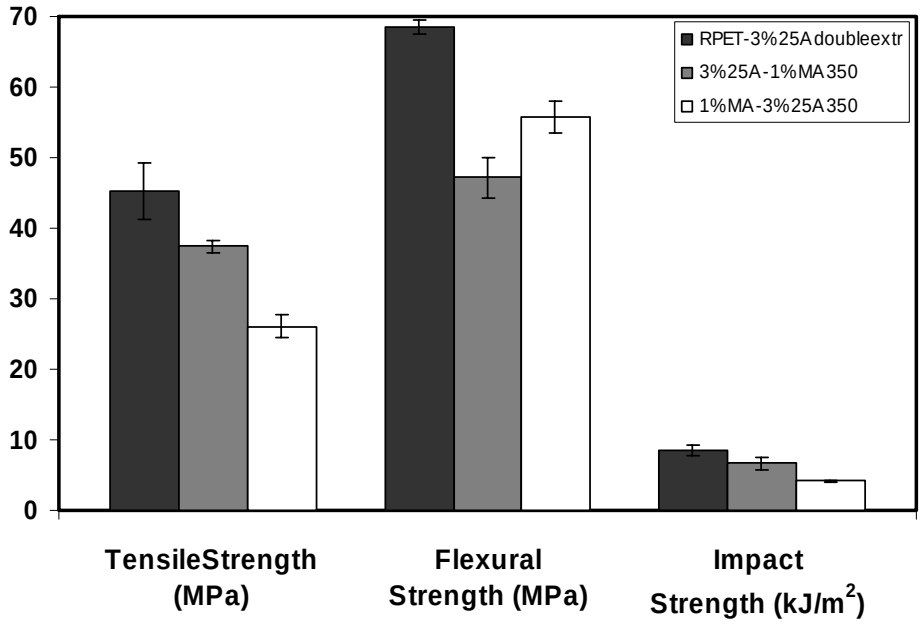

Figure 4.25 Effect of order of addition of chain extenders and organoclay on tensile, flexural and impact strength of nanocomposites

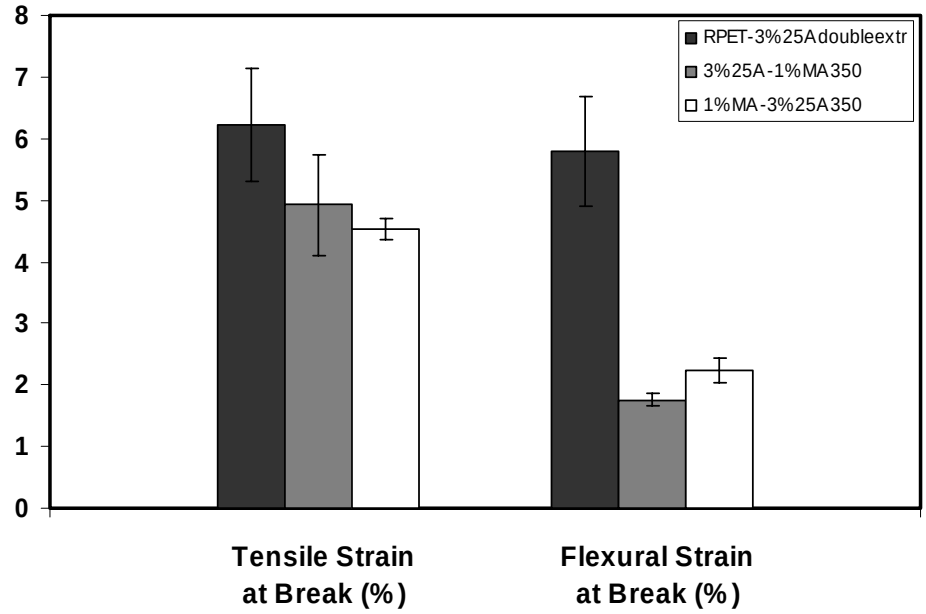

Figure 4.26 Effect of order of addition of chain extenders and organoclay on tensile and flexural strain at break of nanocomposites

The sequence of addition of chain extenders has clear effect on the maximum values of tensile and flexural stress-strain curves. The addition of organoclay followed by the addition of MA reveals higher tensile modulus, flexural modulus, tensile strength, impact strength and tensile strain at break compared to the addition of MA followed by the addition of organoclay. This is due to two main effects. Primarily, the diffusion of smaller chains is easier than diffusion of larger chains into the sheets of the organoclay. Also by adding the clay at the first step, the clay is extruded twice and further dispersion may have been accomplished.

4.2.4 Effect of Repeated Extrusion Cycle on the Mechanical Properties of the Nanocomposites

In order to examine the effects of repeated extrusion cycles on the mechanical properties of nanocomposites, tensile, flexural and impact tests were performed. This feature is illustrated in Figures 4.27 through 4.31.

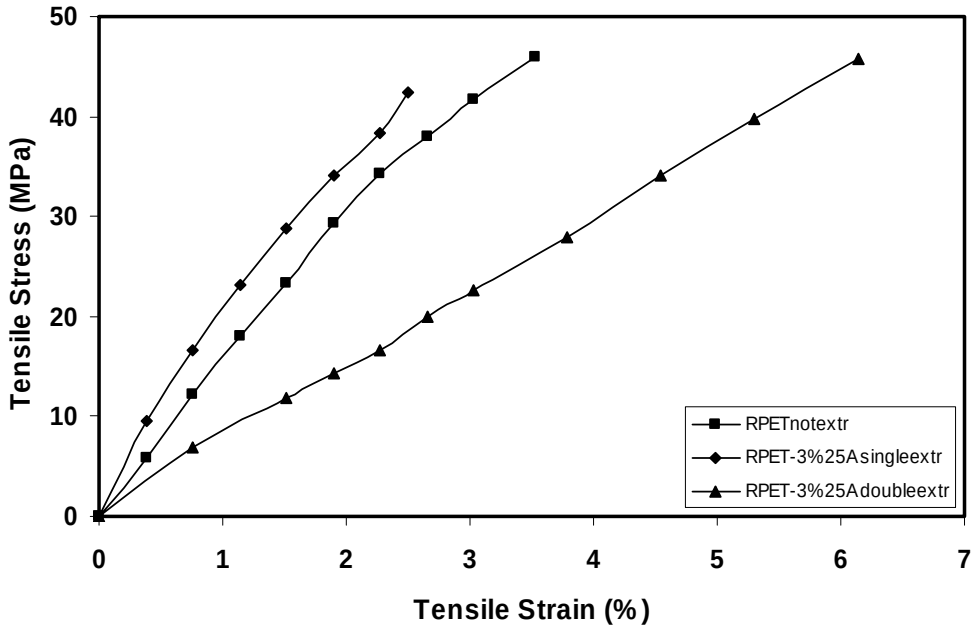

Figure 4.27 Effect of repeated extrusion cycles on tensile stress-strain behavior of nanocomposites

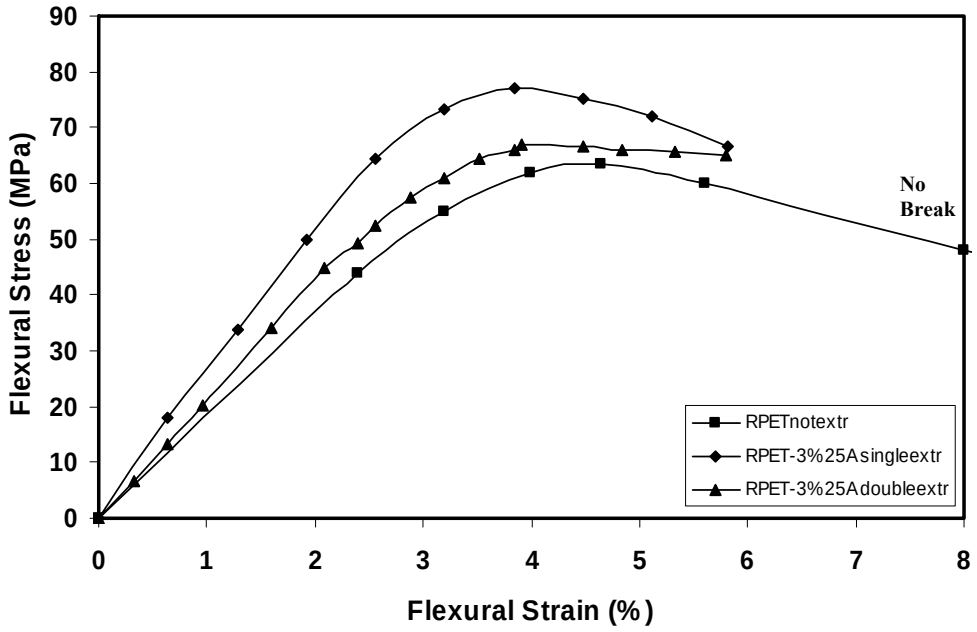

Figure 4.28 Effect of repeated extrusion cycles on flexural stress-strain behavior of nanocomposites

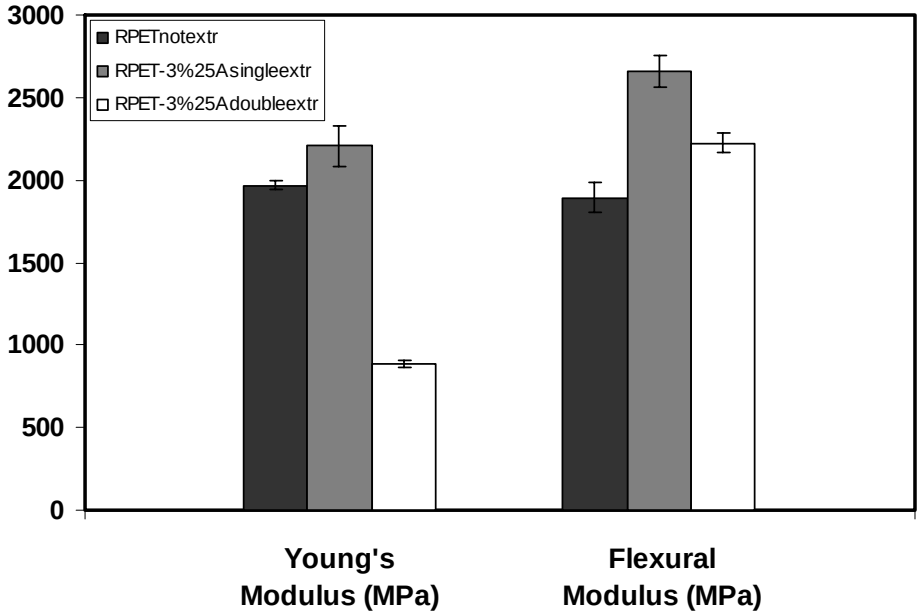

Figure 4.29 Effect of repeated extrusion cycles on Young's and flexural modulus of nanocomposites

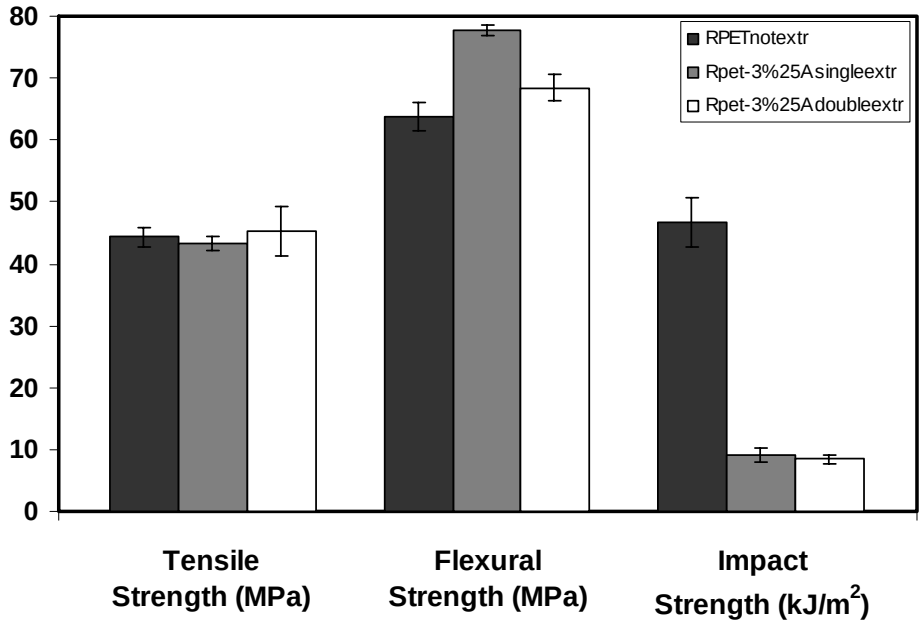

Figure 4.30 Effect of repeated extrusion cycles on tensile, flexural and impact strength of nanocomposites

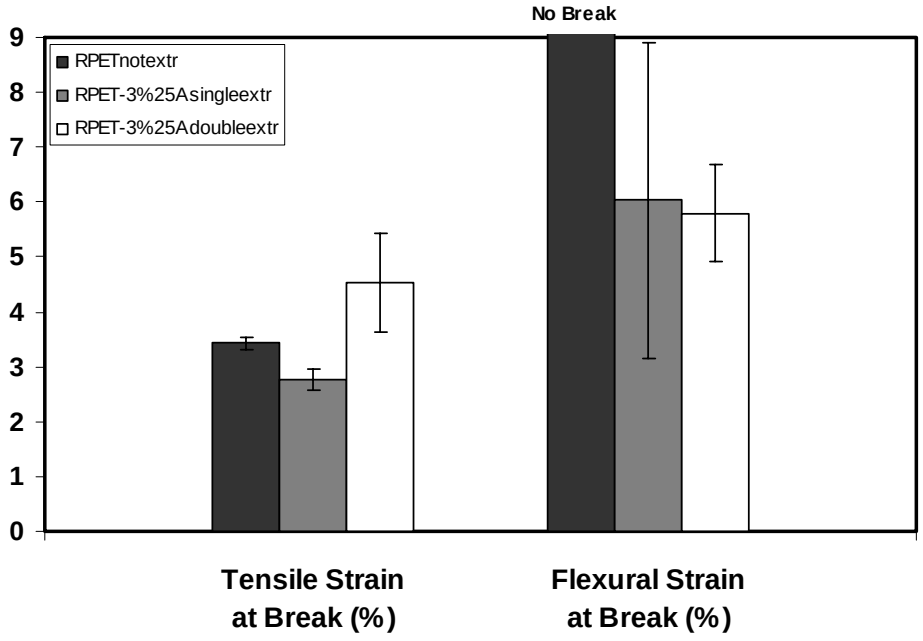

Figure 4.31 Effect of repeated extrusion cycles on tensile and flexural strain at break of nanocomposites

The effect of repeated extrusion cycles on tensile and flexural properties of nanocomposites is illustrated in Figures 4.27 through 4.31. As mentioned in Section 4.2.1 the repeated cycles of extrusion yields lower molecular weight due to the thermo-mechanical degradations. And also as mentioned in Section 4.2.3, the repeated cycles of extrusion yields better dispersion of organoclay with an effective interaction area. After second extrusion, higher tensile strain at break and tensile strength but lower impact strength, flexural modulus and tensile modulus is observed. These results show that the effect of molecular weight decrease in double extrusion is dominant over the further possible effect of organoclay dispersion in double extrusion. This explains why the modulus of the single extruded nanocomposite is higher and the elongation at break is lower the corresponding properties of R-PET. The impact strength results are also consistent with the stress-strain curves. Double extruded R-PET-3%25A has the lowest impact strength.

4.2.5 Effect of MA or PMDA Content on the Mechanical Properties of the Nanocomposites

In order to examine the effects of PMDA content on the mechanical properties of 3 weight % Cloisite25A containing nanocomposites at 350 rpm, tensile, flexural and impact tests were performed. This feature is illustrated in Figures 4.32 through 4.42.

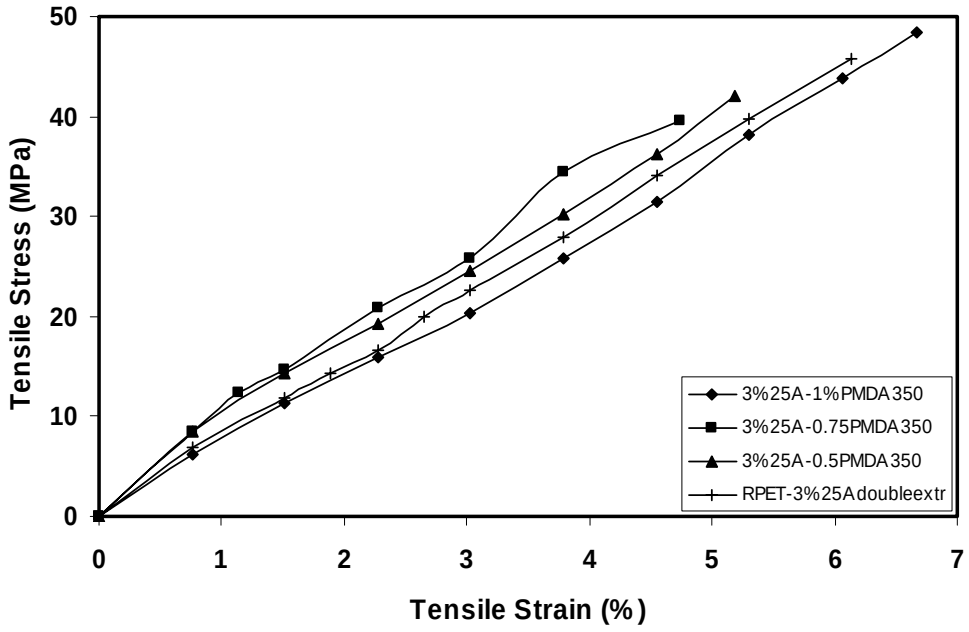

Figure 4.32 Effect of PMDA content on tensile stress-strain behavior of 3 weight % Cloisite25A containing nanocomposites, at 350 rpm

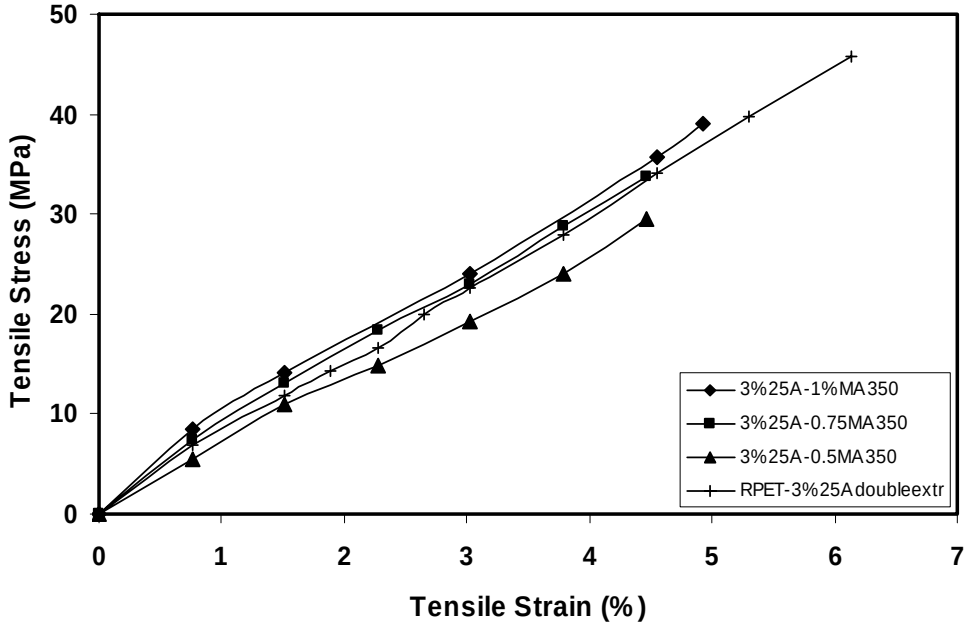

Figure 4.33 Effect of MA content on tensile stress-strain behavior of 3 weight % Cloisite25A containing nanocomposites, at 350 rpm

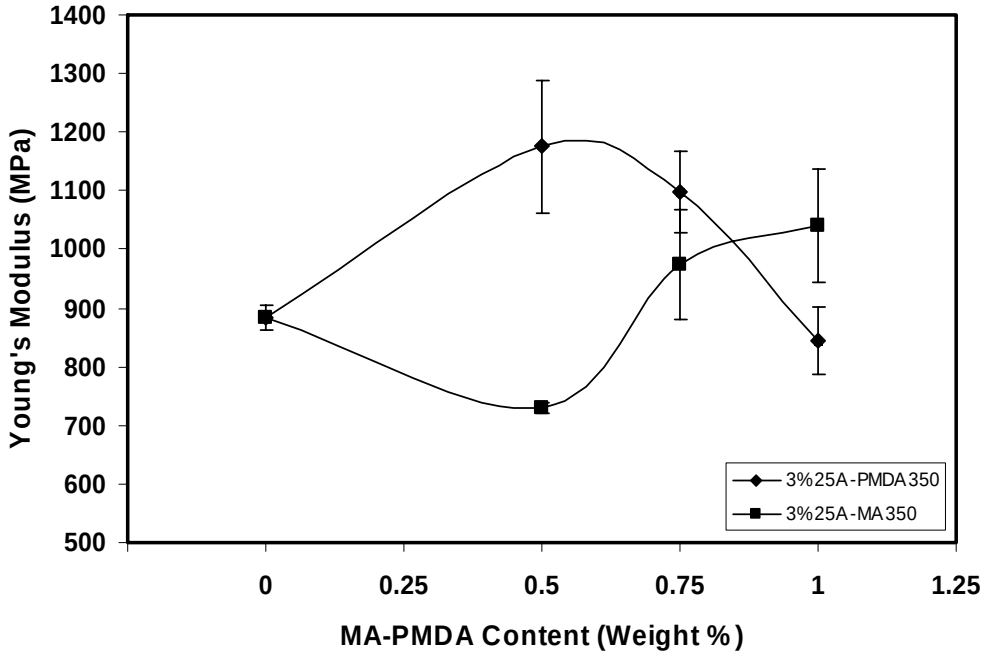

Figure 4.34 Effect of MA or PMDA content on Young's modulus of 3 weight % Cloisite25A containing nanocomposites, at 350 rpm

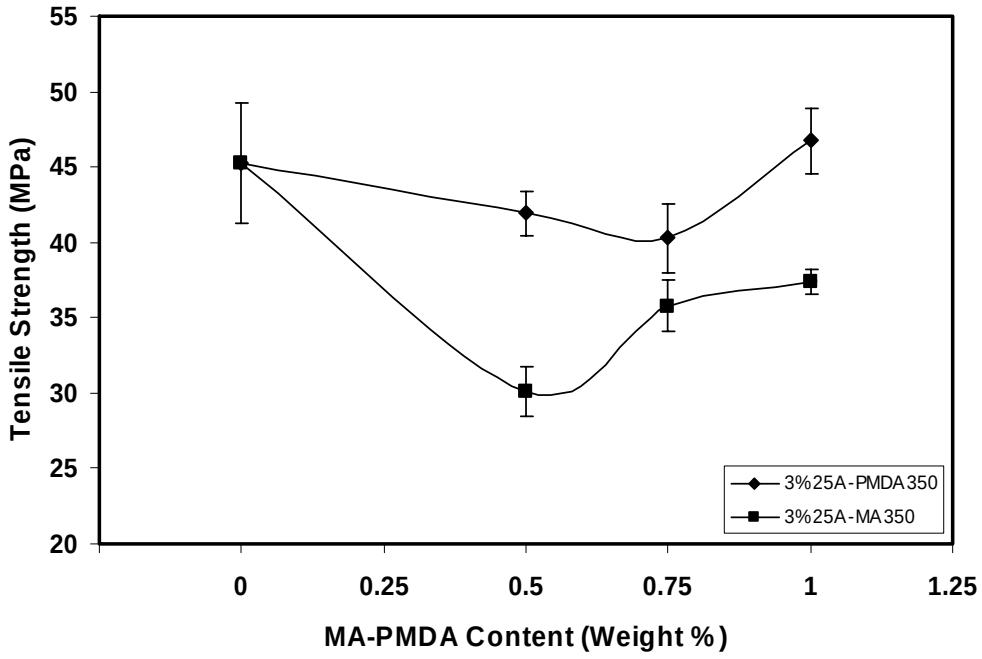

Figure 4.35 Effect of MA or PMDA content on tensile strength of 3 weight % Cloisite25A containing nanocomposites, at 350 rpm

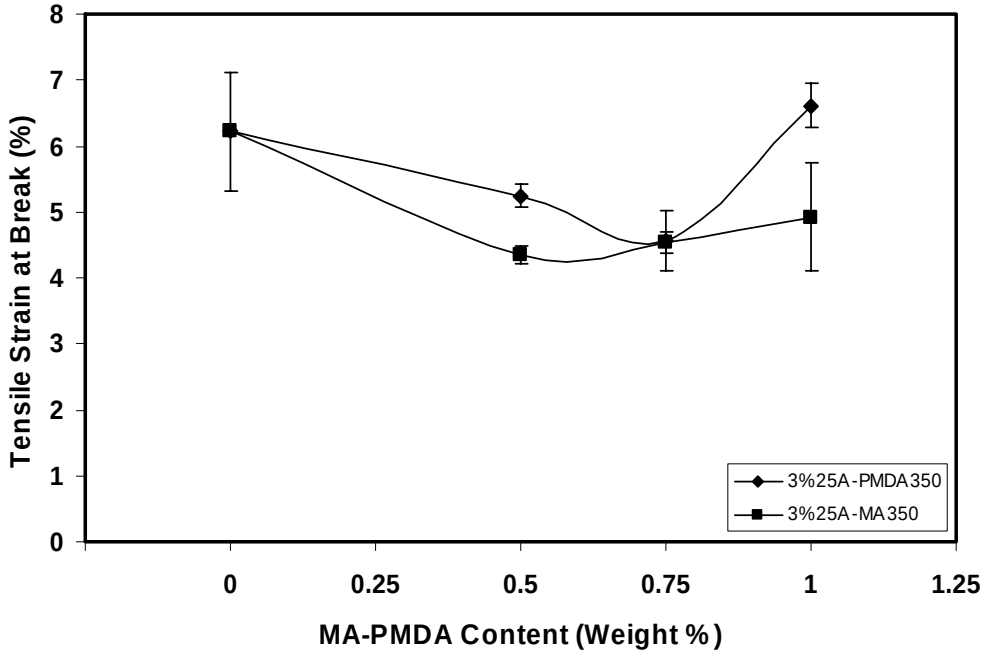

Figure 4.36 Effect of MA or PMDA content on tensile strain at break of 3 weight % Cloisite25A containing nanocomposites, at 350 rpm

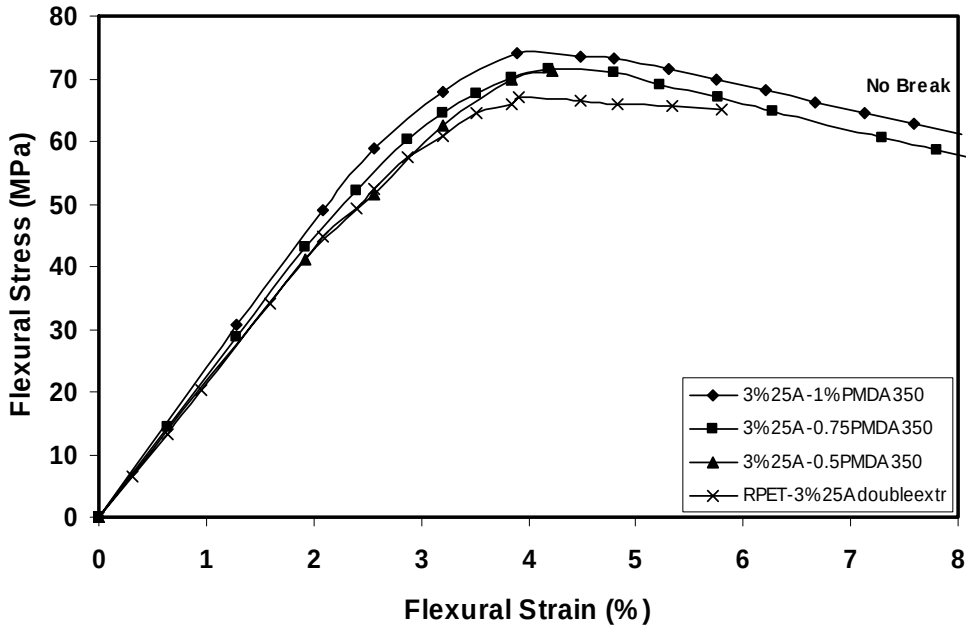

Figure 4.37 Effect of PMDA content on flexural stress-strain behavior of 3 weight % Cloisite25A containing nanocomposites, at 350 rpm

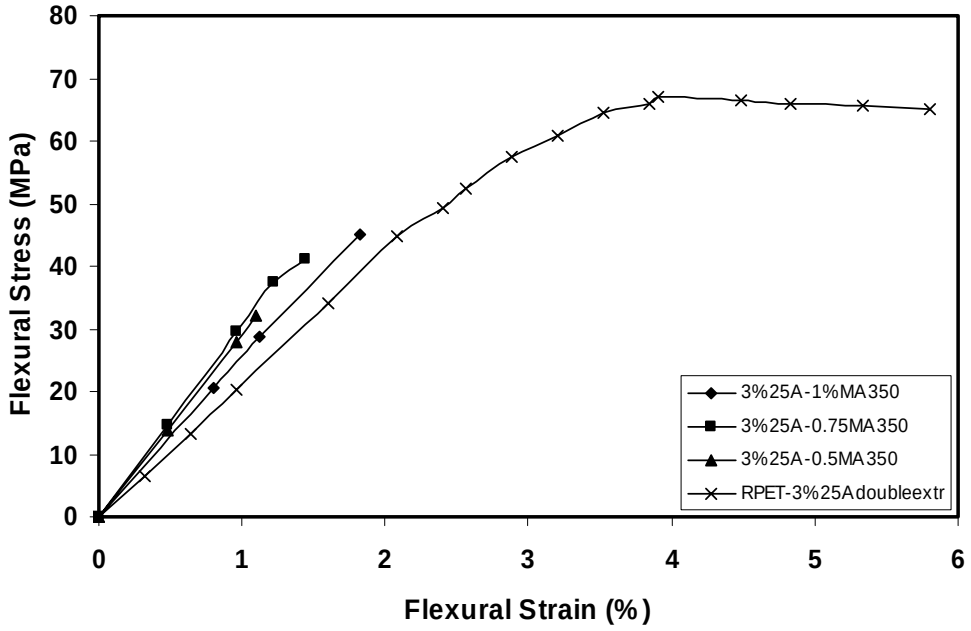

Figure 4.38 Effect of MA content on flexural stress-strain behavior of 3 weight % Cloisite25A containing nanocomposites, at 350 rpm

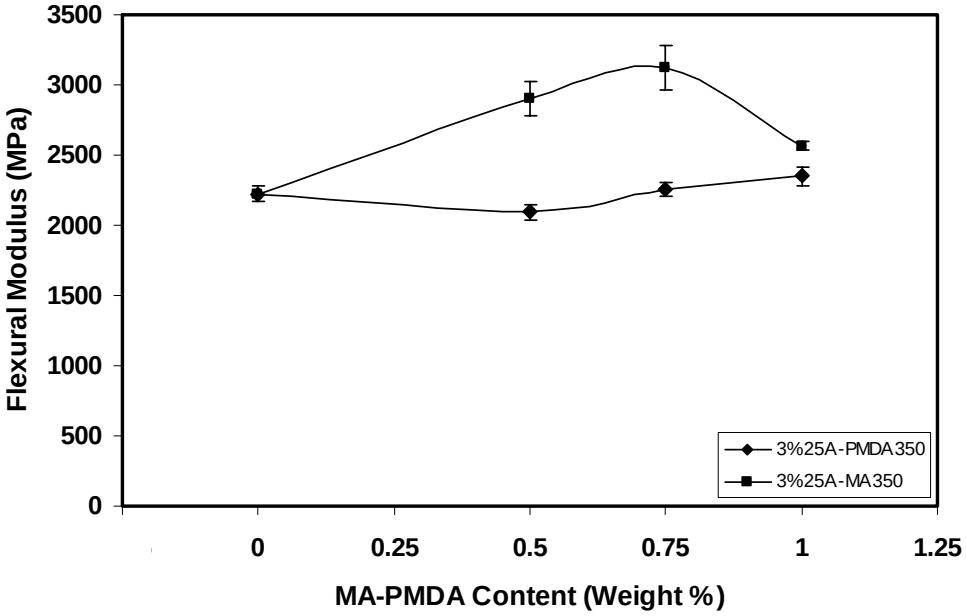

Figure 4.39 Effect of MA or PMDA content on flexural modulus of 3 weight % Cloisite25A containing nanocomposites, at 350 rpm

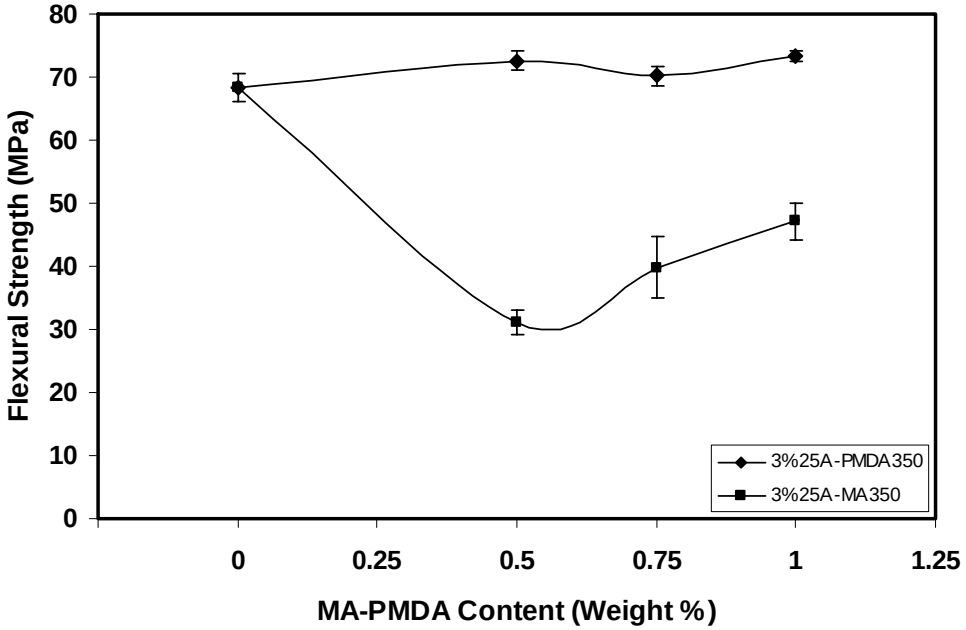

Figure 4.40 Effect of MA or PMDA content on flexural strength of 3 weight % Cloisite25A containing nanocomposites, at 350 rpm

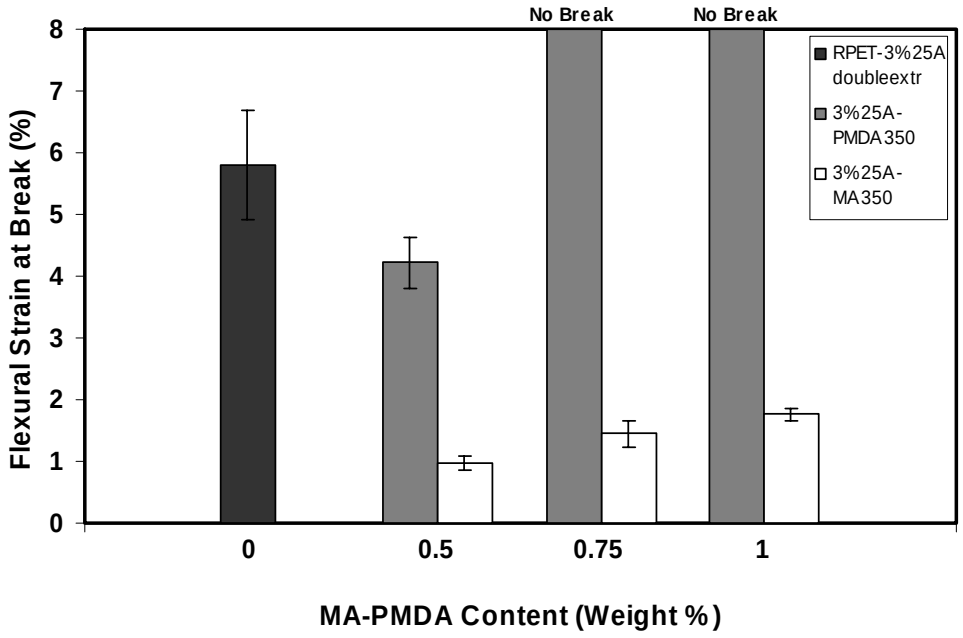

Figure 4.41 Effect of MA or PMDA content on flexural strain at break of 3 weight % Cloisite25A containing nanocomposites, at 350 rpm

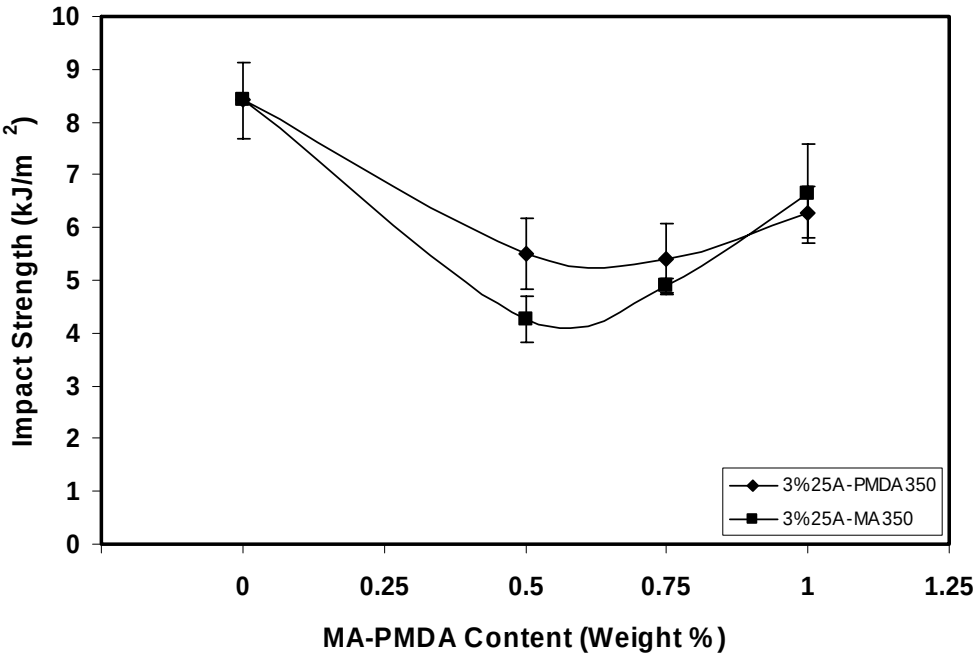

Figure 4.42 Effect of MA or PMDA content on impact strength of 3 weight % Cloisite25A containing nanocomposites, at 350 rpm

Figures 4.32 and 4.33 show the effect of PMDA and MA content on the stress-strain behavior of 3 weight % Cloisite25A containing nanocomposites at 350 rpm respectively. Higher molecular weight of the matrix resin is expected with the addition of anhydride chain extenders. At 0.5 and 0.75 weight % PMDA content, higher modulus values are observed with respect to the double extruded 3 weight % Cloisite25A containing nanocomposites. At 1 weight % PMDA content, the modulus decreased due to the possible plasticizing effect of excess PMDA. This behavior can be deduced from the increasing strain values at 1 weight % PMDA content. Compared to PMDA, MA does not offer significant improvement in mechanical properties.

Effect of MA and PMDA content on Young's modulus of 3 weight % Cloisite25A containing nanocomposites at 350 rpm is shown in Figure 4.34. At 0.5 weight % PMDA content, there is a significant increase in Young's modulus ie. 33% with respect to double extruded 3 weight % Cloisite25A containing nanocomposite. The effect of improving modulus is observed at 0.5 and 0.75 weight % with PMDA nevertheless this effect is observed at 1 weight % with MA. This is an expected result since PMDA contains four reactive groups that can lead to crosslinking or branching while MA contains two reactive groups. Thus, lower concentration ofchain extender is sufficient and more effective in the case of PMDA. Since the modulus or stiffness of a polymer is a function of intermolecular forces, the improvements in the Young's modulus indicate higher molecular weights. At higher concentrations the excess PMDA acts as a plasticizer that lowers modulus and increase elongation at break. By looking at this graph it would be wise to say that PMDA is a more effective chain extender.

Effect of MA and PMDA content on tensile strength of 3 weight % Cloisite25A containing nanocomposites at 350 rpm is shown in Figure 4.35. The tensile strength of PMDA added nanocomposites is higher than MA added nanocomposites at all concentrations which also indicates that PMDA is more effective.

As seen in Figure 4.36, the tensile strain at break decreases with addition of chain extenders except 1 weight % PMDA content. Addition of chain extenders increases the molecular weight, and at higher molecular weights secondary forces dominate over the primary intramolecular forces, thereby the chain slippage is prevented at higher molecular weights and that makes lower molecular weight polymers more extensible. At 1 weight % PMDA content, elongation at break increased due to the possible plasticizing effect of excess PMDA.

Effect of MA and PMDA content on flexural properties of nanocomposites containing 3 weight % Cloisite25A is illustrated in Figures 4.37 through 4.41. Flexural strength shows similar trend to tensile strength however, owing to the nature of the flexural tests, strength values are greater than those of tensile samples. Therefore higher flexural modulus, flexural strength is observed in flexural tests as seen in figures 4.39 and 4.40. Higher flexural strain at break and flexural strength is observed with PMDA. Also, at 0.75 and 1 weight % PMDA content, flexural specimens did not break in flexural test, which indicates the plasticizing effect of excess PMDA.

As expected from stress-strain curves at low PMDA content, the impact strength is higher than the impact strength of the nanocomposites with MA, whereas 1 weight % MA content imparts higher impact strength.

4.2.6 Effect of Screw Speed on the Mechanical Properties of the Nanocomposites

In order to examine the effects of screw speed (rpm) on the mechanical properties of 3 weight % Cloisite25A-1 weight % PMDA containing nanocomposites, tensile, flexural and impact tests were performed. This feature is illustrated in Figures 4.43 through 4.53.

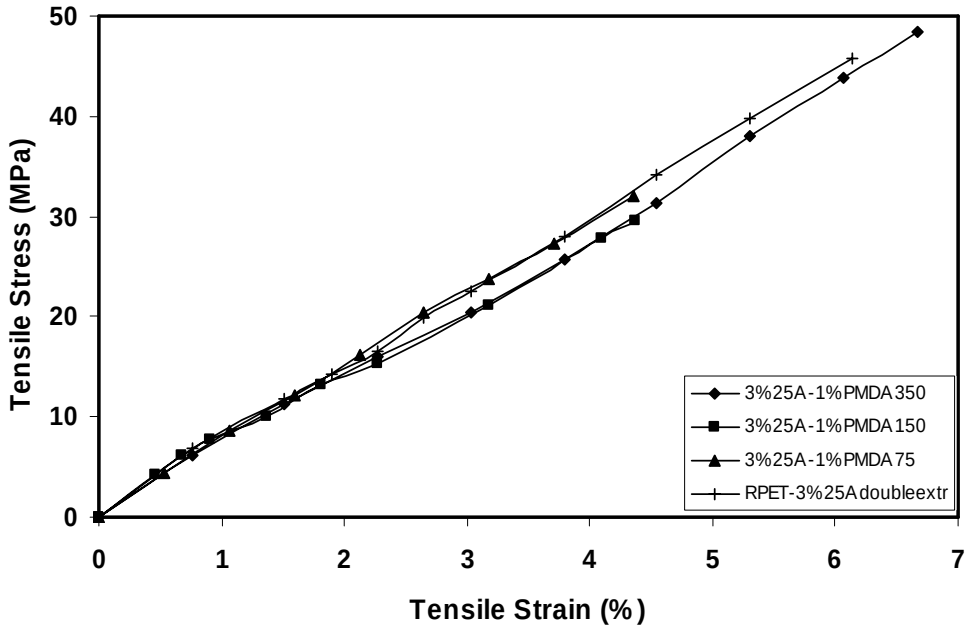

Figure 4.43 Effect of screw speed (rpm) on tensile stress-strain behavior of 3 weight % Cloisite25A - 1 weight % PMDA containing nanocomposites

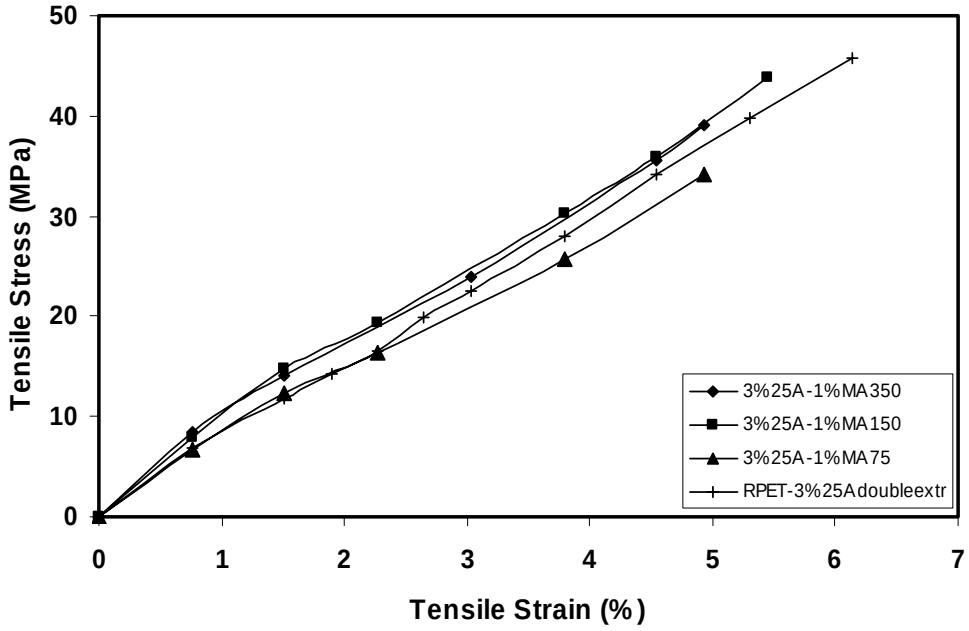

Figure 4.44 Effect of screw speed (rpm) on tensile stress-strain behavior of 3 weight % Cloisite25A - 1 weight % MA containing nanocomposites

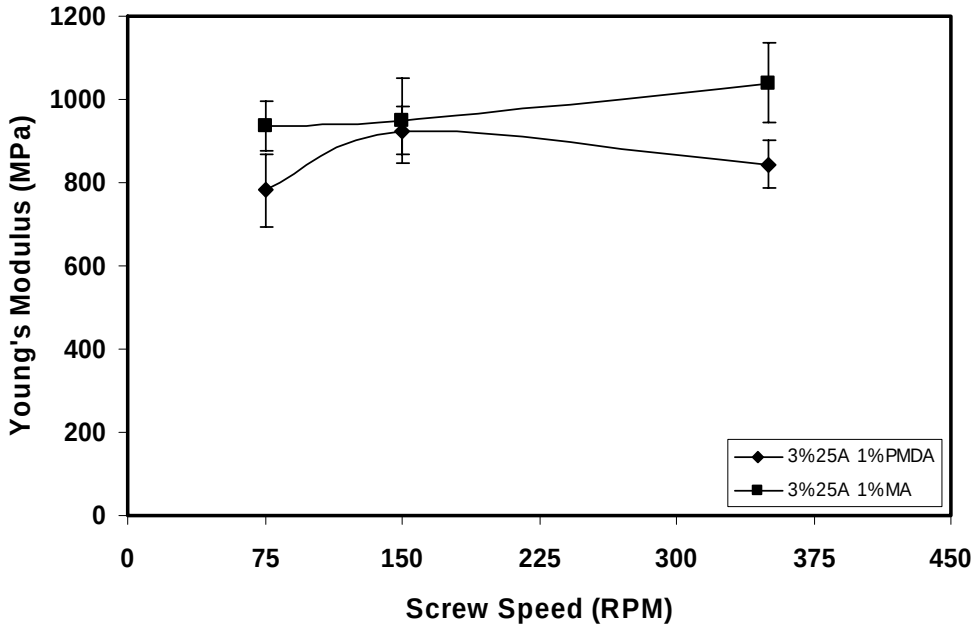

Figure 4.45 Effect of screw speed (rpm) on Young's modulus of 3 weight % Cloisite25A - 1 weight % MA or PMDA containing nanocomposites

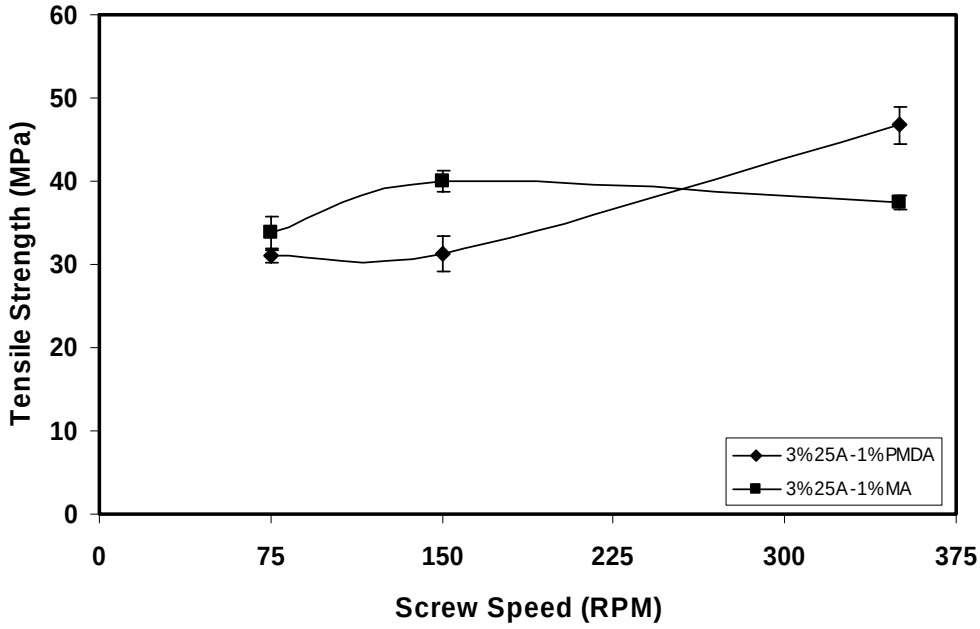

Figure 4.46 Effect of screw speed (rpm) on tensile strength of 3 weight % Cloisite25A - 1 weight % MA or PMDA containing nanocomposites

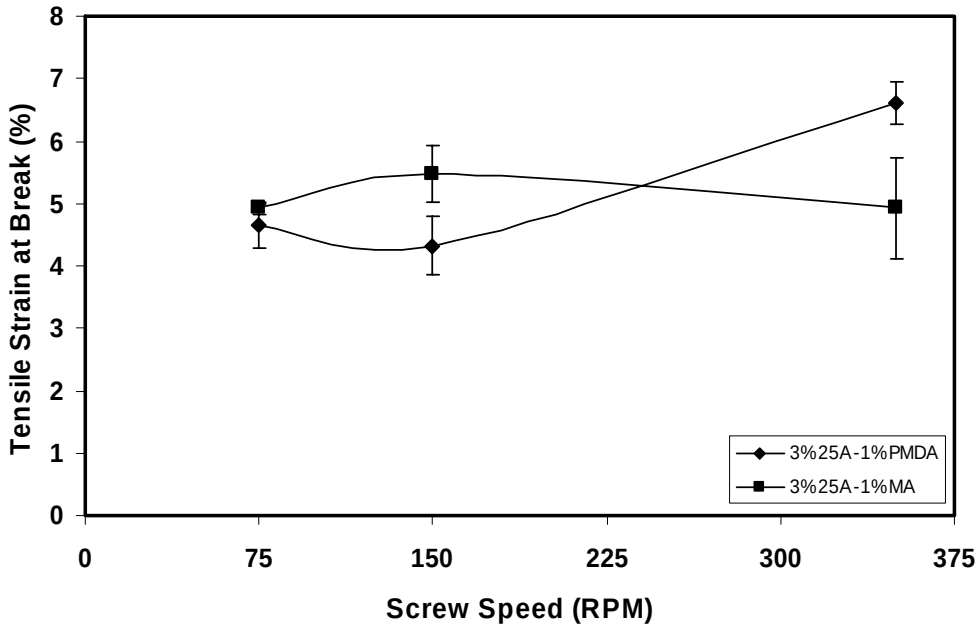

Figure 4.47 Effect of screw speed (rpm) on tensile strain at break of 3 weight % Cloisite25A - 1 weight % MA or PMDA containing nanocomposites

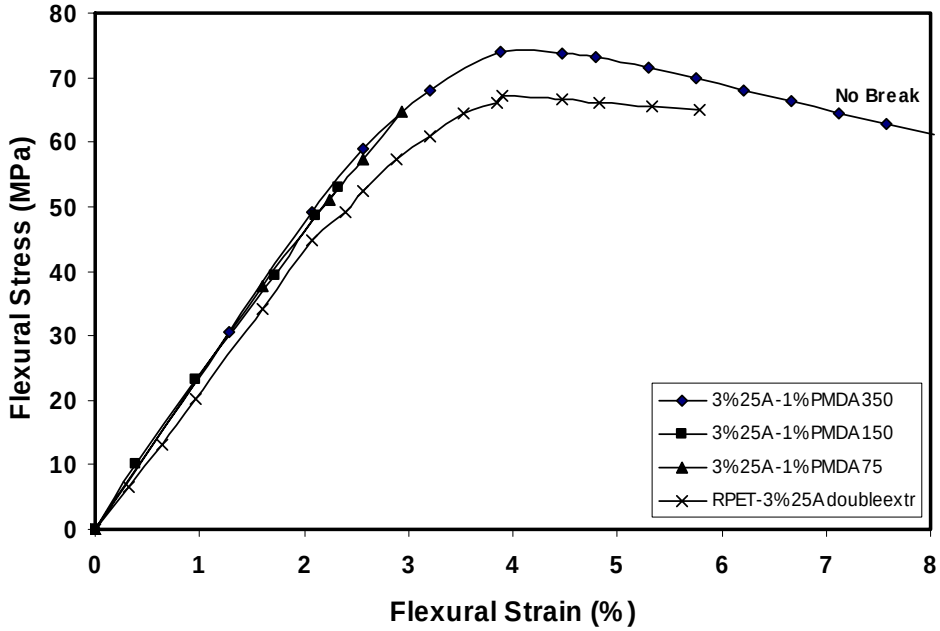

Figure 4.48 Effect of screw speed (rpm) on flexural stress-strain behavior of 3 weight % Cloisite25A - 1 weight % PMDA containing nanocomposites

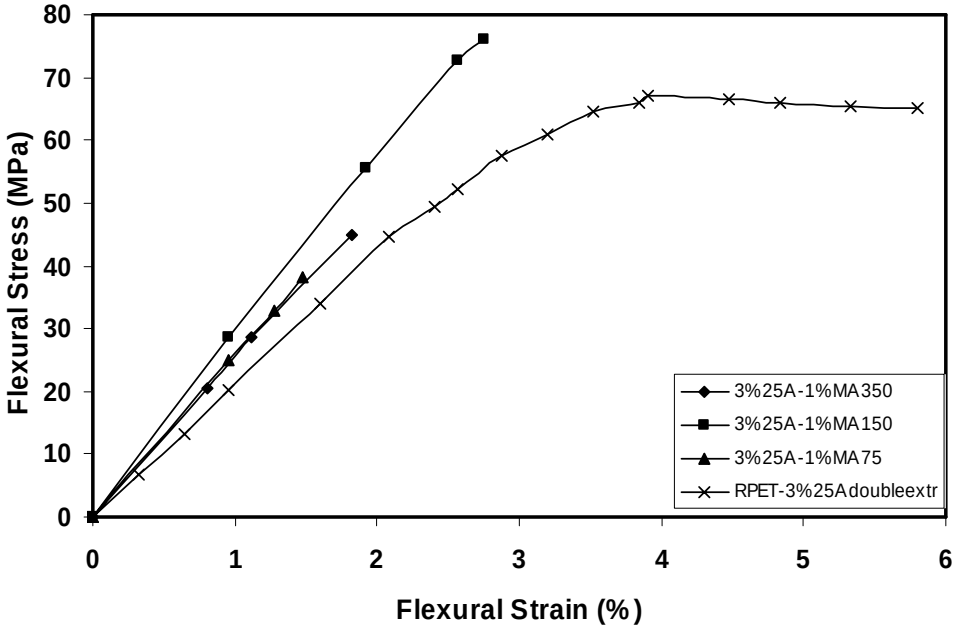

Figure 4.49 Effect of screw speed (rpm) on flexural stress-strain behavior of 3 weight % Cloisite25A - 1 weight % MA containing nanocomposites

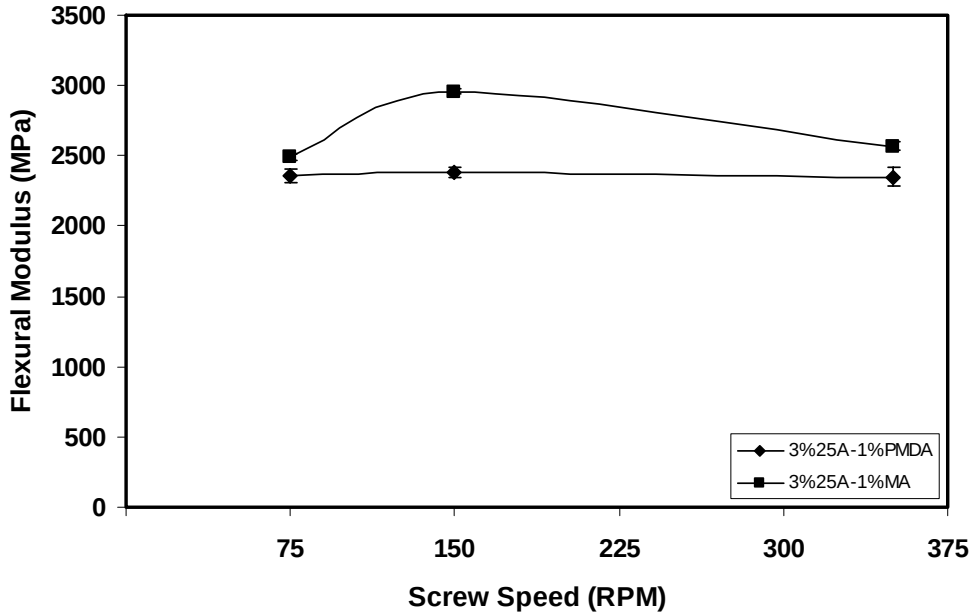

Figure 4.50 Effect of screw speed (rpm) on flexural modulus of 3 weight % Cloisite25A - 1 weight % MA or PMDA containing nanocomposites

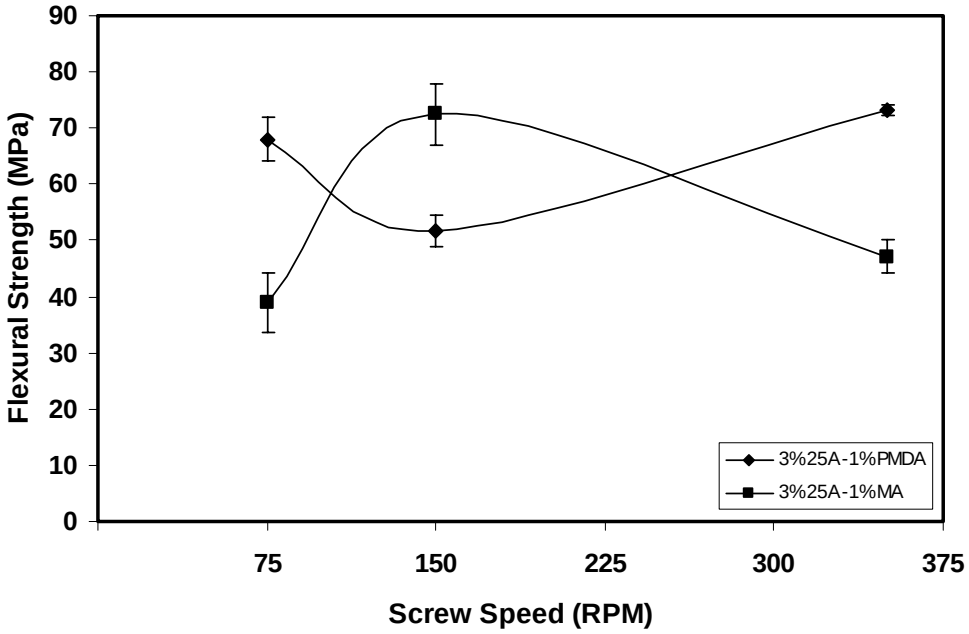

Figure 4.51 Effect of screw speed (rpm) on flexural strength of 3 weight % Cloisite25A - 1 weight % MA or PMDA containing nanocomposites

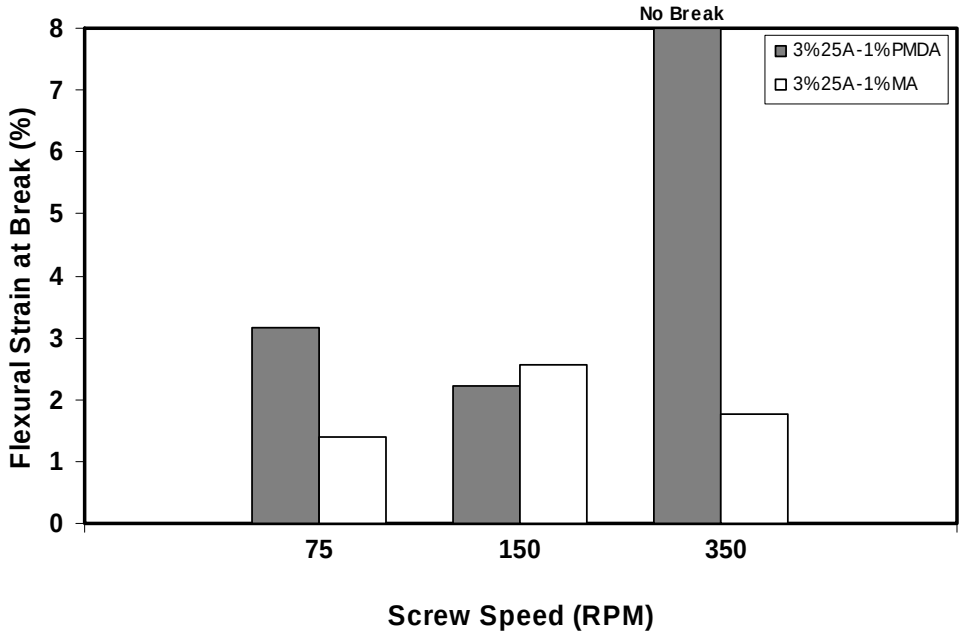

Figure 4.52 Effect of screw speed (rpm) on flexural strain at break of 3 weight % Cloisite25A - 1 weight % MA or PMDA containing nanocomposites

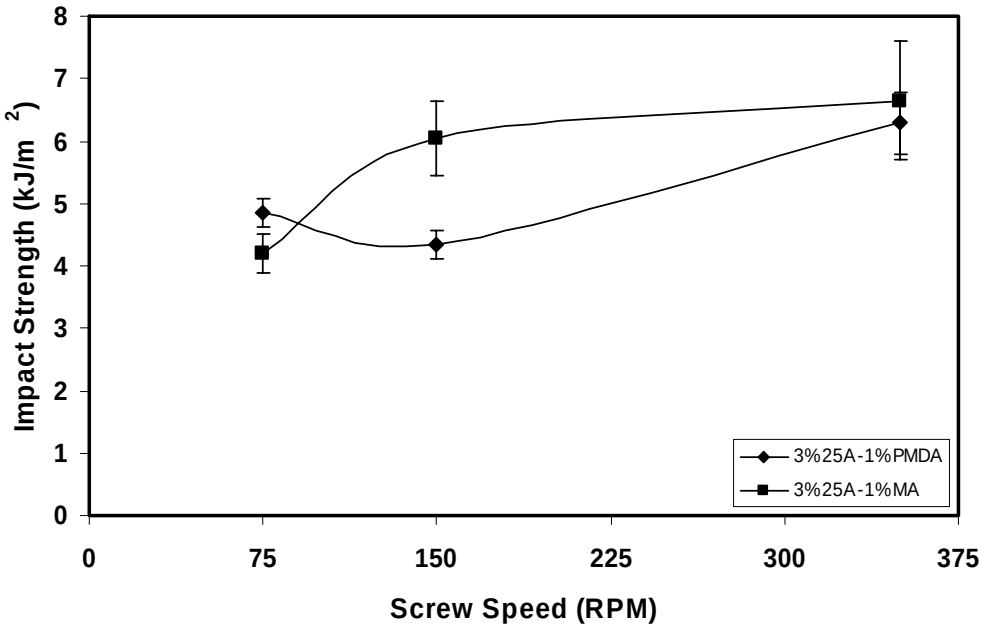

Figure 4.53 Effect of screw speed (rpm) on impact strength of 3 weight % Cloisite25A - 1 weight % MA or PMDA containing nanocomposites

Figures 4.43 and 4.44 show the effect of screw speed on the stress-strain behavior of 3 weight % Cloisite25A - 1 weight % MA or PMDA containing nanocomposites. The stress-strain curves of MA and PMDA with changing screw speed show resemblance. The property change is not significant with changing screw speed in the case of PMDA which indicates that there is enough residence time for chain extension reactions to complete. The screw speed has two different degradation effects; thermal and mechanical degradations. When screw speed increases, mechanical degradation increases, whereas thermal degradation decreases owing to the lower residence time. These effects compensate for each other, since they are both significant.

Although there is only little difference in Young's modulus, flexural modulus and impact strength at different screw speeds. Both MA and PMDA show their best performances at 350 rpm so it can be stated that 350 rpm is the best screw speed for both MA and PMDA among the screw speeds studied. Such a behavior may be the result of increasing the available surface area for filler matrix interactions. At lower

rpm, the degree of dispersion and exfoliation are lower due to the lower shear stresses applied. At all screw speeds MA has better properties since 1 weight % is an excess amount for PMDA as found in the earlier section.

4.3 Differential Scanning Calorimeter (DSC) Analysis

Table 4.2 shows the results of differential scanning calorimetry analyses performed in order to characterize the thermal behavior of samples at different chain extender contents and screw speeds. Differential Scanning Calorimeter (DSC) Analysis involves measuring the heat absorbed by a sample when that sample goes through thermal transitions. The DSC test allows these transitions to be identified by noting the absorption of heat from a plot of heat versus time as the sample is gradually heated. The plots identifying the temperatures of transitions are given in Appendix B.

The glass transition temperature (T_g) increases as the intermolecular forces in the polymer and the regularity or crystallinity of the polymer chain structure increase. Also, if the polymer is highly restricted in some other way, glass transition temperature will be high since glass transition temperature is highly dependent on the molecular mobility of the polymer chains. As seen in Table 4.2, with both PMDA and MA containing nanocomposites higher glass transition temperatures are observed with respect to the double extruded 3 weight % Cloisite 25A containing nanocomposites. These increases may be due to the increase in secondary intermolecular forces as molecular weights increase. Compared to PMDA containing nanocomposites, MA containing nanocomposites have higher glass transition temperatures at all concentrations and screw speeds. The lower glass transition temperatures of PMDA can be attributed to possible chain branches that decrease distance related secondary forces.

The net effect of increasing molecular weight in DSC analysis is an increase in the melting point. Compared to PMDA containing nanocomposites, MA containing nanocomposites have higher melting temperatures at all concentrations and screw

speeds. This result may be due to the possible chain branches that impede close packing of the polymer units and decrease the crystallinity of the polymer.

MA containing nanocomposites have higher T_m and T_g. However PMDA containing nanocomposites have better mechanical properties. This indicates an effective chain extension and branching reaction of PMDA, since PMDA decreases T_m and T_g and increases mechanical properties due to the branched structure.

Table 4.2 Thermal transition temperatures of recycled PET nanocomposites.

Sample Specifications	Glass Transition Temp. T_g, (°C)	Crystallization Temp. T_c, (°C)	Melting Temp. T_m, (°C)
R-PETsingleextr	70.8	137.6	260.8
R-PET-3%25Asigleextr	71.9	117.6	254.0
R-PET-3%25Adoubleextr	69.3	116.3	255.9
R-PET3%25A-1%PMDA350	69.7	119.9	251.4
R-PET3%25A-1%PMDA150	73.6	121.2	250.8
R-PET3%25A-1%PMDA75	71.9	121.4	251.9
R-PET3%25A-0.75%PMDA350	70.0	118.4	252.0
R-PET3%25A-0.5%PMDA350	71.4	118.9	253.0
R-PET3%25A-1%MA350	76.2	120.1	261.7
R-PET3%25A-1%MA150	71.9	119.3	256.0
R-PET3%25A-1%MA75	73.1	117.5	255.7
R-PET3%25A-0.75%MA350	74.3	116.1	256.1
R-PET3%25A-0.5%MA350	72.6	116.5	255.1

4.4 Melt Flow Index (MFI) Test

Melt flow index test was performed in order to get information about important flow characteristics such as viscosity of the polymer that has been found to relate closely with average molecular weight and branching structure of the sample [49]. For pure polymers a high melt index indicates a low molecular weight or less branched structure whereas the opposite is also true; a low melt index means a higher molecular weight or more branched structure. Melt flow index is not an intrinsic or fundamental property of a polymer. It is rather a conventional property.

The mentioned degradation behavior of R-PET in repeated cycles can clearly be seen in Table 4.3. Melt flow index of pure R-PET and 3 weight % organoclay containing nanocomposite tend to increase after the extrusion cycles. The increase in MFI value indicates a decrease in molecular weight probably due to the deterioration during processing by thermo-mechanical degradations.

Effect of addition of organoclay on the MFI values of R-PET can be seen in Table 4.3. Addition of organoclay decreases the MFI values in both single and double extrusion indicating a higher viscosity owing to the filler effect.

As seen in Table 4.3, with both PMDA and MA containing nanocomposites lower MFI values are observed with respect to the double extruded 3 weight % Cloisite25A containing nanocomposites indicating an improving effect on the molecular weight or structure. Compared to PMDA containing nanocomposites, MA containing nanocomposites have higher MFI values at all concentrations and screw speeds since PMDA contains four reactive groups that can lead branching while MA contains two reactive groups. Both MA and PMDA containing nanocomposites show their lowest MFI values at 1 weight % at 350 rpm so it can be stated that 350 rpm is optimum screw speed for both MA and PMDA.

Table 4.3 Melt Flow Index values of recycled PET nanocomposites.

Sample Specifications	MFI (g/10 min)
R-PET not extruded	181
R-PET single extrusion	411
R-PET double extrusion	1058
R-PET-3%25A single extrusion	240
R-PET-3%25A double extrusion	430
R-PET3%25A-1%PMDA350	247
R-PET3%25A-1%PMDA150	529
R-PET3%25A-1%PMDA75	441
R-PET3%25A-0.75%PMA350	315
R-PET3%25A-0.5%PMDA350	329
R-PET3%25A-1%MA350	491
R-PET3%25A-1%MA150	659
R-PET3%25A-1%MA75	711
R-PET3%25A-0.75%MA350	818
R-PET3%25A-0.5%MA350	1599

CHAPTER V

CONCLUSIONS

XRD analysis showed that, the basal spacing of Cloisite 25A increased from 19.21 Å to about 28-34 Å after processing with polymer indicating an intercalated structure. After extrusion, d-spacing of unintercalated clay collapses to 15.5 Å. Organoclay content had no significant effect on the interlayer distance. Also, PMDA content, MA content and screw speed did not have a recognizable effect on the interlayer distance.

From SEM micrographs it is seen that, at 3 weight % of organoclay in R-PET, good dispersion of clay is observed forming a tortuous crack path upon impact. However, at 4 weight % organoclay loading, the organoclay forms agglomerates acting as stress concentrators. PMDA displayed good dispersion at 0.5 weight % and 350 rpm. MA displayed the similar dispersion behavior at 1 weight % and 350 rpm. Both PMDA and MA show more tortuous crack path with smaller distances between crack propagation lines at these conditions.

In single extruded R-PET, tensile modulus, tensile strength and impact strength reduced dramatically compared to the neat resin. Tensile modulus and tensile strength increased for twice extruded R-PET with respect to the single extruded R-PET. Flexural strength and modulus, on the other hand, increased at repeated extrusion cycles.

Highest improvement in mechanical properties including Young's modulus, tensile strength, flexural modulus and flexural strength was obtained at 3 weight % organoclay loading. Thus, an optimized structure is obtained at 3 weight %

organoclay content. As expected, tensile strain, flexural strain, and impact strength decreased as the organoclay content increased in the nanocomposites.

A clear difference was observed in the mechanical properties with changing sequence of addition of chain extenders and organoclay. The addition of organoclay followed by the addition of MA exhibited higher Young's modulus, flexural modulus, tensile strength, tensile strain and impact strength than the opposite order of addition of the ingredients.

Tensile and flexural modulus decreased, after the second extrusion of 3 weight % organoclay containing nanocomposite.

Addition of PMDA or MA at 350 rpm to 3 weight % organoclay containing nanocomposites increased the Young's modulus. At lower contents (0.5 and 0.75) PMDA is more effective in increasing Young's modulus compared to MA, whereas at 1 weight % MA is more effective. Flexural modulus increased with the addition of MA; however PMDA has no significant effect on the flexural modulus. At 0.75 and 1 weight % PMDA content, the samples showed no break in flexural test indicating diminishing brittle behavior. PMDA proved to be a better chain extender with respect to MA. A recognizable effect of screw speed was not observed on MA or PMDA containing nanocomposites.

The MFI values of the neat R-PET, increased with increasing number of extrusion cycles. The MFI value of single extruded and double extruded R-PET reduced with the addition of 3 weight % organoclay. At all contents, PMDA yielded lower MFI values than did MA.

DSC analysis showed that both Tg and Tm of the nanocomposites containing MA were higher than the nanocomposites containing PMDA at the same chain extender content. Nanocomposites containing 1 weight % MA showed the maximum Tg and Tm values.

REFERENCES

1. Kornman X., Synthesis and Characterisation of Thermoset-Clay Nanocomposites, Licenciate Thesis : Luleå University of Technology, Sweden (2000)
2. LeBaron P C., Wang Z. and Pinnavaia T J., Applied Clay Science, 15, 11-29 (1999)
3. Carter L W., Hendricks J G. and Bolley D S., United States Patent No. 2,531,396, 1950 (Assigned to National Lead Co.)
4. Usuki A., Kojima Y., Kawasumi M., Okada A., Fukushima Y., Karauchi T. and Kamigatio O., J. Mater. Res., 8, 1179 (1993)
5. Usuki A., Koiwai A., Kojima Y., Kawasumi M., Okada A., Karauchi T. and Kamigatio O., J. Appl. Polym. Sci., 55, 119 (1995)
6. Okada A. and Usuki A., Mater. Sci. Engng., C, 3:109 (1995)
7. Okada A., Fukushima Y., Kawasumi M., Inagaki S., Usuki A., Sugiyama S., Karauchi T. and Kamigaito O., United States Patent No. 4,739,007, 1988
8. La Mantia F P., 'Handbook of Plastics Recycling', Rapra Technology Limited, Shrewsbury, UK, (2002)
9. La Mantia F P., 'Recycling of Plastic Materials', ChemTec Publishing, Toronto-Scarborough, Ontario, Canada (1993)
10. Lubin G., 'Handbook of Composites', Van Nostrand Reinhold, New York, (1982)
11. Mazumdar S K., 'Composites Manufacturing', CRC Press, Boca Raton, London, New York, Washington, D.C., (2002)
12. Strong A B., 'Fundamentals of Composites Manufacturing: Materials, Methods and Applications', Society of Manufacturing Engineers, Publications Development Dept., Reference Publications Division, Dearborn, Michigan, (1989)

13. Phillips L N., 'Design with Advanced Composite Materials', The Design Council, Springer Verlag, London, (1989)
14. Chawla K K., 'Composite Materials: Science and Engineering', Springer-Verlag, New York, (1998)
15. Strong A B., 'High Performance and Engineering Thermoplastic Composites', Technomic Pub. Co., Lancaster, Pennsylvannia, (1993)
16. Cogswell F N., 'Thermoplastic Aromatic Polymer Composites', Butterworth-Hinemann Limited, London, (1992)
17. Akovalı G., 'Handbook of Composite Fabrication', Rapra Tehnology Limited, Shawbury, UK, (2001)
18. Chung D D L., 'Composite Materials: Science and Applications', Springer-Verlag, London, (2003)
19. Ajayan P M., Schadler L S. and Braun P V., 'Nanocomposite Science and Technology', Wiley-VCH Verlag GmbH&Co., Weinheim, (2003)
20. Schmidt D., Shah D., Giannelis E P., Current Opinion in Solid State and Materials Science, 6, 205–212 (2002)
21. Manias E., 'Concurrent Enhancement of Various Materials Properties in Polymer/Clay Nanocomposites', http://zeus.plmsc.psu.edu/nano.html
22. Dennis H R., Hunter D L., Chang D., Kim S., White J L., Cho J W. and Paul D R., Polymer, 42, 9513-9522 (2001)
23. Seymour R B., 'Reinforced Plastics: Properties&Applications', ASM International, Katleen Mills Editorial, USA, (1993)
24. Hay J N., Shaw S J., 'A Review of Nanocomposites 2000', http://www.btwebworld.com/nano/nanocomposites_review.pdf
25. Alexandre M., Dubois P., Materials Science and Engineering, 28, 1-63 (2000)
26. Beyer G., Plastics Additives & Compounding, 22-28, October 2002
27. Krishnamoorti R, Yurekli K, Current Opinion in Colloid & Interface Science, 6, 464-470 (2001)
28. Turaçlı H., 'Ekstrüzyon Teknolojisine Giriş', Pagev, İstanbul, (1999)
29. Rauwendaal C., 'Understanding Extrusion', Hanser Publishers, Munich, (1998)

30. A web page on extrusion of plastics, www.tut.fi/plastics/tyreschool/moduulit/moduuli_6/hypertext/3/3_2.html
31. A web page on extrusion of plastics, www.engr.unconn.edu/cheg/
32. Xanthos M., 'Reactive Extrusion: Principles and Practice', Carl Hanser Verlag, Munich, (1992)
33. Birley A W., Haworth B. and Batchelor J., 'Physics of Plastics: Processing, Properties and Materials Engineering', Carl Hanser Verlag, Munich, (1992)
34. De Paoli M A. and Silva Spinace M A., J. Appl. Polym. Sci., 80, 20-25 (2001)
35. Paci M. and La Mantia F.P., Polymer Degradation and Stability, 61, 417-420 (1998)
36. Torres N., Robin J J. and Boutevin B., J. Appl. Polym. Sci., 79, 1816-1824 (2001)
37. Martinez J M., Eguiazabal J I., and Nazabal J., J. Macromol. Sci.-Phys., B34 (1&2), 171-176 (1995)
38. Ehrig R.J., 'Plastics Recycling', Hanser Publishers, Munich, (1992)
39. Paci M. and La Mantia F.P., Polymer Degradation and Stability, 63, 11-14 (1999)
40. Karayannidis P G. and Psalida E A., J. Appl. Polym. Sci., 77, 2206-2211 (2000)
41. Incarnatoa L., Scarfatoa P., Di Maioa L. and Aciernob D., Polymer, 41, 6825-6831 (2000)
42. Yılmazer U., Xantos M., Bayram G. and Tan V., J. Appl. Polym. Sci., 75, 1371- 1377 (2000)
43. Shah V., 'Handbook of Plastic Testing Technology', 2nd Edition, Wiley-Interscience Publication, (1998)
44. 'Annual Book of ASTM Standards', Vol.08.01, American Society for Testing and Materials ASTM D638-91a, Philadelphia, USA (1993)
45. 'Annual Book of ASTM Standards', Vol.08.01, American Society for Testing and Materials ASTM D790M, Philadelphia, USA (1993)
46. Seymour R B., Carraher C E., 'Structure-Property Relationships in Polymers', Plenum Press, New York, (1984)

47. ‘Annual Book of ASTM Standards’, Vol.08.01, American Society for Testing and Materials ASTM D256, Philadelphia, USA (1993)
48. Gilman J.W., Jackson C.L., Morgan A.B.,Haris R., Manias E., Giannelis E.P.,Wuthenow M., Hilton D., and Phillips S.H., Chem. Mater., 12, 1866-1873 (2000)
49. Strong A B., ‘Plastics: Materials and Processing’, Prentice Hall, New Jersey (2000)
50. Pegretti A., Kolarik J., Peroni C. and Migliaresi C., Polymer, Article In Press, Accepted 11 February 2004
51. Solis A S., Rejan A G. and Manero O., Macromol. Symp., 192, 281-292 (2003)
52. Ke Y., Long C. and Qi Z., J. Appl. Polym. Sci., 71, 1139-1146 (1999)
53. Karabulut M., ‘Production and Characterization of Nanocomposite Materials From Recycled Thermoplastics’, METU M.Sc. Thesis, Ankara, Turkey, (2003)
54. Yoon J T., Jo W H., Lee M S. and Ko M B., Polymer, 42, 329-336 (2001)
55. Fornes T D., Yoon P J., Keskkula H. and Paul D R., Polymer, 42, 9929-9940 (2001)
56. Nielsen L. and Landel R., ‘Mechanical Properties of Polymers and Composites’, Second Edition, Marcel Dekker Inc., USA (1993)

APPENDIX A

A.1 Stress-Strain Data for All Compositions

Table A.1.1 The data of tensile stress-strain curves of recycled PET

NOT extruded		Single Extruded		Double Extruded	
Stress	**Strain (%)**	**Stress**	**Strain (%)**	**Stress**	**Strain (%)**
0	0	0	0	0	0
5.81	0.37	18.31	1.51	5.94	0.37
1.51	0.75	25.74	2.27	12.87	0.75
2.27	1.13	30.69	3.03	18.06	1.13
3.03	1.51	35.14	3.78	22.77	1.51
3.78	1.89	40.34	4.54	27.72	1.89
4.54	2.27			32.67	2.27
38.04	2.65			36.38	2.65
41.74	3.03			39.60	3.03
45.97	3.52			41.58	3.40
				44.05	3.78

Table A.1.2 The data of tensile stress-strain curves of nanocomposites containing only Cloisite 25A

2 % Cloisite25A		3 % Cloisite25A		4 % Cloisite25A		3 % Cloisite25A doubleextruded	
Stress	**Strain (%)**	**Stress**	**Strain (%)**	**Stress**	**Strain (%)**	**Stress**	**Strain (%)**
0	0	0	0	0	0	0	0
9.84	0.75	9.59	0.37	10.10	0.37	6.83	0.75
18.68	1.51	16.66	0.75	17.42	0.75	11.88	1.51
27.27	2.27	23.23	1.13	22.72	1.13	14.25	1.89
30.80	2.65	28.78	1.51	27.27	1.36	16.63	2.27
33.83	3.03	34.09	1.89			19.90	2.65
37.87	3.56	38.38	2.27			22.57	3.03
		42.42	2.49			27.92	3.78
						34.15	4.54
						39.80	5.30
						45.74	6.13

Table A.1.3 The data of tensile stress-strain curves of nanocomposites containing PMDA and 3 weight percent Cloisite 25A

1% PMDA at 350 rpm		1% PMDA at 150 rpm		1% PMDA at 75 rpm	
Stress	**Strain (%)**	**Stress**	**Strain (%)**	**Stress**	**Strain (%)**
0.00	0.00	0.00	0.00	0.00	0.00
6.18	0.76	4.23	0.45	4.36	0.53
11.33	1.52	6.24	0.68	8.71	1.06
15.96	2.27	7.80	0.91	12.08	1.59
20.34	3.03	10.02	1.36	16.24	2.12
25.74	3.79	13.14	1.82	20.40	2.65
31.41	4.55	15.37	2.27	23.76	3.18
38.10	5.30	21.16	3.18	27.33	3.71
43.76	6.06	27.85	4.09	32.08	4.35
48.40	6.67	29.63	4.36		

0,75% PMDA at 350 rpm		0,5% PMDA at 350 rpm	
Stress	**Strain (%)**	**Stress**	**Strain (%)**
0.00	0.00	0.00	0.00
8.42	0.76	8.42	0.76
12.38	1.14	14.36	1.52
14.60	1.52	19.31	2.27
20.79	2.27	24.50	3.03
25.74	3.03	30.20	3.79
34.41	3.79	36.14	4.55
39.60	4.73	42.08	5.19

Table A.1.4 The data of tensile stress-strain curves of nanocomposites containing MA and 3 weight percent Cloisite 25A

1% MA at 350 rpm		1% MA at 150		1%MA 75 rpm	
Stress	**Strain (%)**	**Stress**	**Strain (%)**	**Stress**	**Strain (%)**
0.00	0.00	0.00	0.00	0.00	0.00
8.42	0.76	7.93	0.76	6.68	0.76
14.11	1.52	14.86	1.52	12.38	1.52
24.01	3.03	19.32	2.27	16.34	2.27
35.64	4.55	30.22	3.79	25.74	3.79
39.11	4.92	35.92	4.55	34.16	4.92
		43.85	5.45		

0,75% MA at 350 rpm		0,5% MA at 350 rpm	
Stress	**Strain (%)**	**Stress**	**Strain (%)**
0.00	0.00	0.00	0.00
7.43	0.76	5.45	0.76
13.12	1.52	10.89	1.52
18.32	2.27	14.85	2.27
23.02	3.03	19.31	3.03
28.71	3.79	24.01	3.79
33.66	4.47	29.46	4.47

Table A.1.5 The data of flexural stress-strain curves of recycled PET

Not Extruded		Single Extruded		Double Extruded	
Stress	**Strain (%)**	**Stress**	**Strain (%)**	**Stress**	**Strain (%)**
0.00	0.00	0.00	0.00	0.00	0.00
43.89	2.40	42.67	1.92	42.17	1.92
54.87	3.20	64.52	3.20	64.52	3.20
61.78	4.00	70.62	3.84	72.14	4.35
63.40	4.64	72.14	4.61	71.12	5.12
60.15	5.60	68.08	5.76	56.90	7.68
47.96	8.00	57.41	7.68	49.28	8.96
38.20	10.40	46.74	9.60		

Table A.1.6. The data of flexural stress-strain curves of nanocomposites containing only Cloisite 25A

2% Cloisite25A		3% Cloisite25A		4% Cloisite25A		3% Cloisite25A doubleextruded	
Stress	**Strain (%)**	**Stress**	**Strain (%)**	**Stress**	**Strain (%)**	**Stress**	**Strain (%)**
0.00	0.00	0.00	0.00	0.00	0.00	0.00	0.00
7.56	0.32	17.84	0.64	7.51	0.32	6.60	0.32
16.07	0.64	33.81	1.28	23.48	0.96	20.32	0.96
24.58	0.96	49.77	1.92	36.16	1.44	34.04	1.60
39.24	1.60	64.33	2.56	46.49	1.86	49.28	2.40
46.33	1.92	73.25	3.20	51.18	2.05	57.41	2.88
53.42	2.24	77.01	3.84			60.96	3.20
60.04	2.56	75.13	4.48			67.06	3.90
68.07	3.20	71.84	5.12			66.55	4.48
70.91	3.49	66.68	5.82			65.03	5.80

Table A.1.7 The data of flexural stress-strain curves of nanocomposites containing PMDA and 3 weight percent Cloisite 25A

1% PMDA at 350 rpm		0.75% PMDA at 350 rpm		0.5% PMDA at 350 rpm	
Stress	**Strain (%)**	**Stress**	**Strain (%)**	**Stress**	**Strain (%)**
0.00	0.00	0.00	0.00	0.00	0.00
30.68	1.28	14.32	0.64	41.16	1.92
49.10	2.08	42.96	1.92	51.55	2.56
58.91	2.56	52.16	2.40	62.60	3.20
67.92	3.20	64.44	3.20	69.99	3.84
74.05	3.89	70.06	3.84	71.19	4.22
71.50	5.30	69.00	5.22		
68.03	6.21	64.83	6.27		
64.56	7.13	60.65	7.30		
61.09	8.04	56.48	8.32		

1% PMDA at 150 rpm		1% PMDA 75 rpm	
Stress	**Strain (%)**	**Stress**	**Strain (%)**
0.00	0.00	0.00	0.00
10.02	0.38	37.64	1.60
23.27	0.96	51.14	2.24
39.38	1.73	57.28	2.56
48.69	2.11	64.64	2.94
52.98	2.33		

Table A.1.8. The data of flexural stress-strain curves of nanocomposites containing MA and 3 weight percent Cloisite 25A

1% MA at 350 rpm		1% MA at 150 rpm		1% MA at 75 rpm	
Stress	**Strain (%)**	**Stress**	**Strain (%)**	**Stress**	**Strain (%)**
0	0	0	0	0	0
20.45	0.80	28.63	0.95	24.95	0.95
28.63	1.12	55.64	1.91	32.73	1.27
45.00	1.82	72.82	2.55	38.04	1.47
		76.09	2.75		

0,75% MA at 350 rpm		0,5% MA at 350 rpm	
Stress	**Strain (%)**	**Stress**	**Strain (%)**
0	0	0	0
14.72	0.48	13.91	0.48
29.45	0.96	27.82	0.96
37.43	1.22	32.11	1.10
41.11	1.44		

A.2 Tensile Data for All Compositions

Table A.2.1 Young's modulus data for all compositions

Composition	Young's Modulus (MPa)	std. dev.
R-PET Not Extruded	1965.12	26.18
R-PET Single Extruded	1222.22	5.00
R-PET Double Extruded	1503.52	87.89
R-PET-2%25Asigleextr	1405.24	225.19
R-PET-3%25Asigleextr	2204.74	123.18
R-PET-4%25Asigleextr	1980.91	571.33
R-PET-3%25Adoubleextr	884.35	21.43
R-PET3%25A-1%PMDA350	844.22	58.45
R-PET3%25A-1%PMDA150	924.64	57.17
R-PET3%25A-1%PMDA75	781.76	87.56
R-PET3%25A-0.75%PMDA350	1098.53	69.09
R-PET3%25A-0.5%PMDA350	1175.76	113.12
R-PET3%25A-1%MA350	1039.60	96.86
R-PET3%25A-1%MA150	948.91	103.23
R-PET3%25A-1%MA75	936.53	58.99
R-PET3%25A-0.75%MA350	975.30	93.52
R-PET3%25A-0.5%MA350	729.39	10.41
R-PET1%MA-3%25A350	659.13	96.86

Table A.2.2 Tensile strength data for all compositions

Composition	Tensile Strength (Mpa)	std. dev
R-PET Not Extruded	44.28	1.53
R-PET Single Extruded	40.37	0.78
R-PET Double Extruded	42.54	1.53
R-PET-2%25Asingleextr	37.38	1.65
R-PET-3%25Asingleextr	43.23	1.13
R-PET-4%25Asingleextr	30.15	5.20
R-PET-3%25Adoubleextr	45.29	3.99
R-PET3%25A-1%PMDA350	46.72	2.18
R-PET3%25A-1%PMDA150	31.27	2.13
R-PET3%25A-1%PMDA75	31.05	0.93
R-PET3%25A-0.75%PMDA350	40.30	2.28
R-PET3%25A-0.5%PMDA350	41.93	1.43
R-PET3%25A-1%MA350	37.40	0.84
R-PET3%25A-1%MA150	40.06	1.23
R-PET3%25A-1%MA75	33.81	2.01
R-PET3%25A-0.75%MA350	35.75	1.71
R-PET3%25A-0.5%MA350	30.08	1.65
R-PET1%MA-3%25A350	26.09	1.57

Table A.2.3 Tensile strain at break (%) data for all compositions

Composition	Tensile Strain at Break (%)	std. dev
R-PET Not Extruded	3.43	0.11
R-PET Single Extruded	4.55	0.15
R-PET Double Extruded	3.60	0.40
R-PET-2%25Asigleextr	3.37	0.25
R-PET-3%25Asigleextr	2.77	0.20
R-PET-4%25Asigleextr	1.55	0.33
R-PET-3%25Adoubleextr	6.22	0.90
R-PET3%25A-1%PMDA350	6.61	0.34
R-PET3%25A-1%PMDA150	4.33	0.47
R-PET3%25A-1%PMDA75	4.65	0.35
R-PET3%25A-0.75%PMDA350	4.57	0.46
R-PET3%25A-0.5%PMDA350	5.25	0.18
R-PET3%25A-1%MA350	4.92	0.82
R-PET3%25A-1%MA150	5.48	0.46
R-PET3%25A-1%MA75	4.92	0.11
R-PET3%25A-0.75%MA350	4.55	0.17
R-PET3%25A-0.5%MA350	4.36	0.13
R-PET1%MA-3%25A350	4.53	0.18

A.3 Flexural Data for All Compositions

Table A.3.1 Flexural modulus data for all compositions

Composition	Flexural Modulus (MPa)	std. dev.
R-PET Not Extruded	1894.97	91.61
R-PET Single Extruded	2146.48	62.10
R-PET Double Extruded	2110.79	55.57
R-PET-2%25Asigleextr	2479.15	34.32
R-PET-3%25Asigleextr	2659.98	99.69
R-PET-4%25Asigleextr	2464.41	82.76
R-PET-3%25Adoubleextr	2225.59	55.26
R-PET3%25A-1%PMDA350	2349.41	63.95
R-PET3%25A-1%PMDA150	2384.35	39.81
R-PET3%25A-1%PMDA75	2352.96	49.81
R-PET3%25A-0.75%PMDA350	2253.00	48.35
R-PET3%25A-0.5%PMDA350	2092.38	52.92
R-PET3%25A-1%MA350	2565.76	29.24
R-PET3%25A-1%MA150	2957.31	19.48
R-PET3%25A-1%MA75	2495.49	24.35
R-PET3%25A-0.75%MA350	3125.82	157.94
R-PET3%25A-0.5%MA350	2905.08	119.60
R-PET1%MA-3%25A350	2232.21	46.84

Table A.3.2 Flexural strength data for all compositions

Composition	Flexural Strength (MPa)	std. dev
R-PET Not Extruded	63.73	2.29
R-PET Single Extruded	71.17	1.26
R-PET Double Extruded	69.73	1.99
R-PET-2%25Asigleextr	72.74	2.07
R-PET-3%25Asigleextr	77.76	0.78
R-PET-4%25Asigleextr	52.49	2.63
R-PET-3%25Adoubleextr	68.42	2.21
R-PET3%25A-1%PMDA350	73.33	0.93
R-PET3%25A-1%PMDA150	51.74	2.90
R-PET3%25A-1%PMDA75	68.03	3.91
R-PET3%25A-0.75%PMDA350	70.20	1.51
R-PET3%25A-0.5%PMDA350	72.63	1.45
R-PET3%25A-1%MA350	47.13	2.94
R-PET3%25A-1%MA150	72.44	5.46
R-PET3%25A-1%MA75	39.01	5.26
R-PET3%25A-0.75%MA350	39.83	4.84
R-PET3%25A-0.5%MA350	31.21	1.93
R-PET1%MA-3%25A350	55.80	2.32

Table A.3.3 Flexural strain at break (%) data for all compositions

Composition	Flexural Strain at Break (%)	std. dev
R-PET Not Extruded	No Break	No Break
R-PET Single Extruded	No Break	No Break
R-PET Double Extruded	No Break	No Break
R-PET-2%25Asigleextr	3.96	0.47
R-PET-3%25Asigleextr	6.04	1.87
R-PET-4%25Asigleextr	2.26	0.20
R-PET-3%25Adoubleextr	5.79	0.89
R-PET3%25A-1%PMDA350	No Break	No Break
R-PET3%25A-1%PMDA150	2.22	0.17
R-PET3%25A-1%PMDA75	3.16	0.20
R-PET3%25A-0.75%PMDA350	No Break	No Break
R-PET3%25A-0.5%PMDA350	4.22	0.42
R-PET3%25A-1%MA350	1.76	0.09
R-PET3%25A-1%MA150	2.55	0.16
R-PET3%25A-1%MA75	1.41	0.05
R-PET3%25A-0.75%MA350	1.45	0.22
R-PET3%25A-0.5%MA350	0.96	0.11
R-PET1%MA-3%25A350	2.24	0.20

A.4 Impact Strength Data

A.4.1 Impact strength data for all compositions

Composition	Impact Strength (MPa)	std. dev.
R-PET Not Extruded	46.51	2.00
R-PET Single Extruded	15.22	1.56
R-PET Double Extruded	9.60	0.84
R-PET-2%25Asigleextr	7.71	0.26
R-PET-3%25Asigleextr	9.14	1.13
R-PET-4%25Asigleextr	4.28	0.86
R-PET-3%25Adoubleextr	8.42	0.72
R-PET3%25A-1%PMDA350	6.29	0.49
R-PET3%25A-1%PMDA150	4.34	0.22
R-PET3%25A-1%PMDA75	4.84	0.23
R-PET3%25A-0.75%PMDA350	5.40	0.67
R-PET3%25A-0.5%PMDA350	5.51	0.66
R-PET3%25A-1%MA350	6.64	0.95
R-PET3%25A-1%MA150	6.04	0.60
R-PET3%25A-1%MA75	4.21	0.31
R-PET3%25A-0.75%MA350	4.89	0.13
R-PET3%25A-0.5%MA350	4.26	0.43
R-PET1%MA-3%25A350	4.18	0.15

APPENDIX B

DIFFERENTIAL SCANNING CALORIMETER (DSC) ANALYSIS

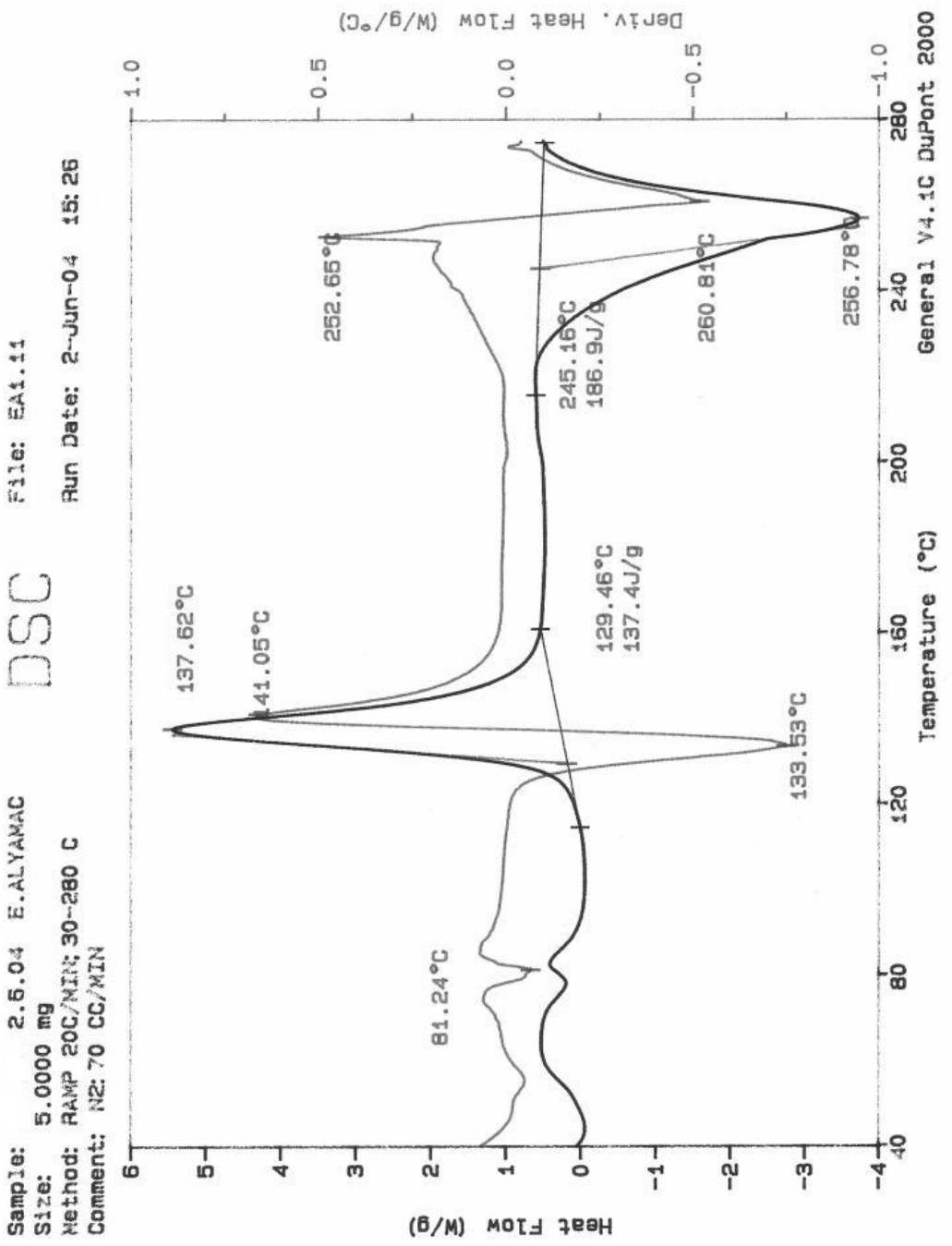

Figure B.1 DSC diagram of single extruded recycled PET

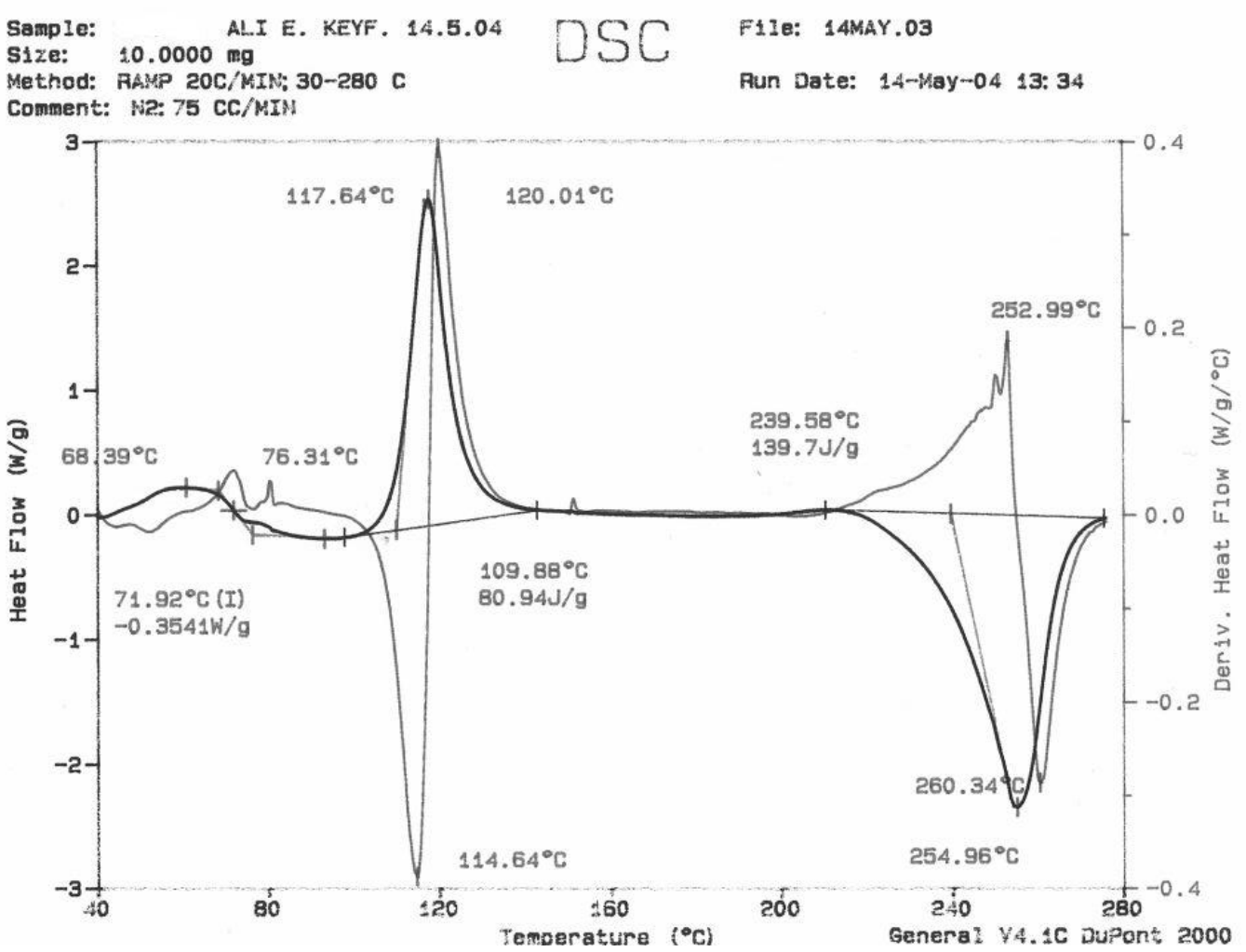

Figure B.2 DSC diagram of the sample containing 3 weight % Cloisite25A at 350 rpm

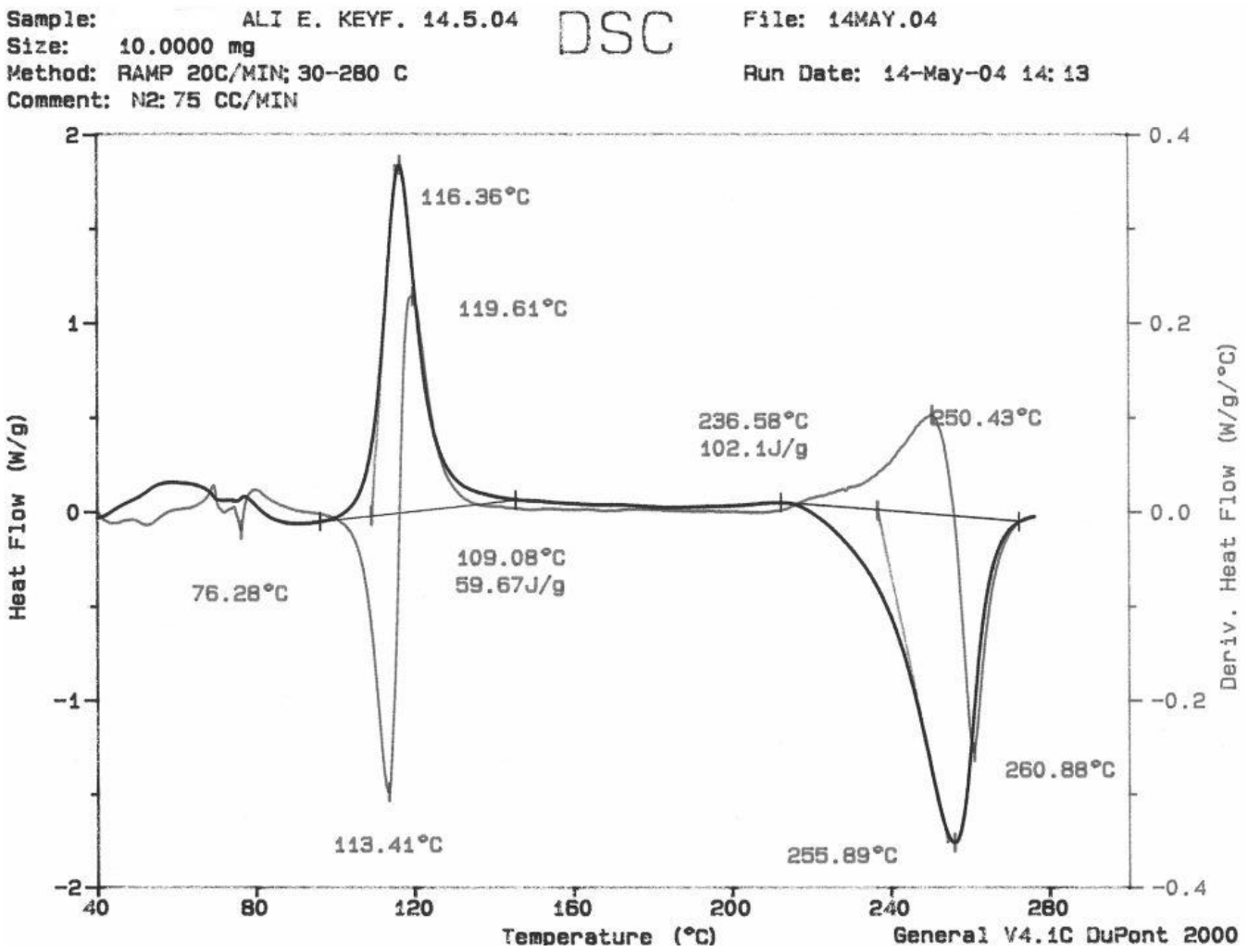

Figure B.3 DSC diagram of the sample containing double extruded 3 weight % Cloisite25A at 350 rpm

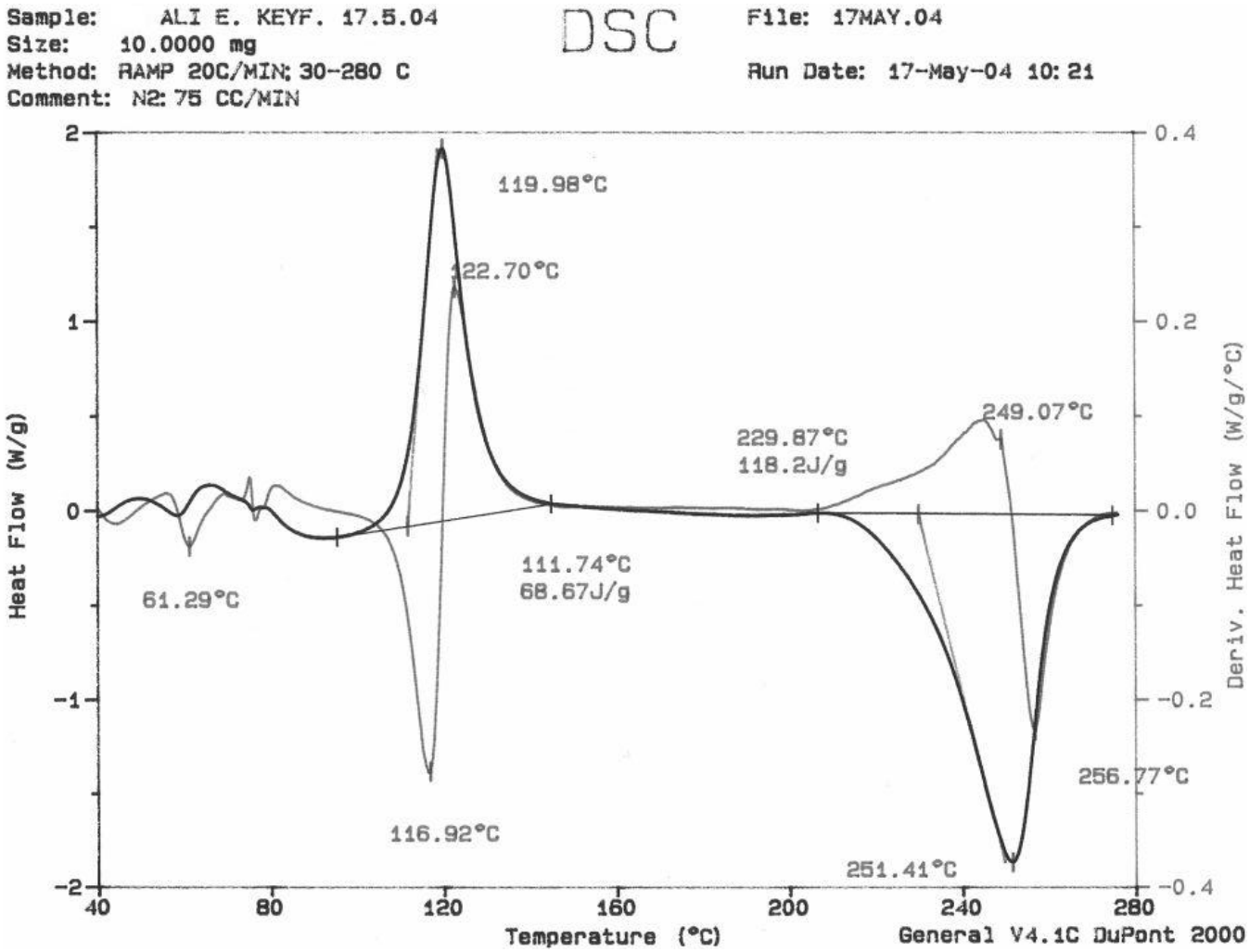

Figure B.4 DSC diagram of the sample containing 3 weight % Cloisite25A and 1 weight % PMDA at 350 rpm

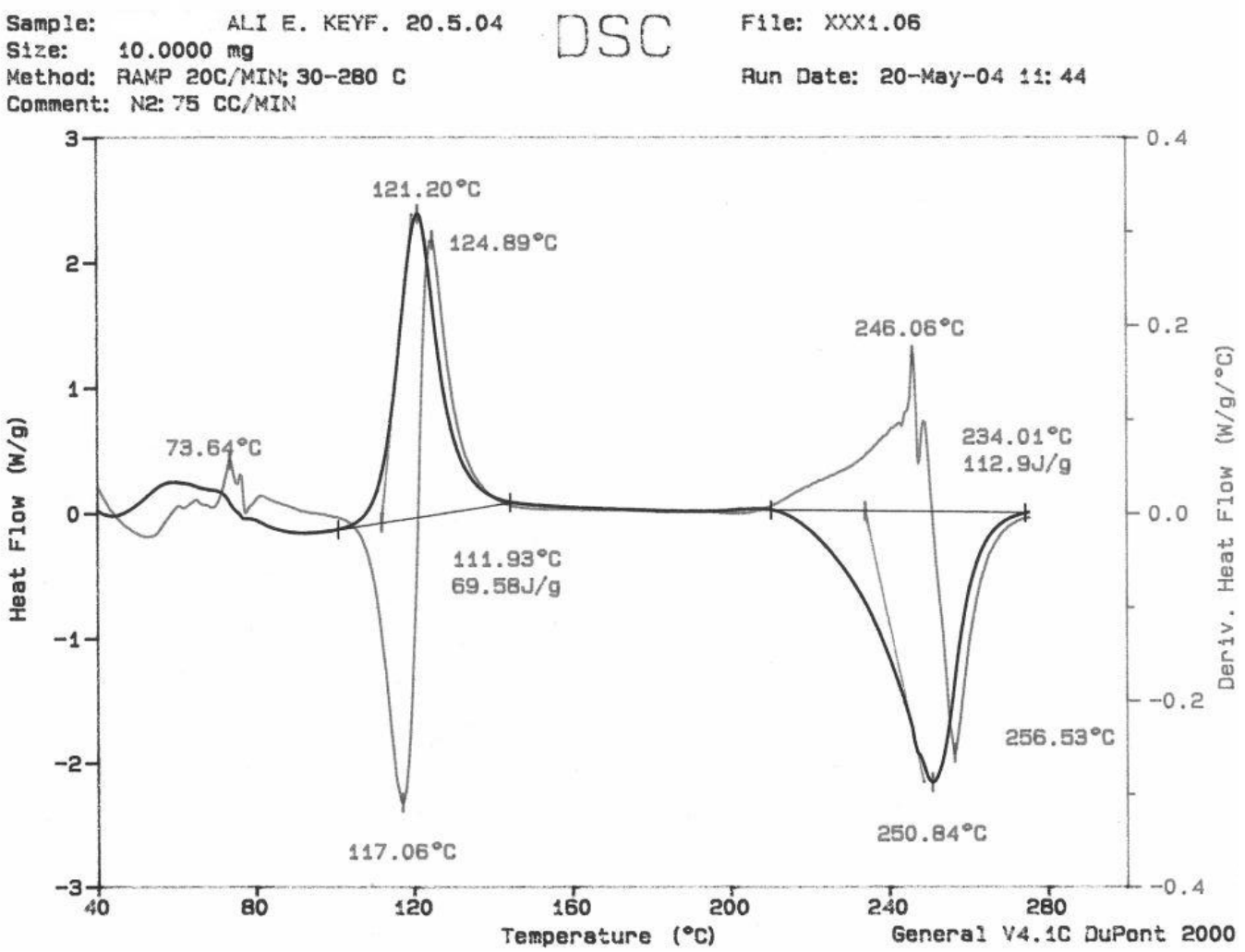

Figure B.5 DSC diagram of the sample containing 3 weight % Cloisite25A and 1 weight % PMDA at 150 rpm

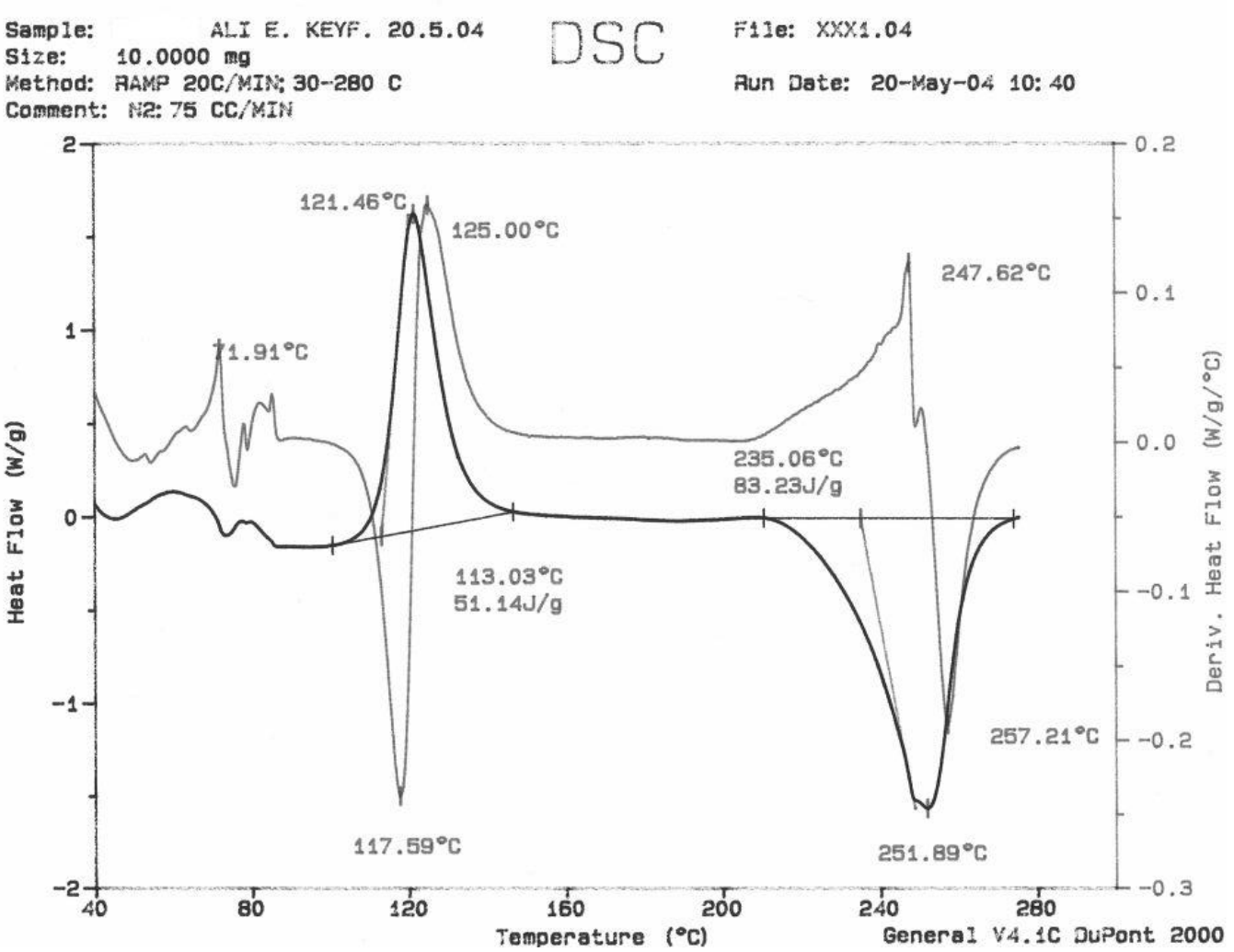

Figure B.6 DSC diagram of the sample containing 3 weight % Cloisite25A and 1 weight % PMDA at 75 rpm

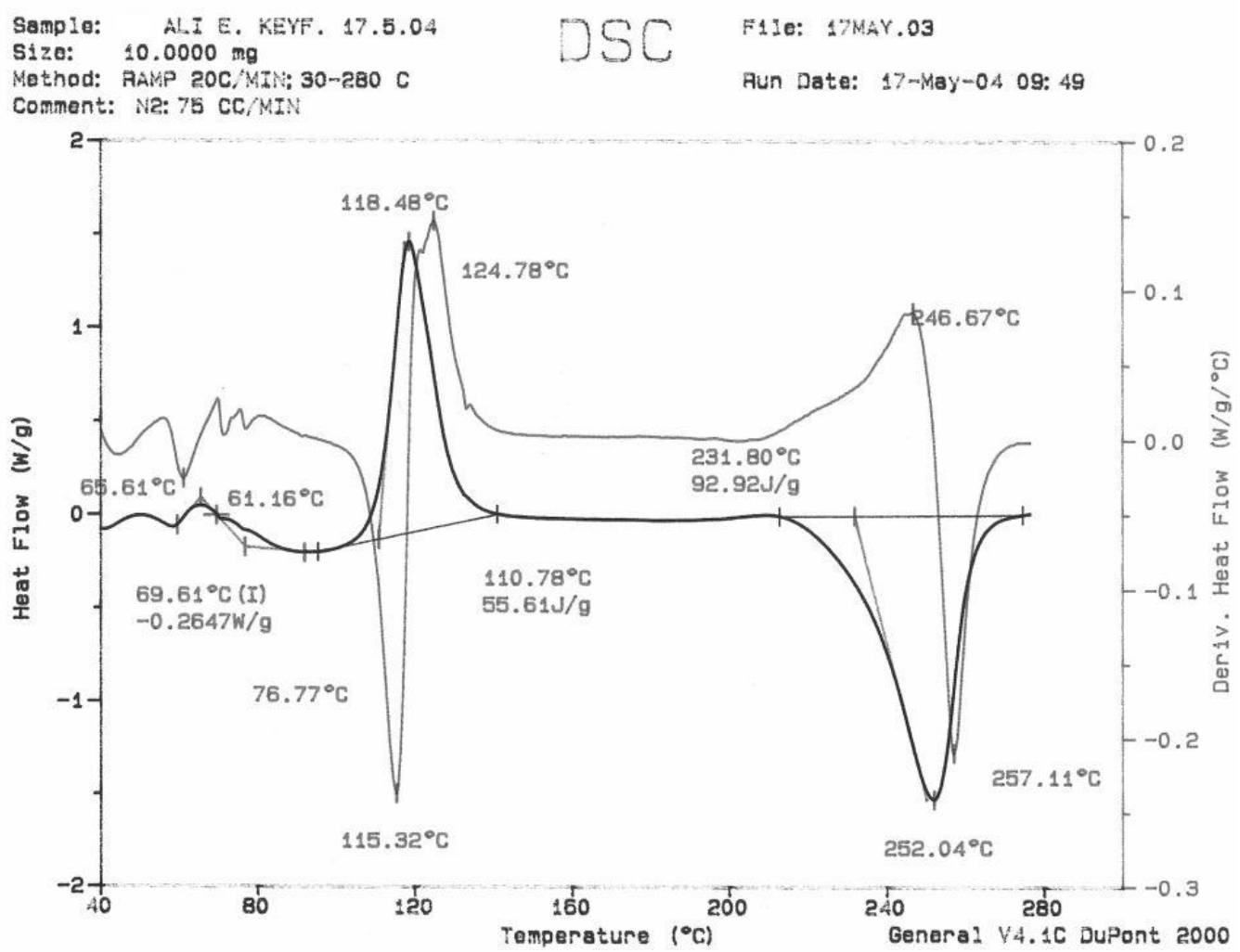

Figure B.7 DSC diagram of the sample containing 3 weight % Cloisite 25A and 0.75 weight % PMDA at 350 rpm

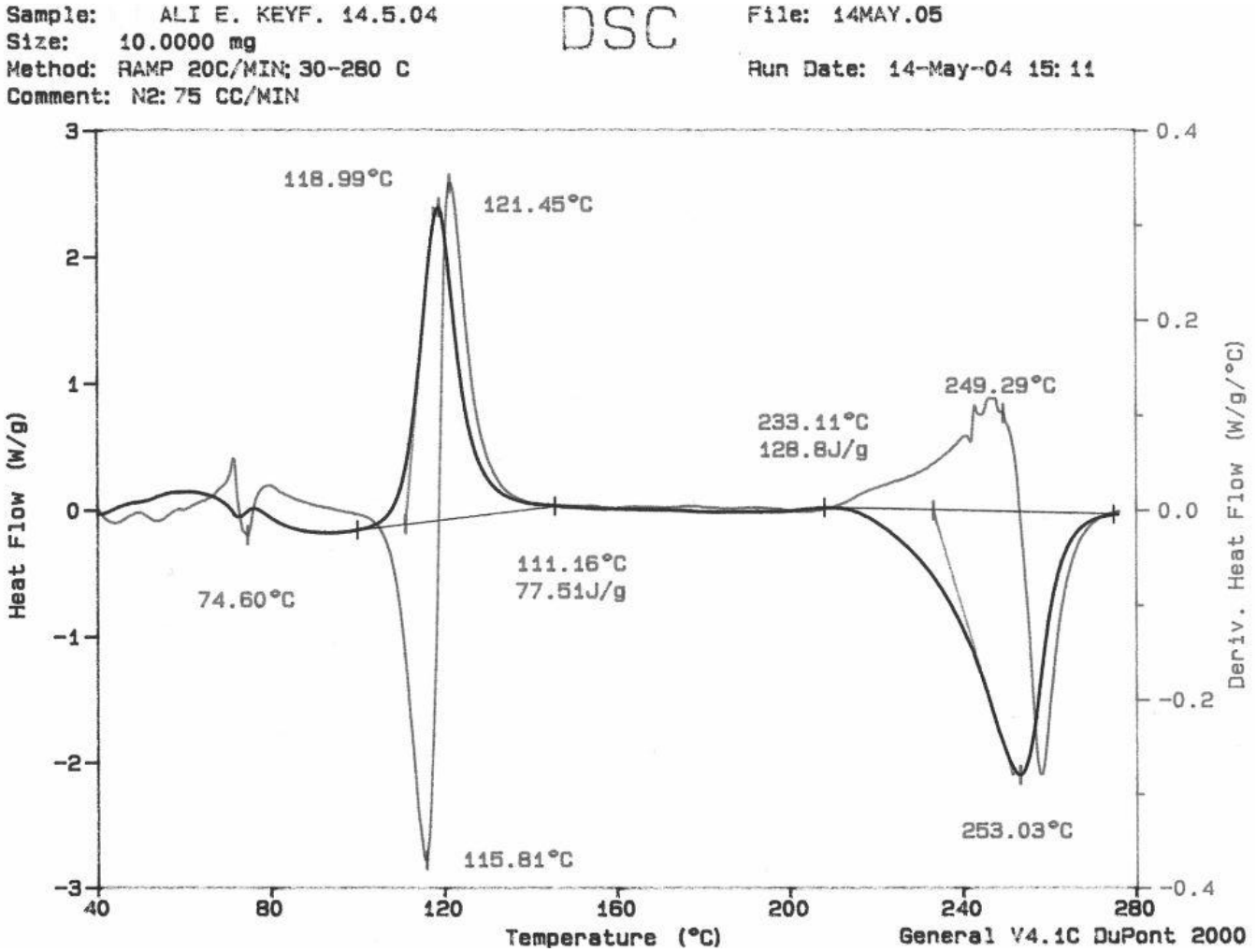

Figure B.8 DSC diagram of the sample containing 3 weight % Cloisite25A and 0.5 weight % PMDA at 350 rpm

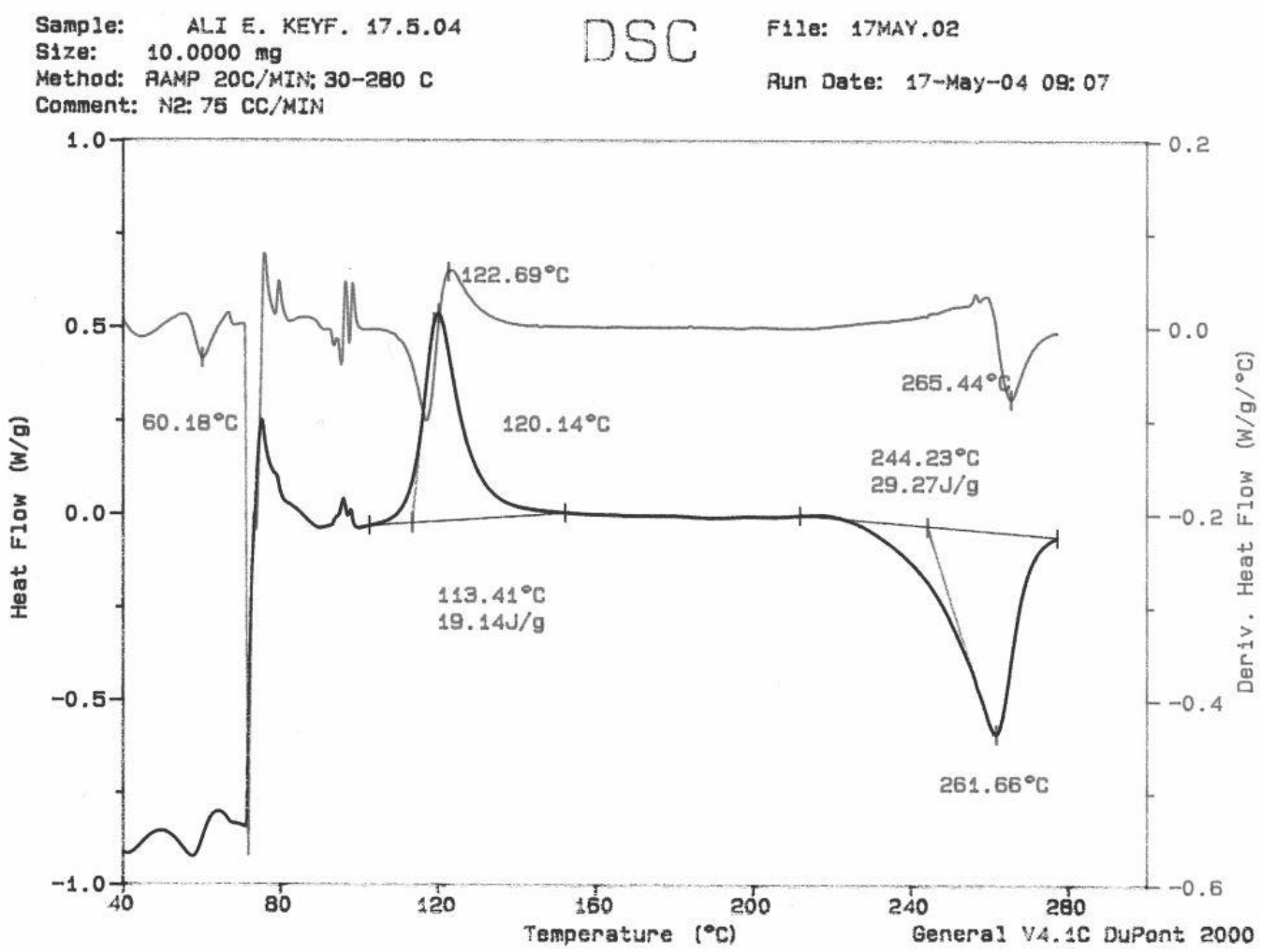

Figure B.9 DSC diagram of the sample containing 3 weight % Cloisite25A and 1 weight % MA at 350 rpm

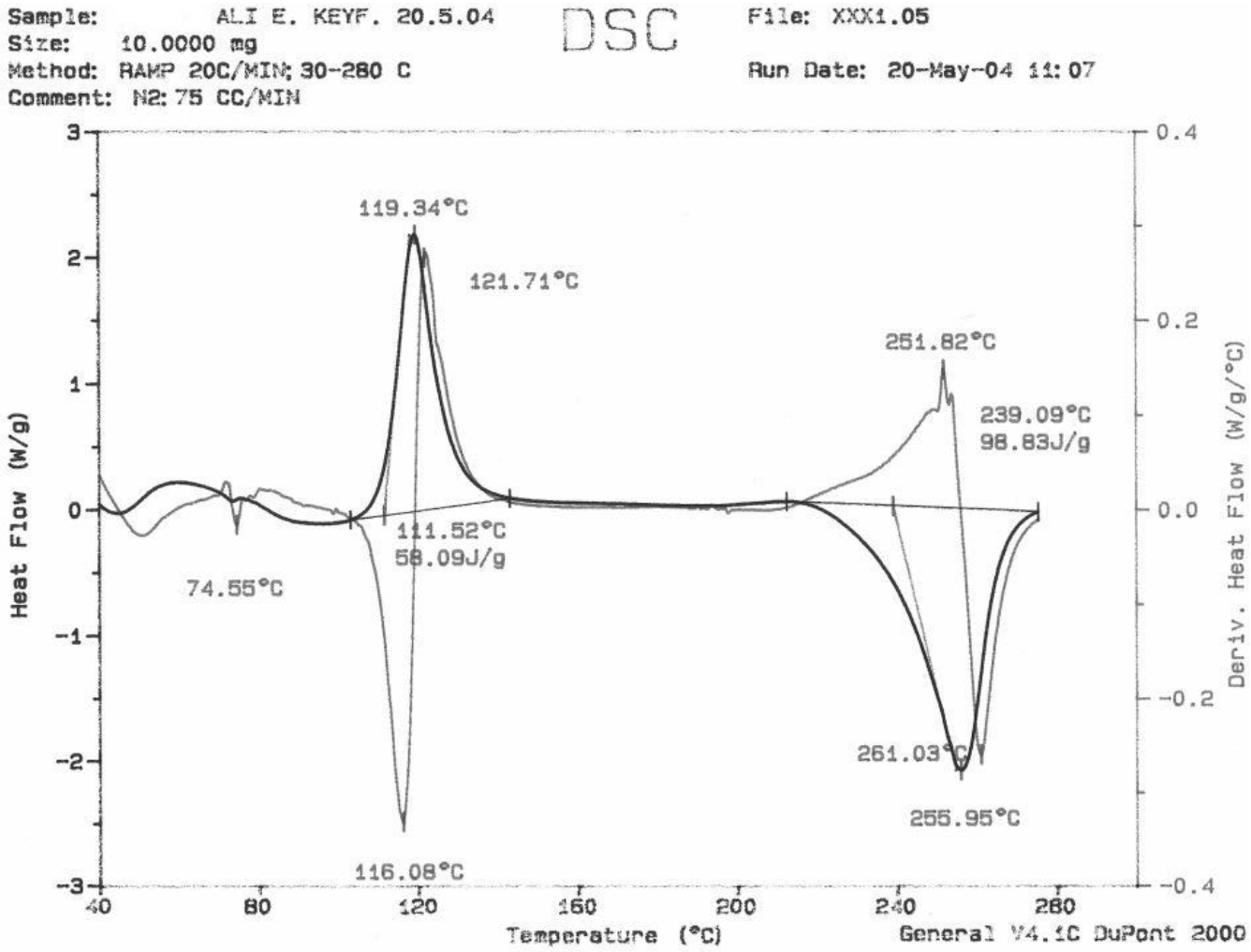

Figure B.10 DSC diagram of the sample containing 3 weight % Cloisite25A and 1 weight % MA at 150 rpm

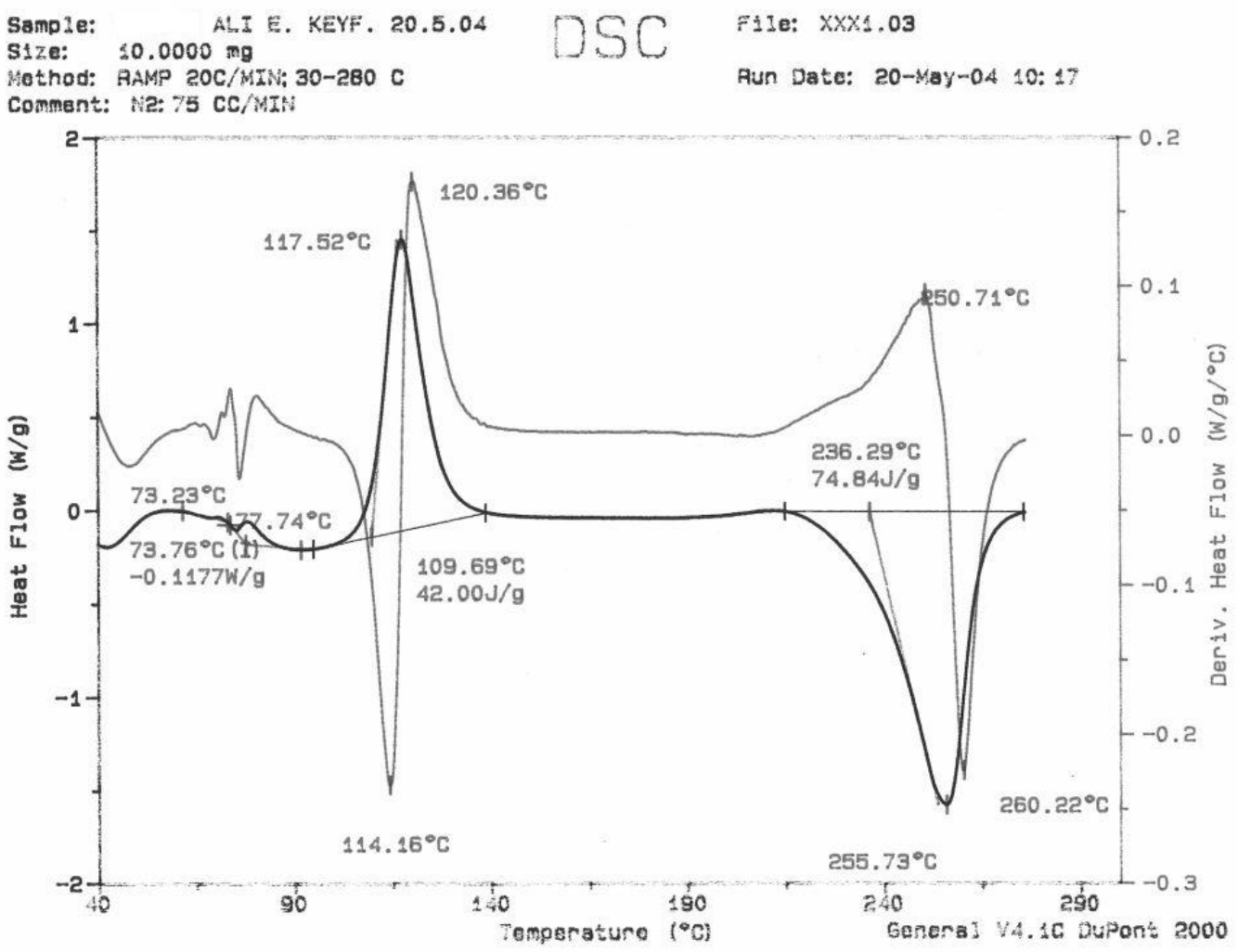

Figure B.11 DSC diagram of the sample containing 3 weight % Cloisite25A and 1 weight % MA at 75 rpm

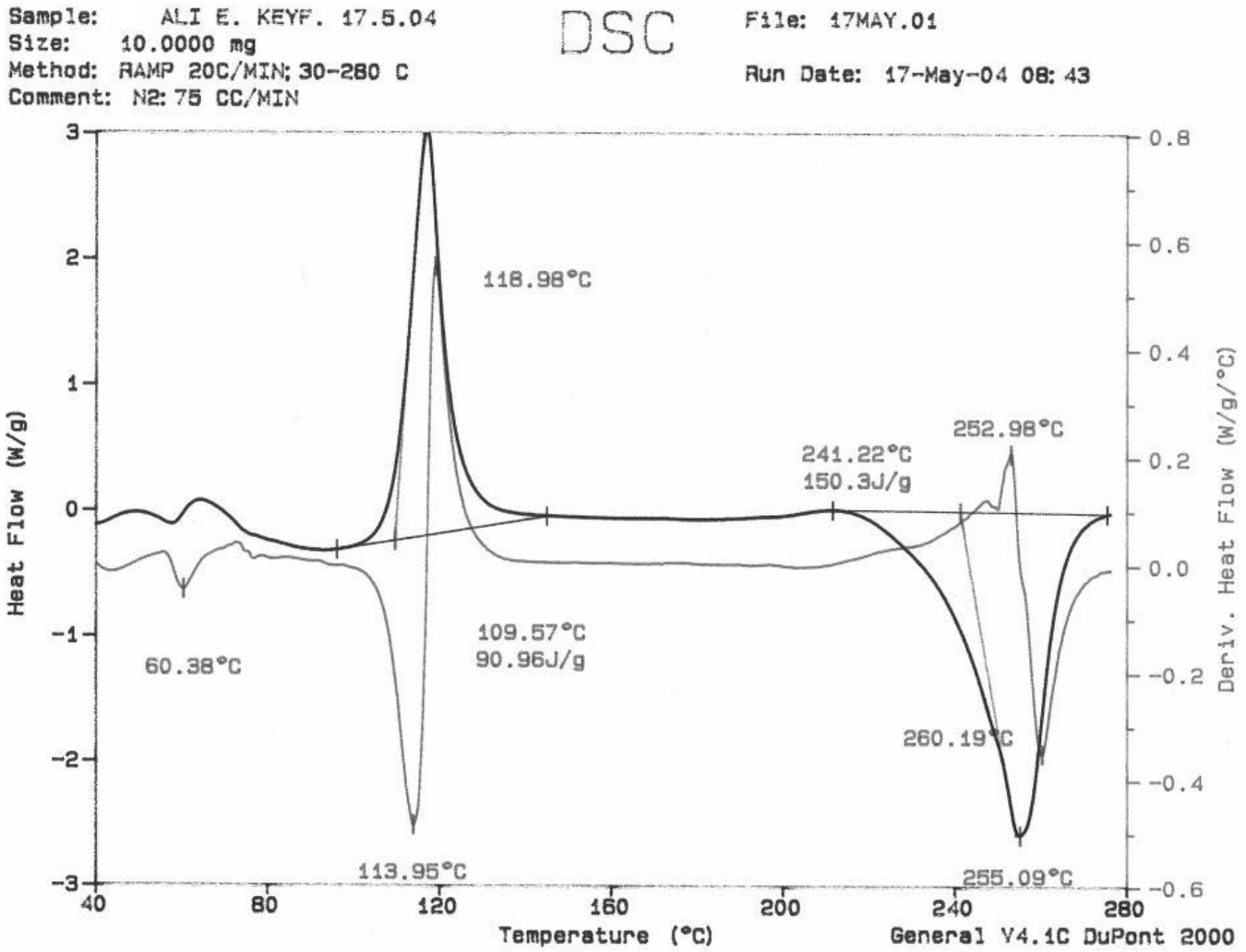

Figure B.12 DSC diagram of the sample containing 3 weight % Cloisite25A and 0.75 weight % MA at 350 rpm

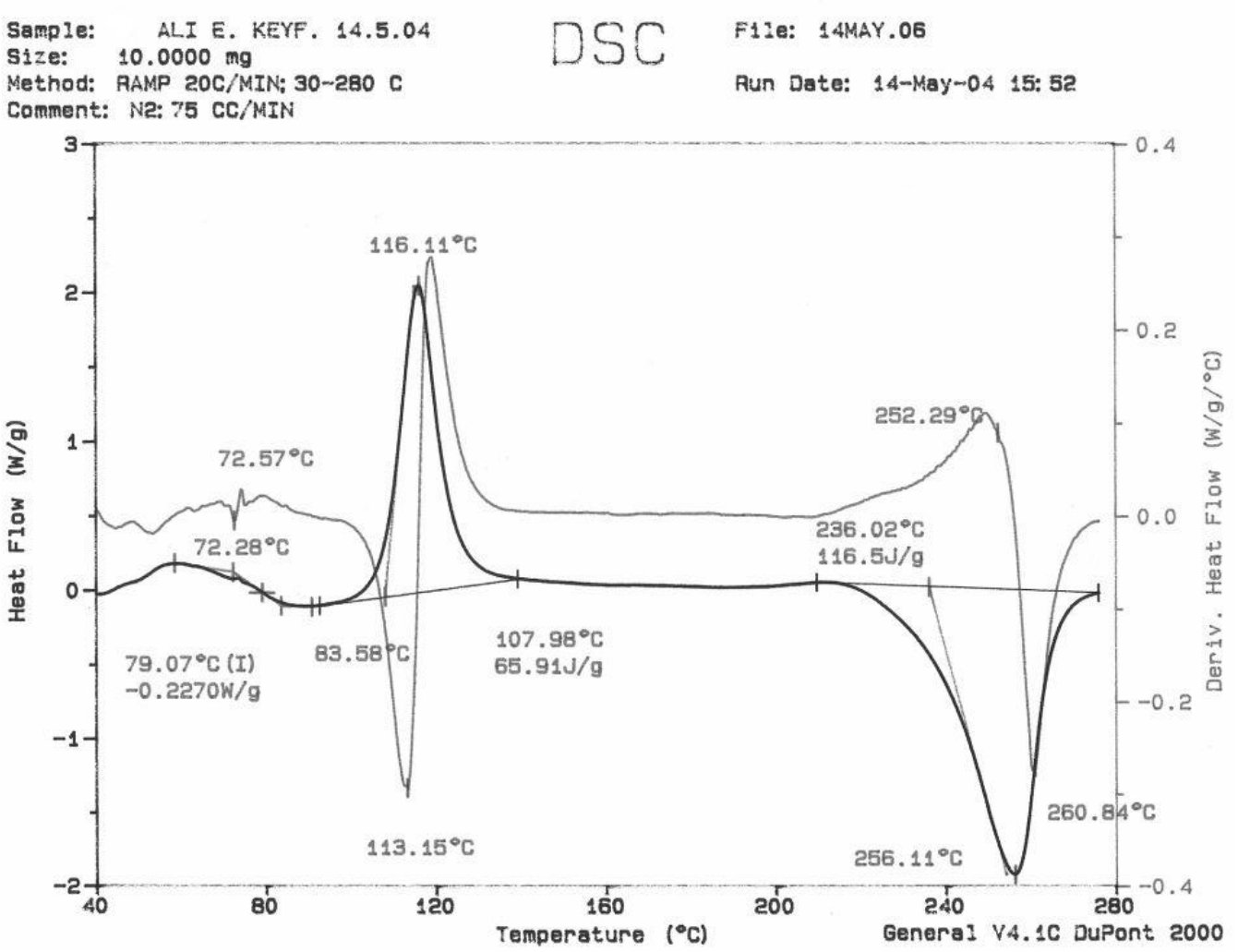

Figure B.13 DSC diagram of the sample containing 3 weight % Cloisite25A and 0.5 weight % MA at 350 rpm

APPENDIX C

X-RAY ANALYSIS

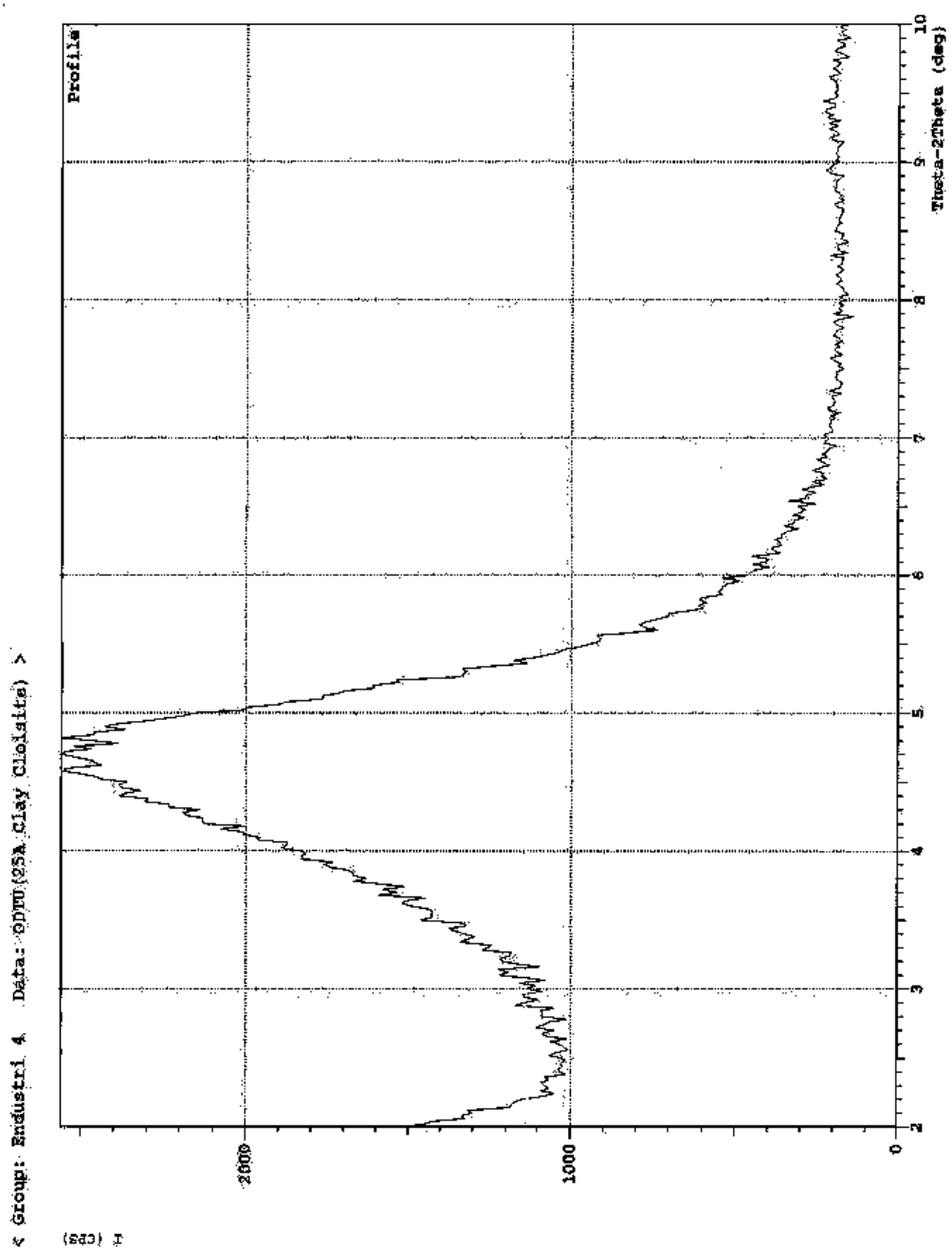

Figure C.1 XRD pattern of Cloisite 25A

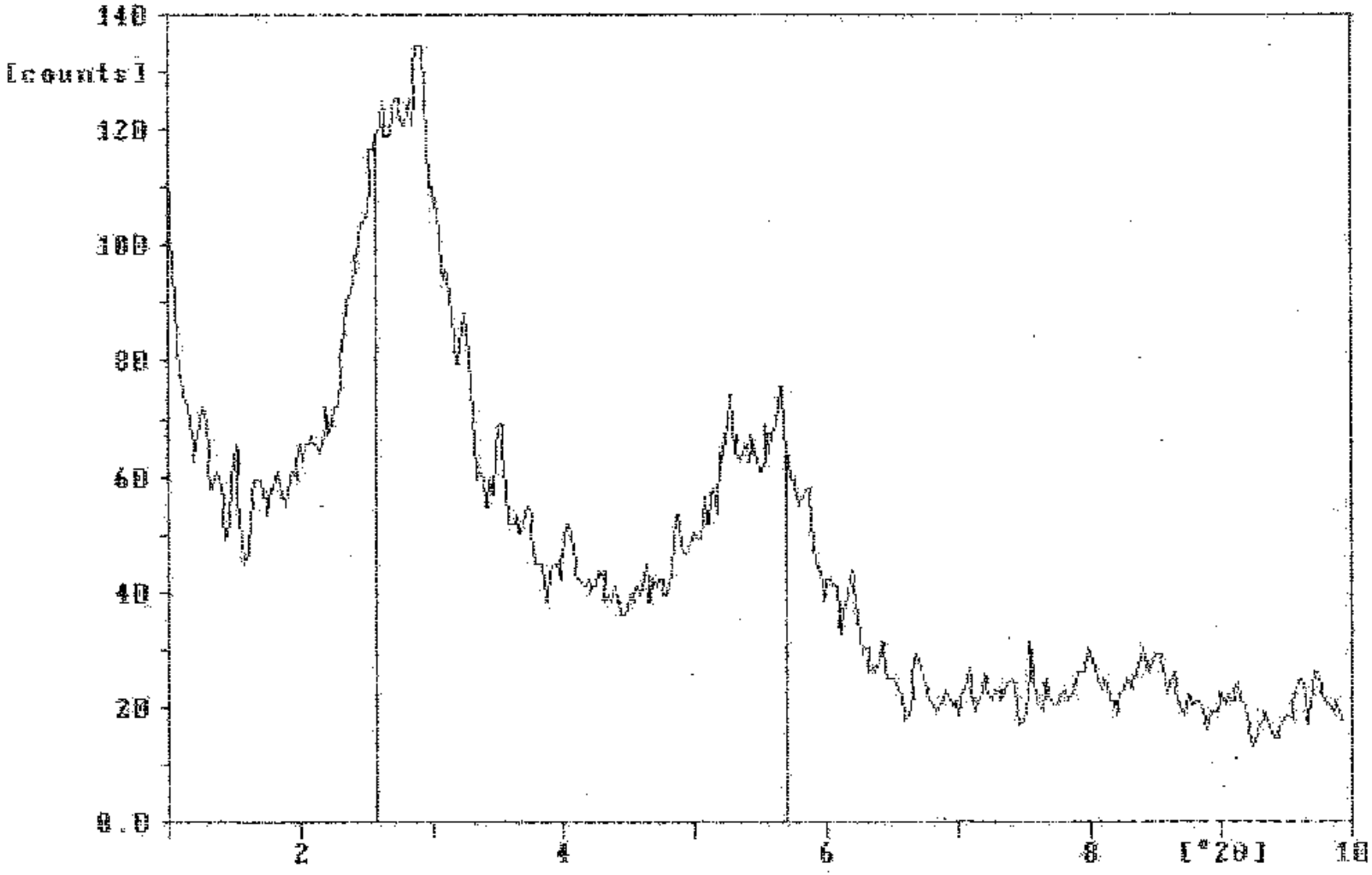

Figure C.2 XRD pattern of sample containing 2 weight % Cloiste 25A at 350 rpm

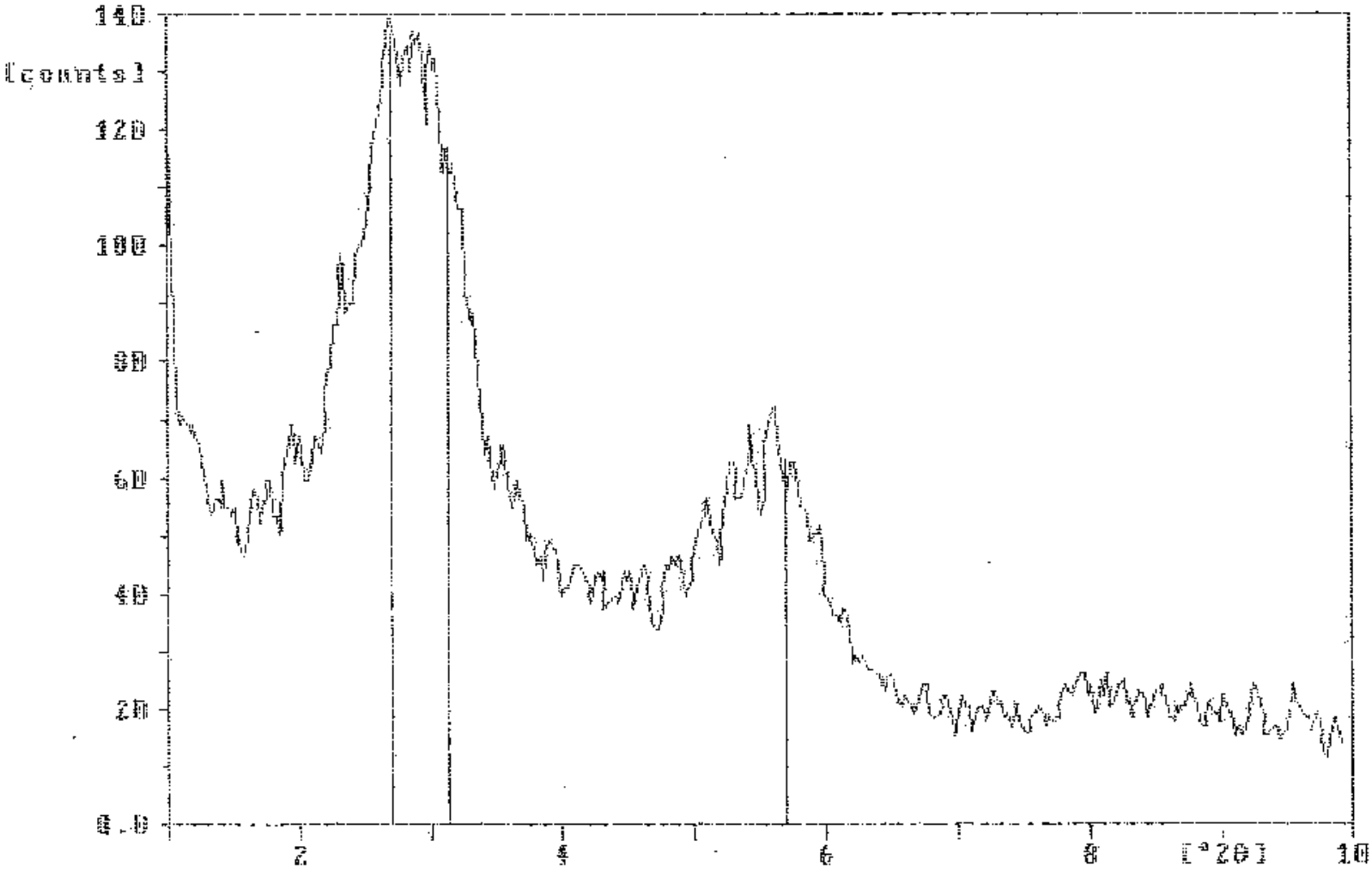

Figure C.3 XRD pattern of sample containing 3 weight % Cloiste 25A at 350 rpm

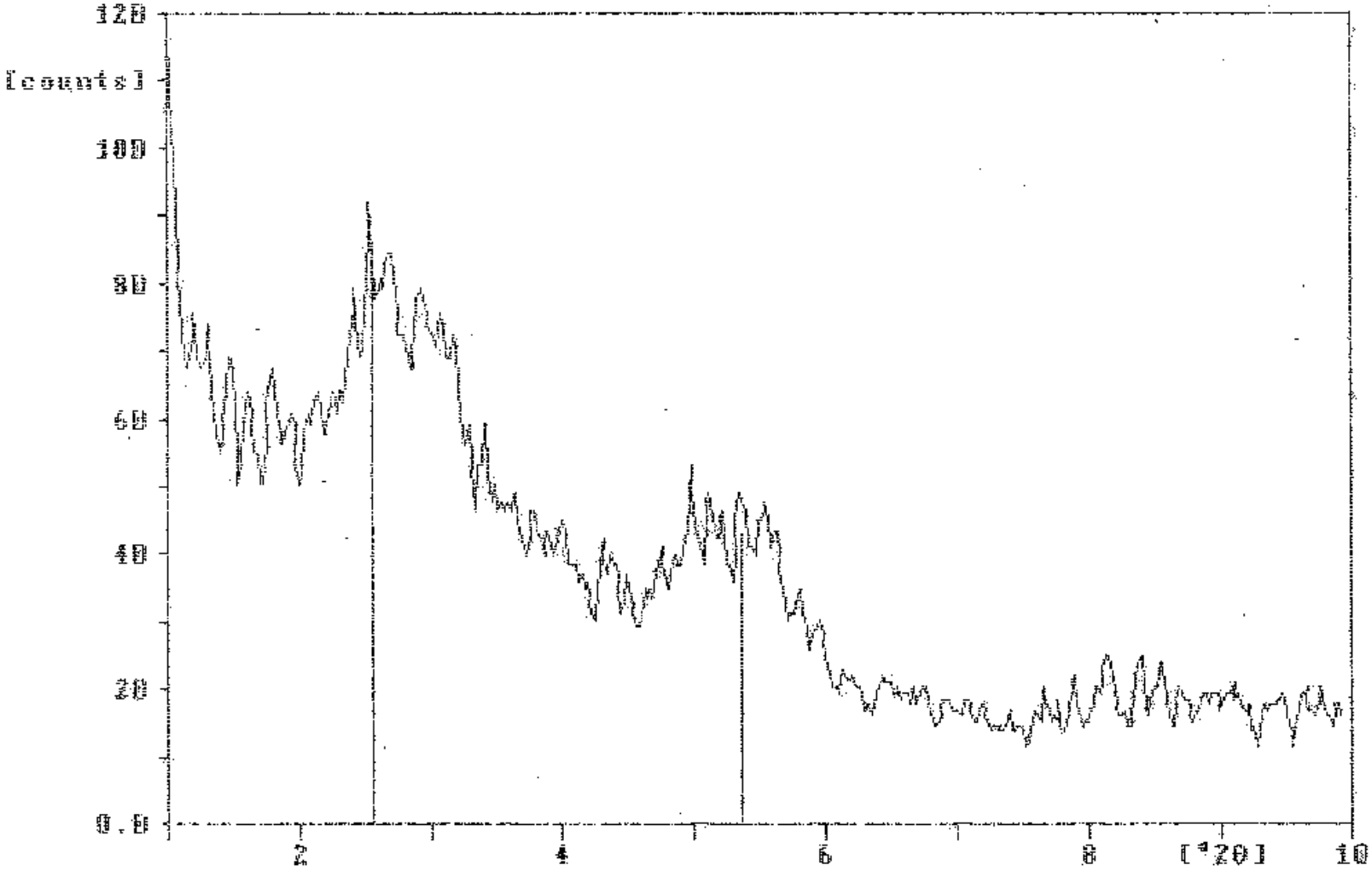

Figure C.4 XRD pattern of sample containing 4 weight % Cloiste 25A at 350 rpm

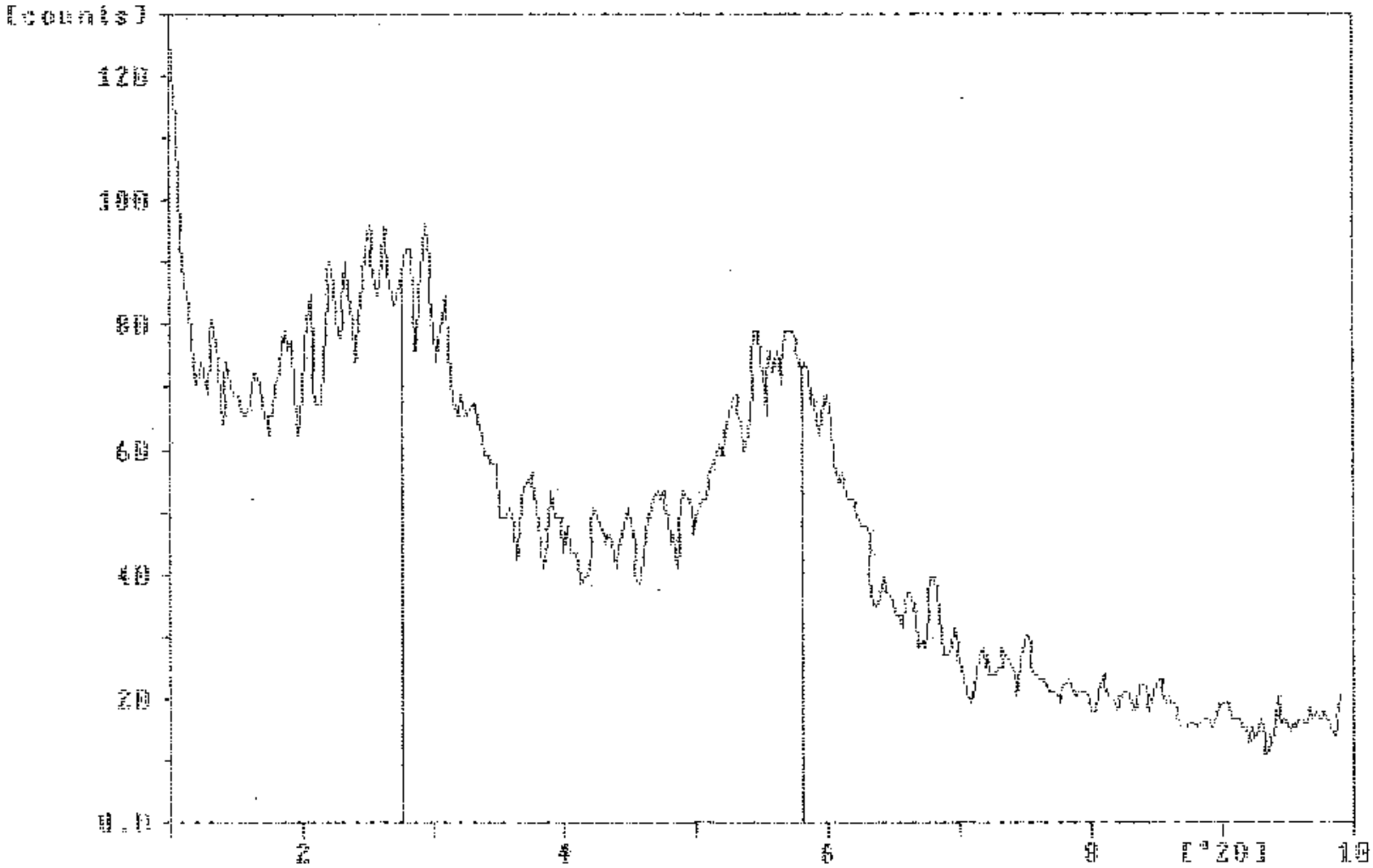

Figure C.5 XRD pattern of sample containing double extruded 3 weight % Cloiste 25A at 350 rpm

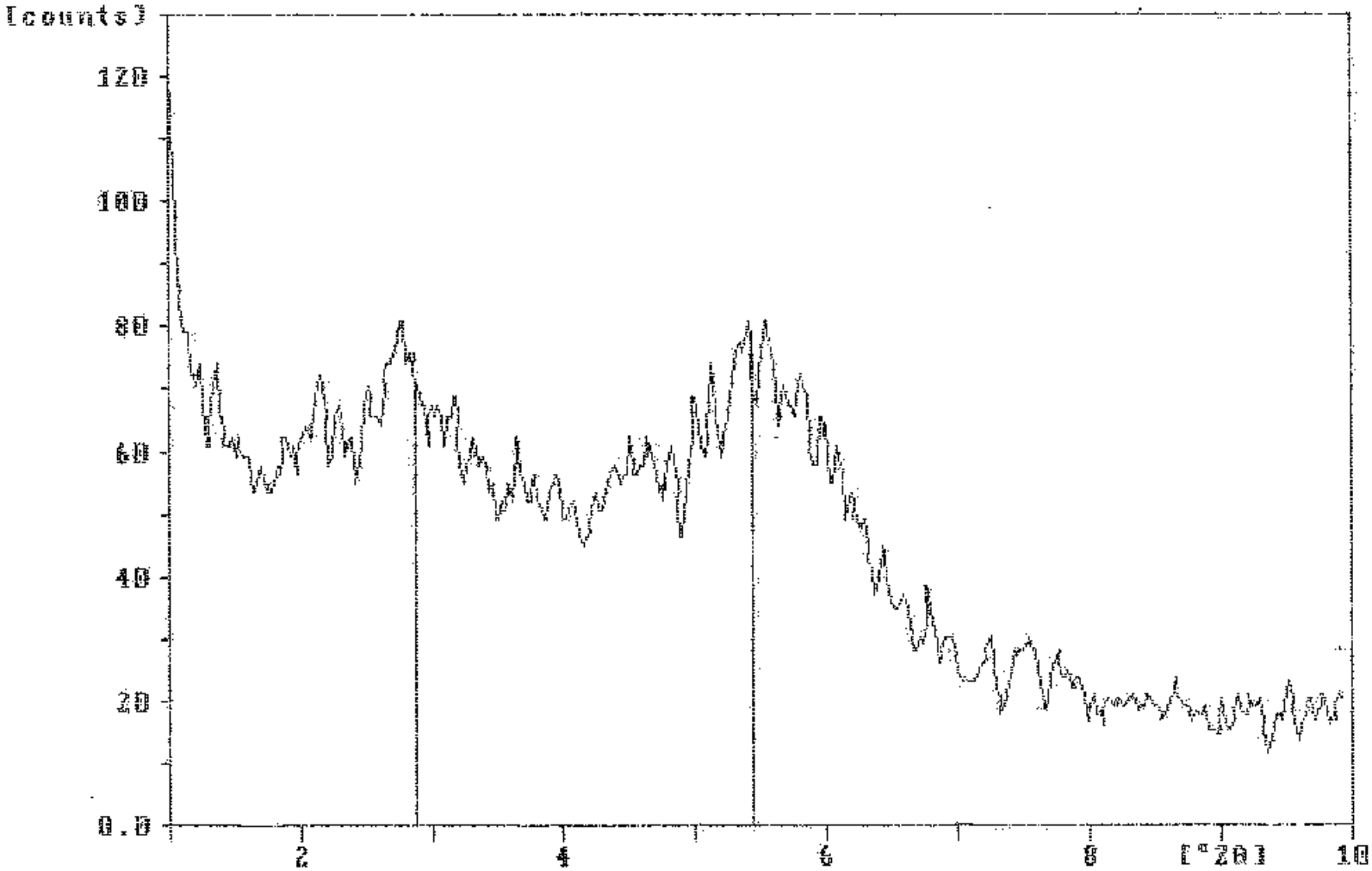

Figure C.6 XRD pattern of sample containing 3 weight % Cloiste 25A and 1 weight % PMDA at 350 rpm

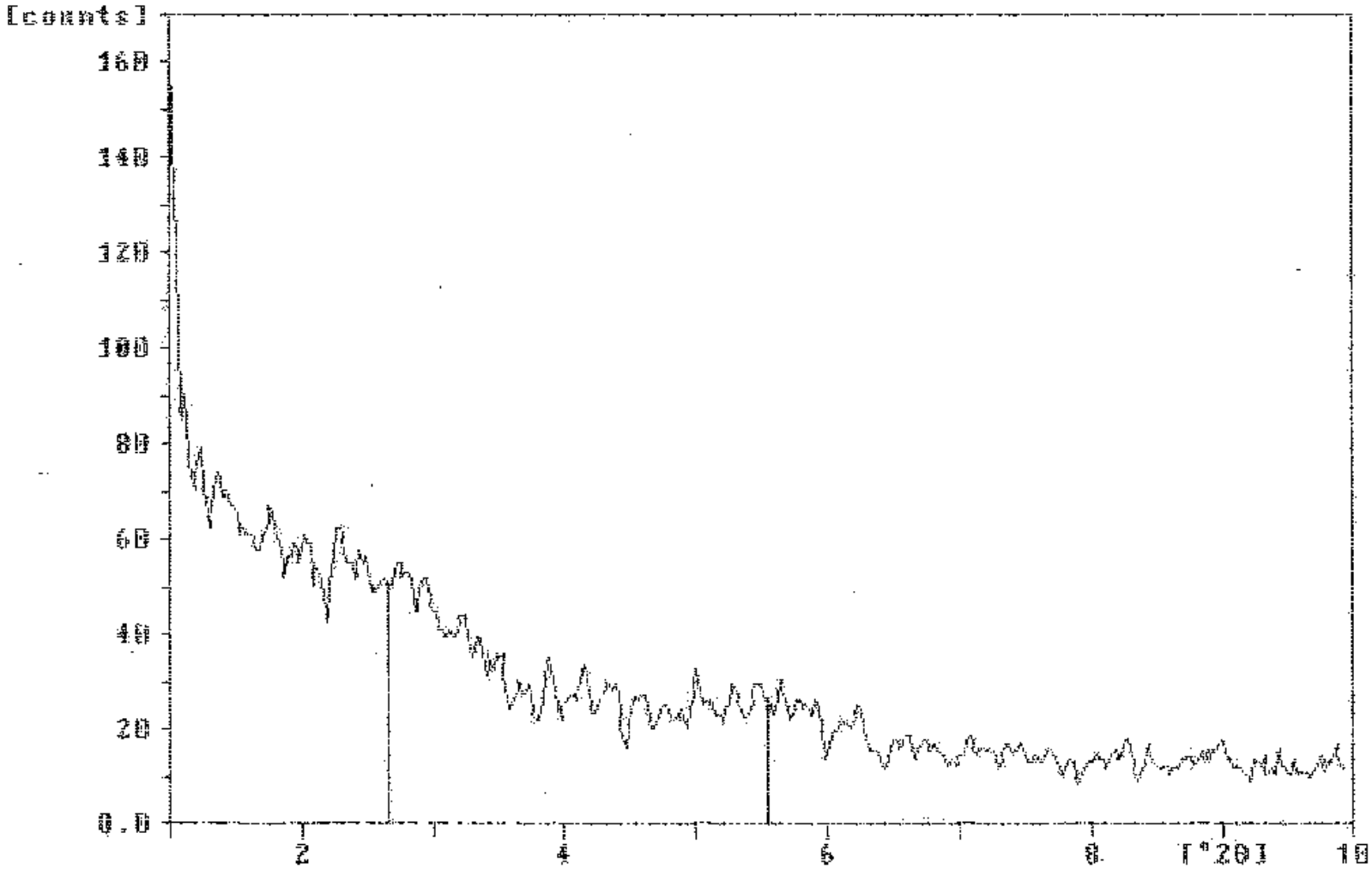

Figure C.7 XRD pattern of sample containing 3 weight % Cloiste 25A and 1 weight % PMDA at 150 rpm

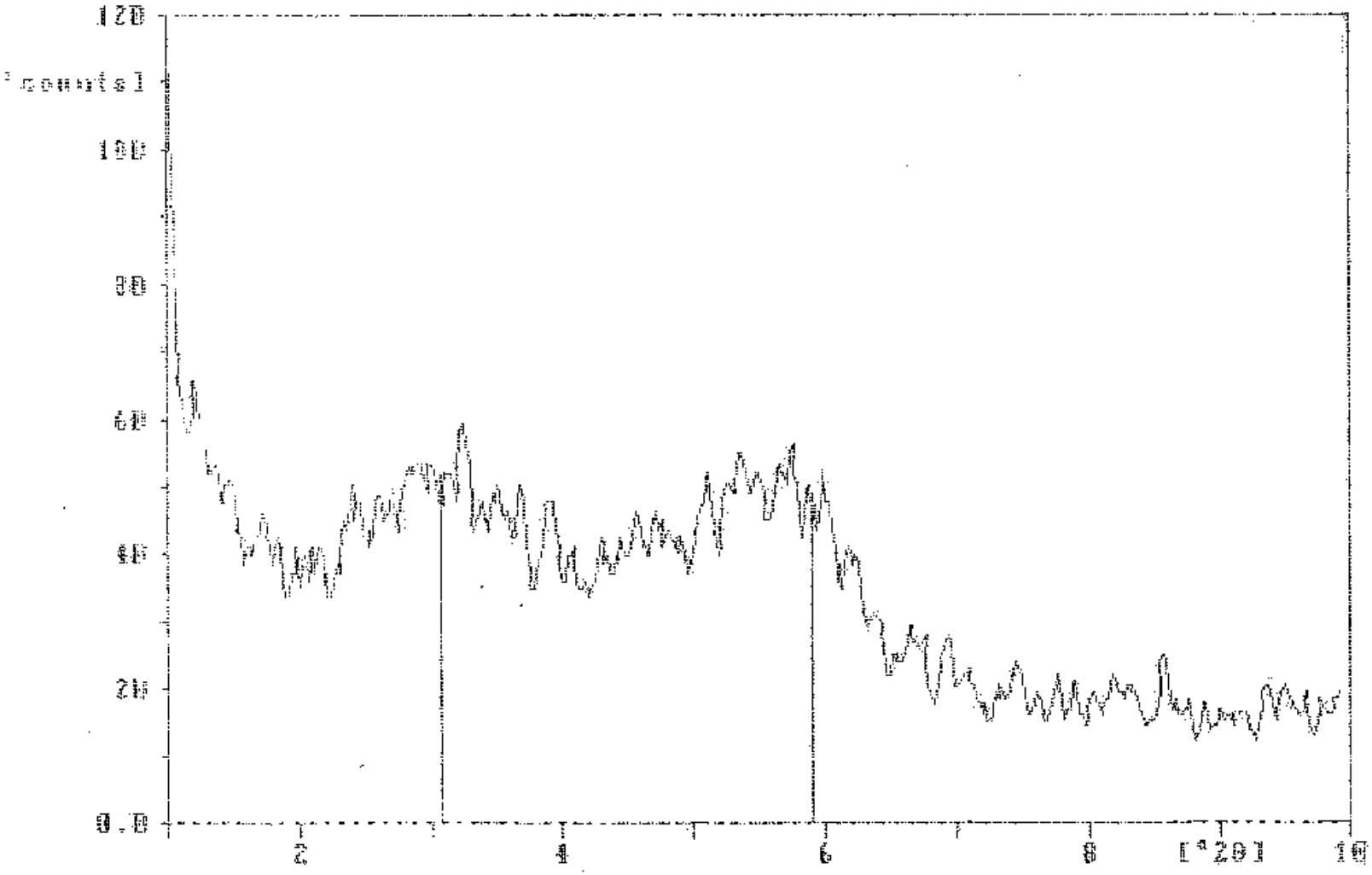

Figure C.8 XRD pattern of sample containing 3 weight % Cloiste 25A and 1 weight % PMDA at 75 rpm

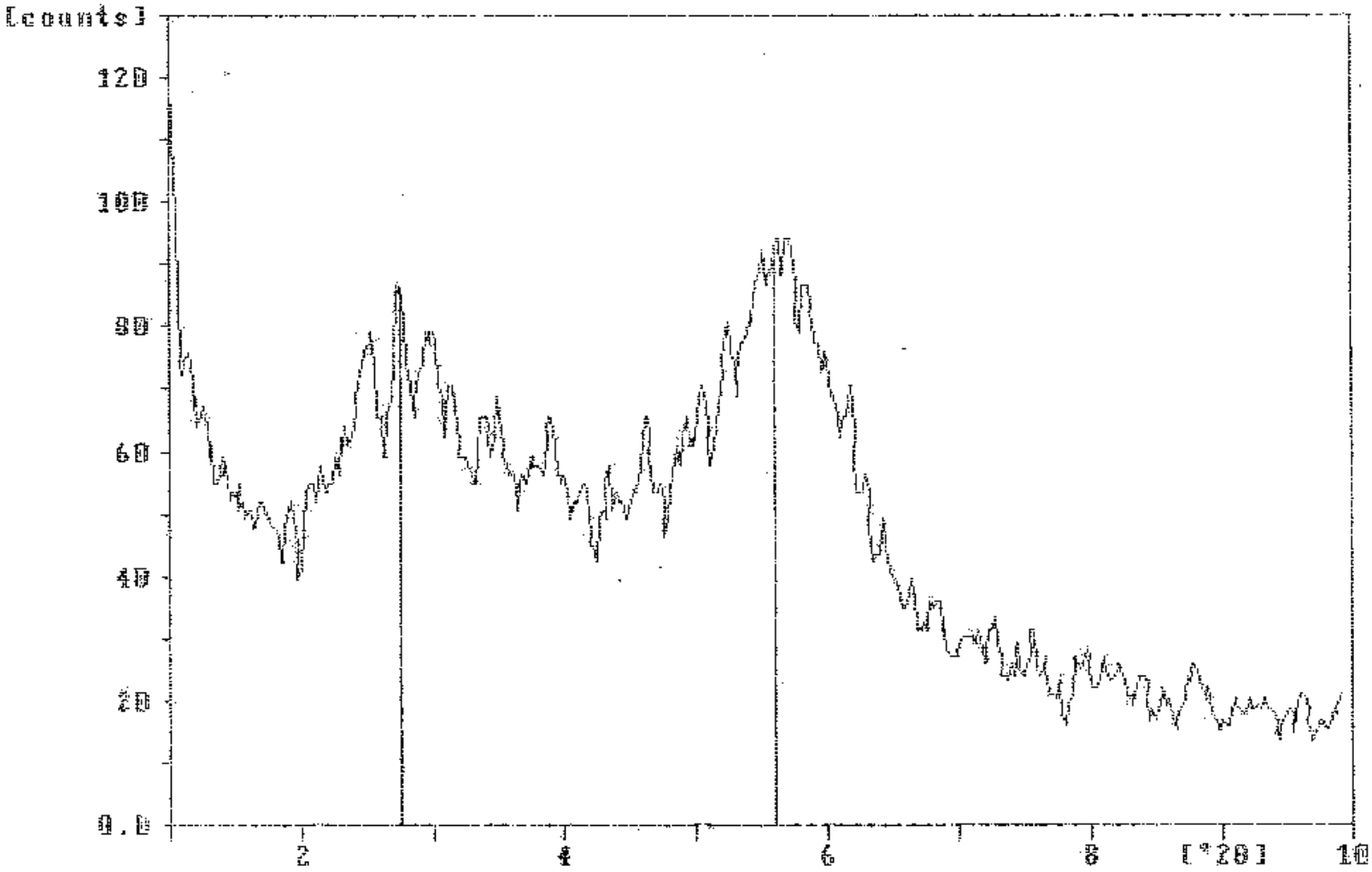

Figure C.9 XRD pattern of sample containing 3 weight % Cloiste 25A and 0.75 weight % PMDA at 350 rpm

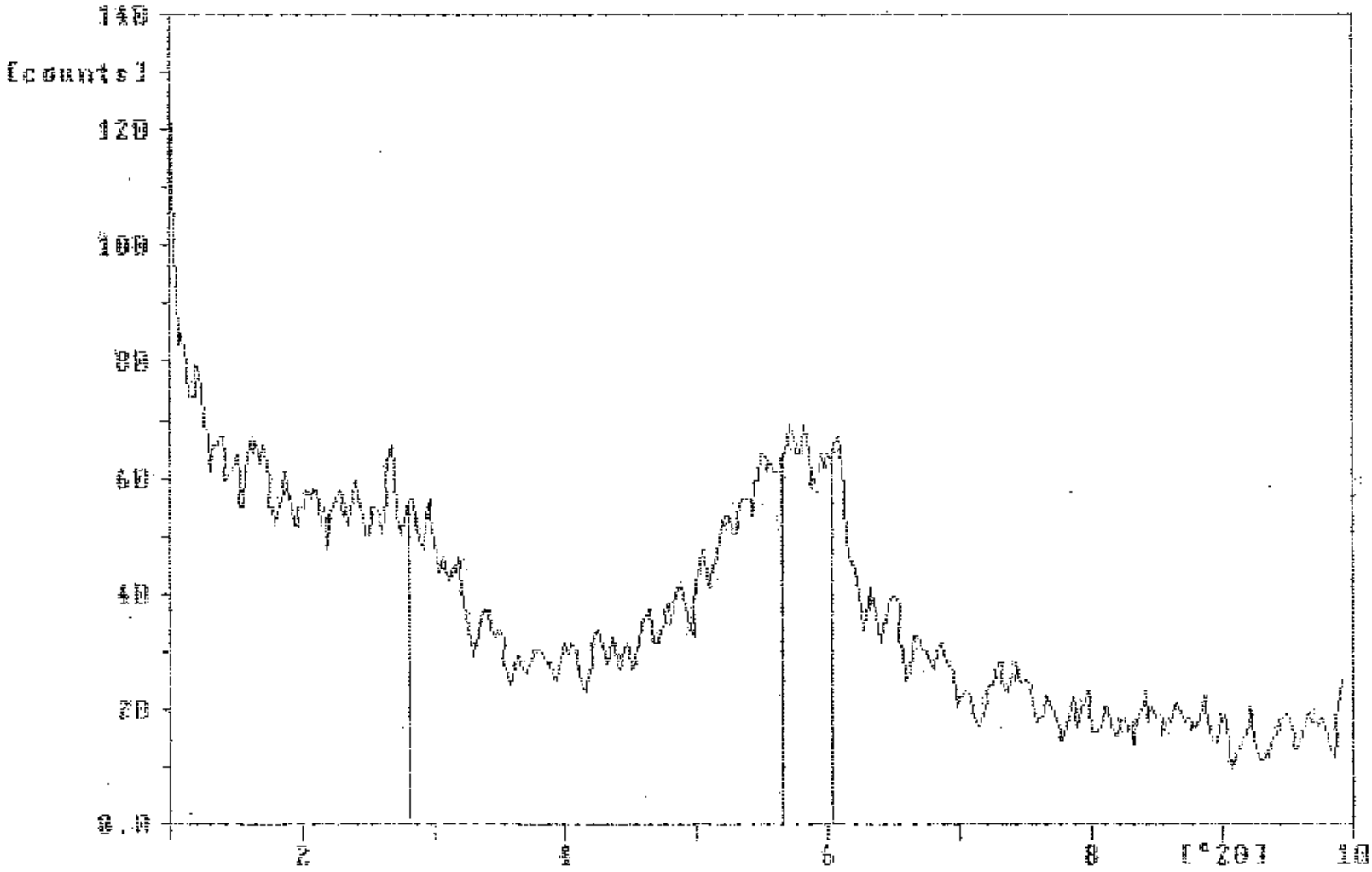

Figure C.10 XRD pattern of sample containing 3 weight % Cloiste 25A and 0.5 weight % PMDA at 350 rpm

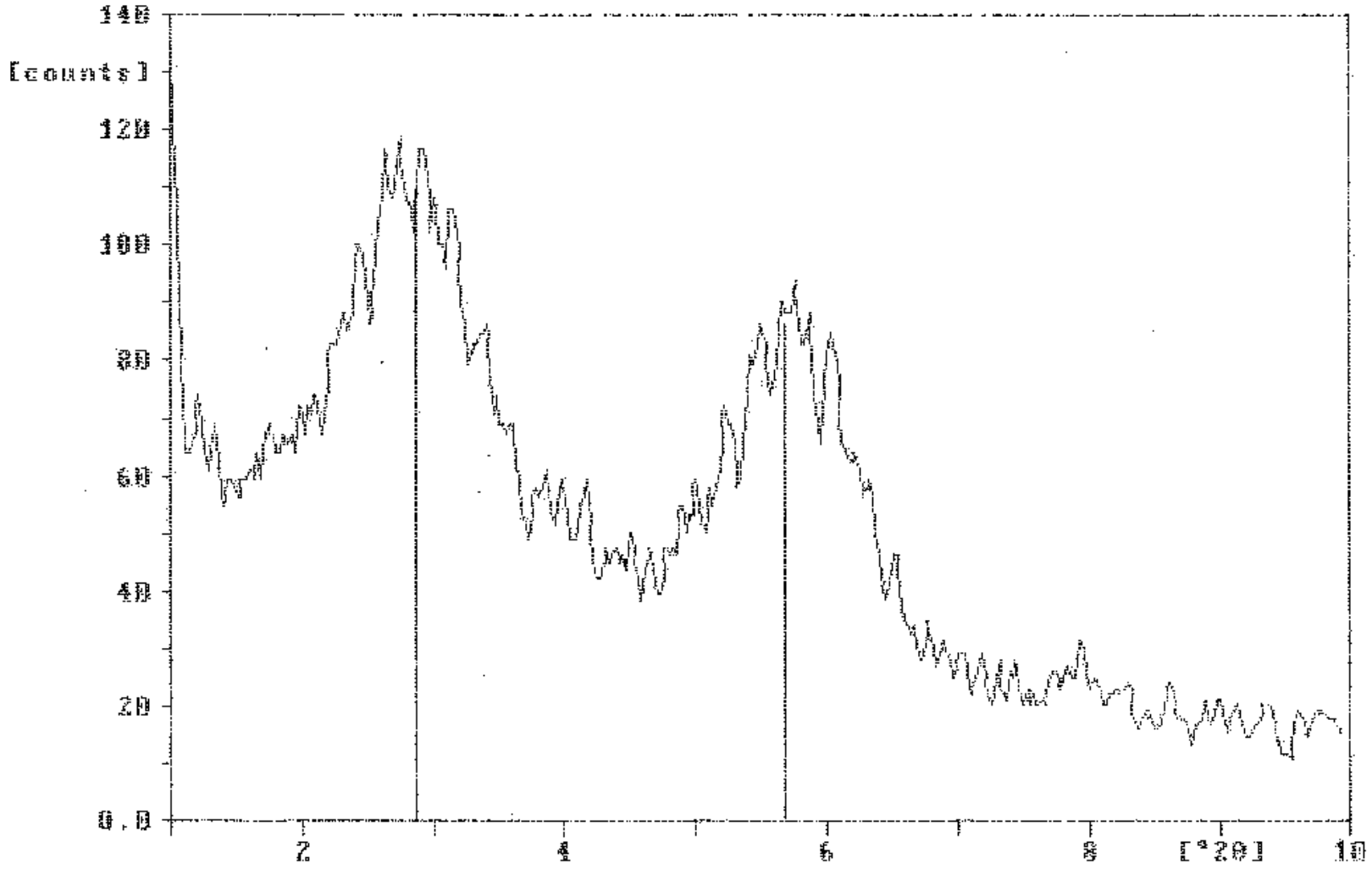

Figure C.11 XRD pattern of sample containing 3 weight % Cloiste 25A and 1 weight % MA at 350 rpm

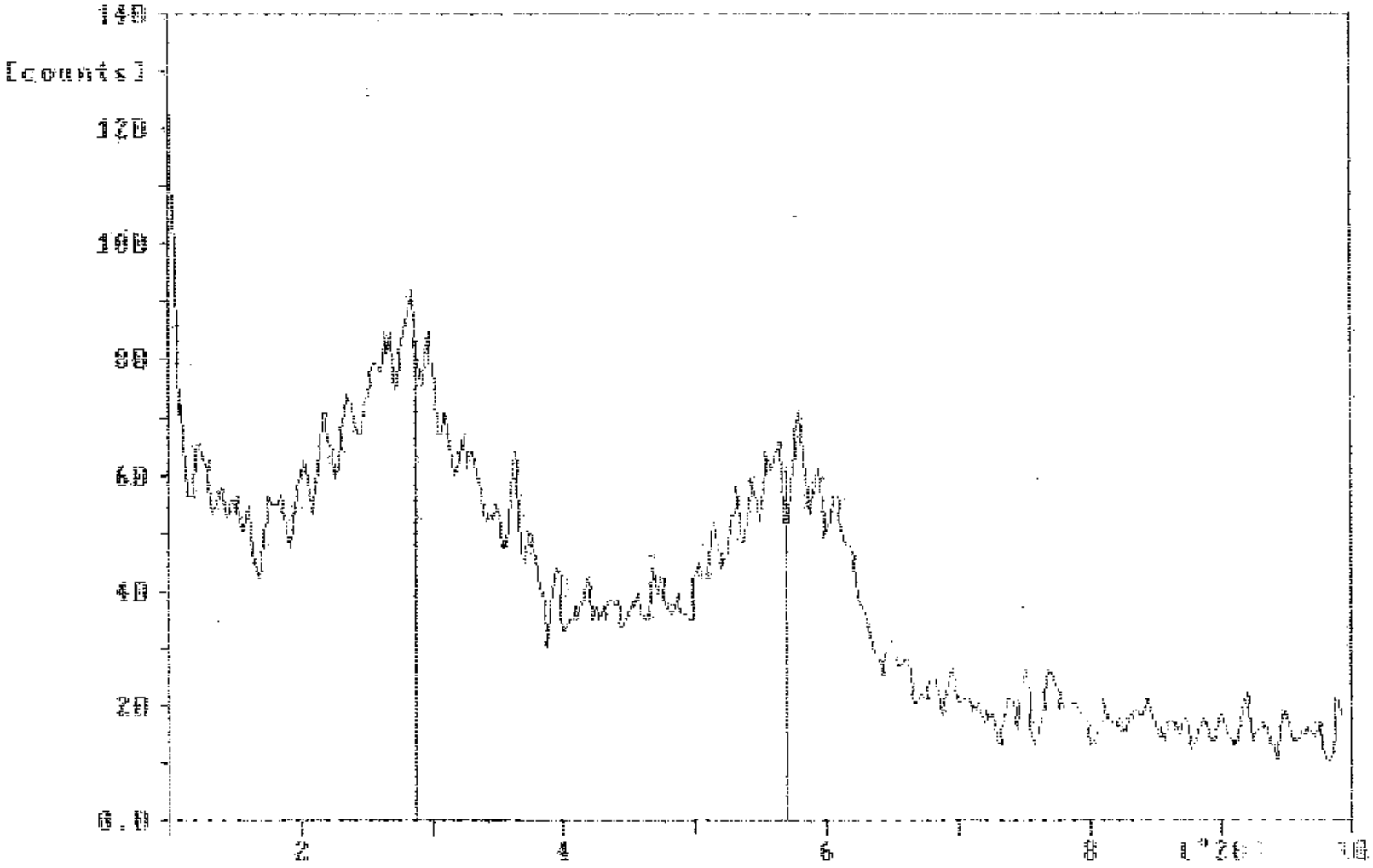

Figure C.12 XRD pattern of sample containing 3 weight % Cloiste 25A and 1 weight % MA at 150 rpm

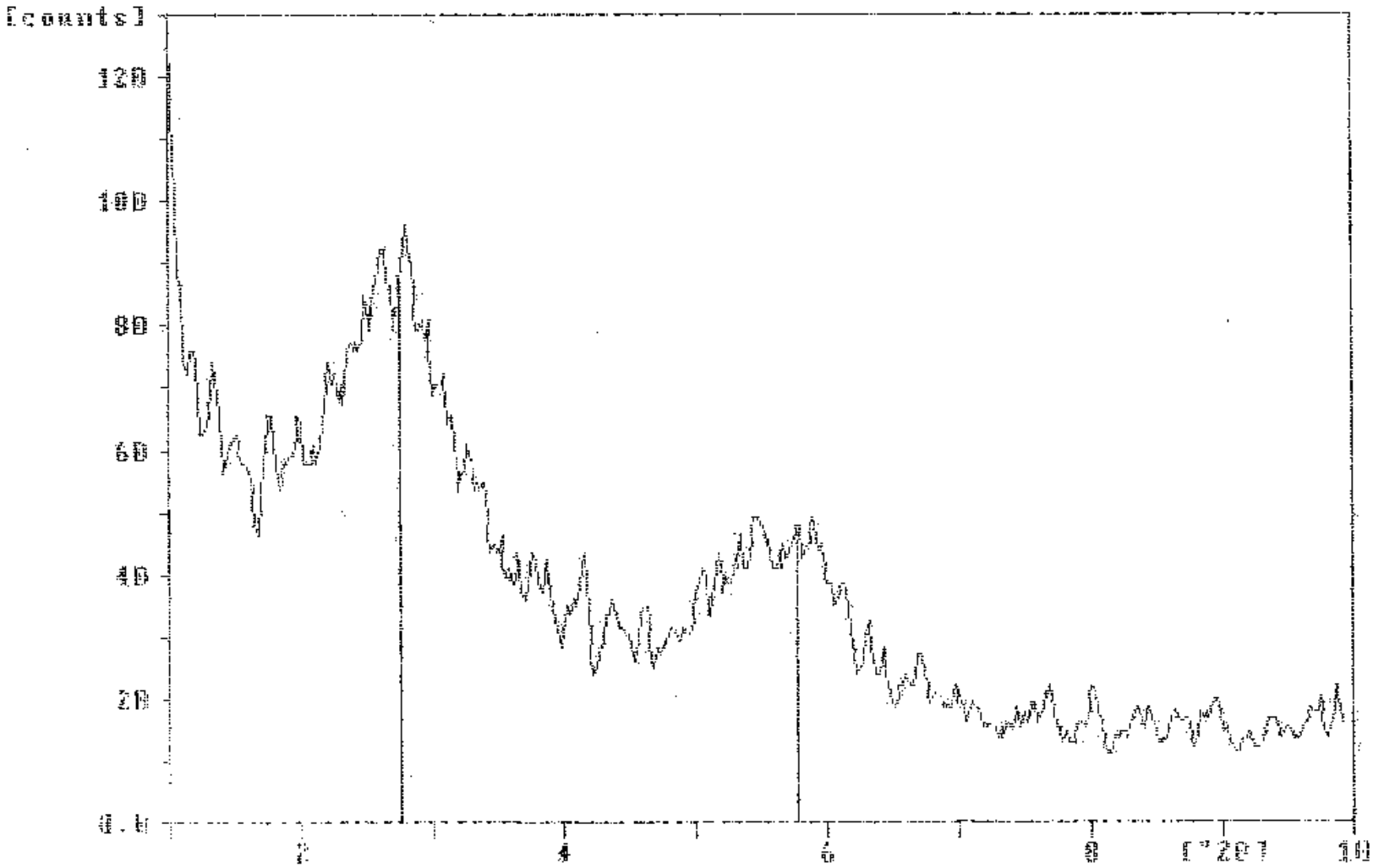

Figure C.13 XRD pattern of sample containing 3 weight % Cloiste 25A and 1 weight % MA at 75 rpm

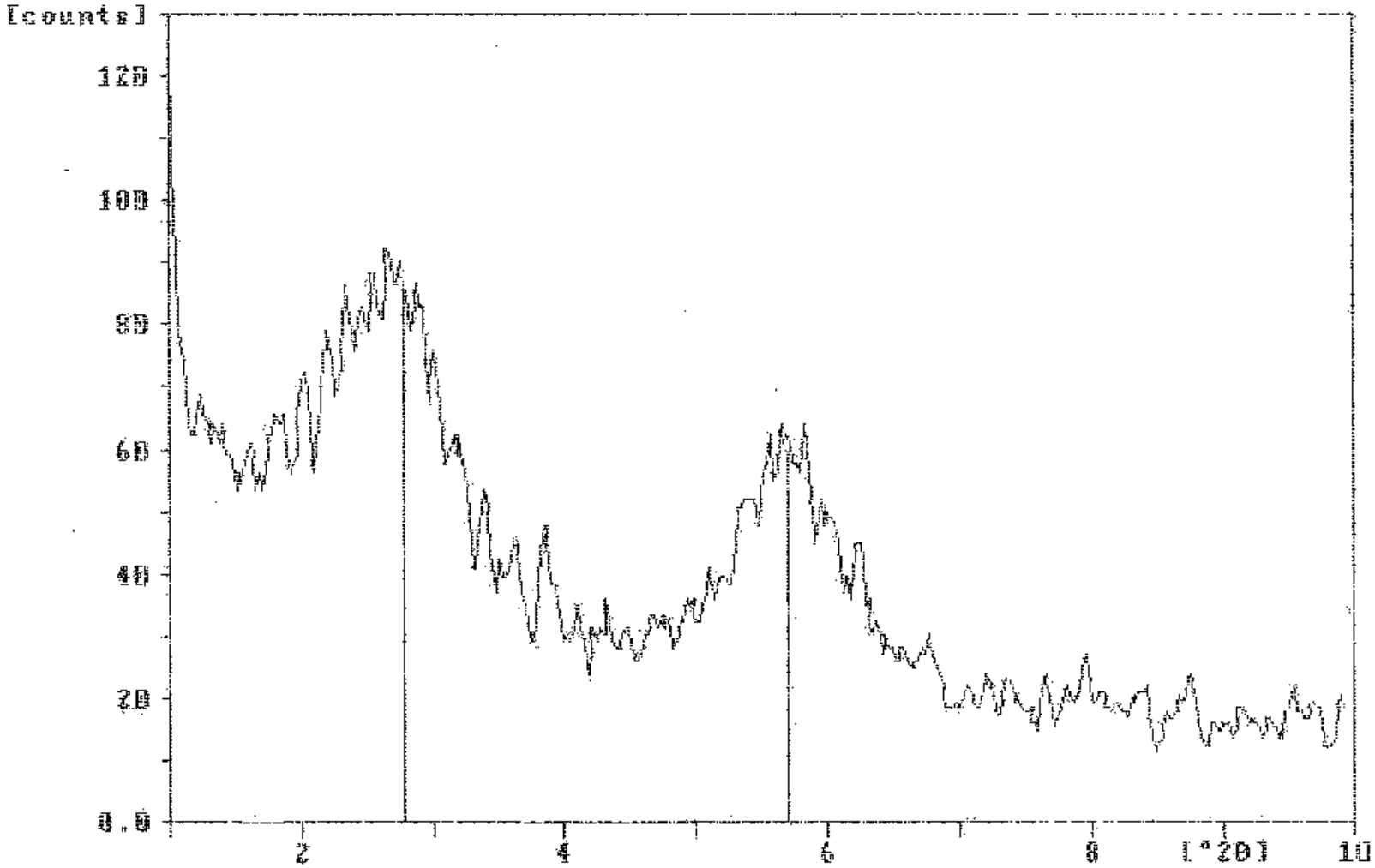

Figure C.14 XRD pattern of sample containing 3 weight % Cloiste 25A and 0.75 weight % MA at 350 rpm

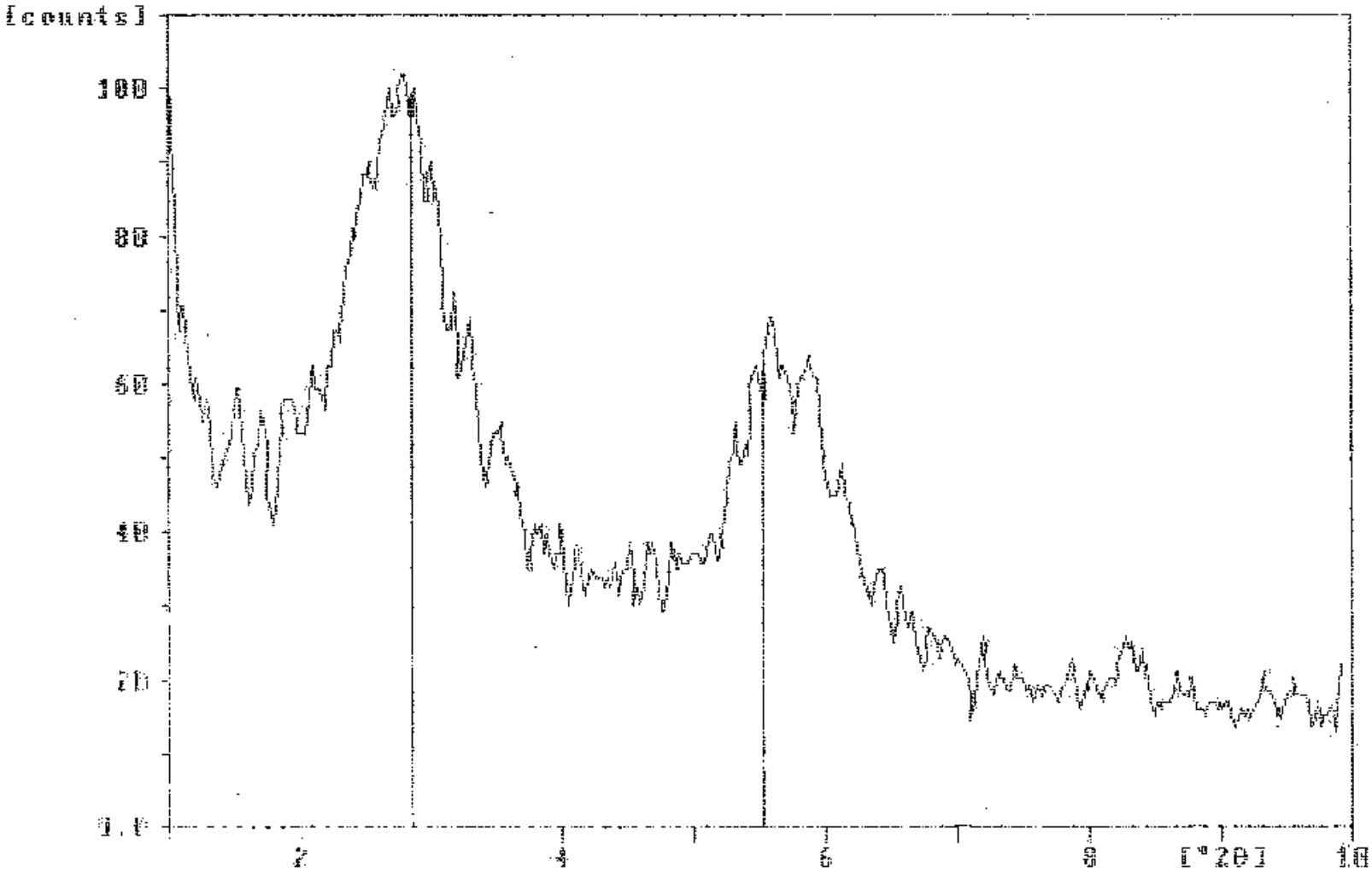

Figure C.15 XRD pattern of sample containing 3 weight % Cloiste 25A and 0.5 weight % MA at 350 rpm

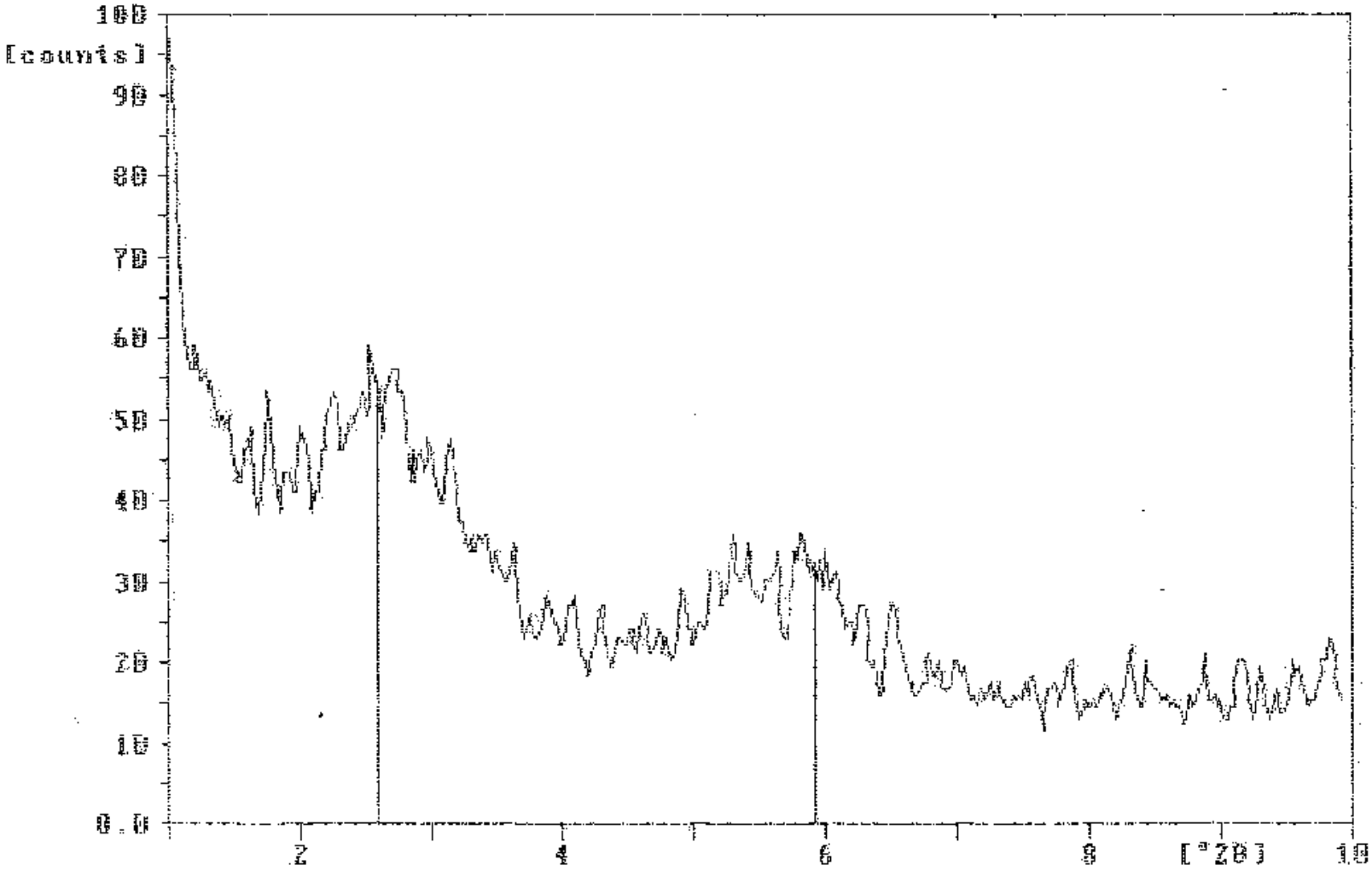

Figure C.16 XRD pattern of sample containing 0.5 weight % MA and 3 weight % Cloiste 25A and at 350 rpm

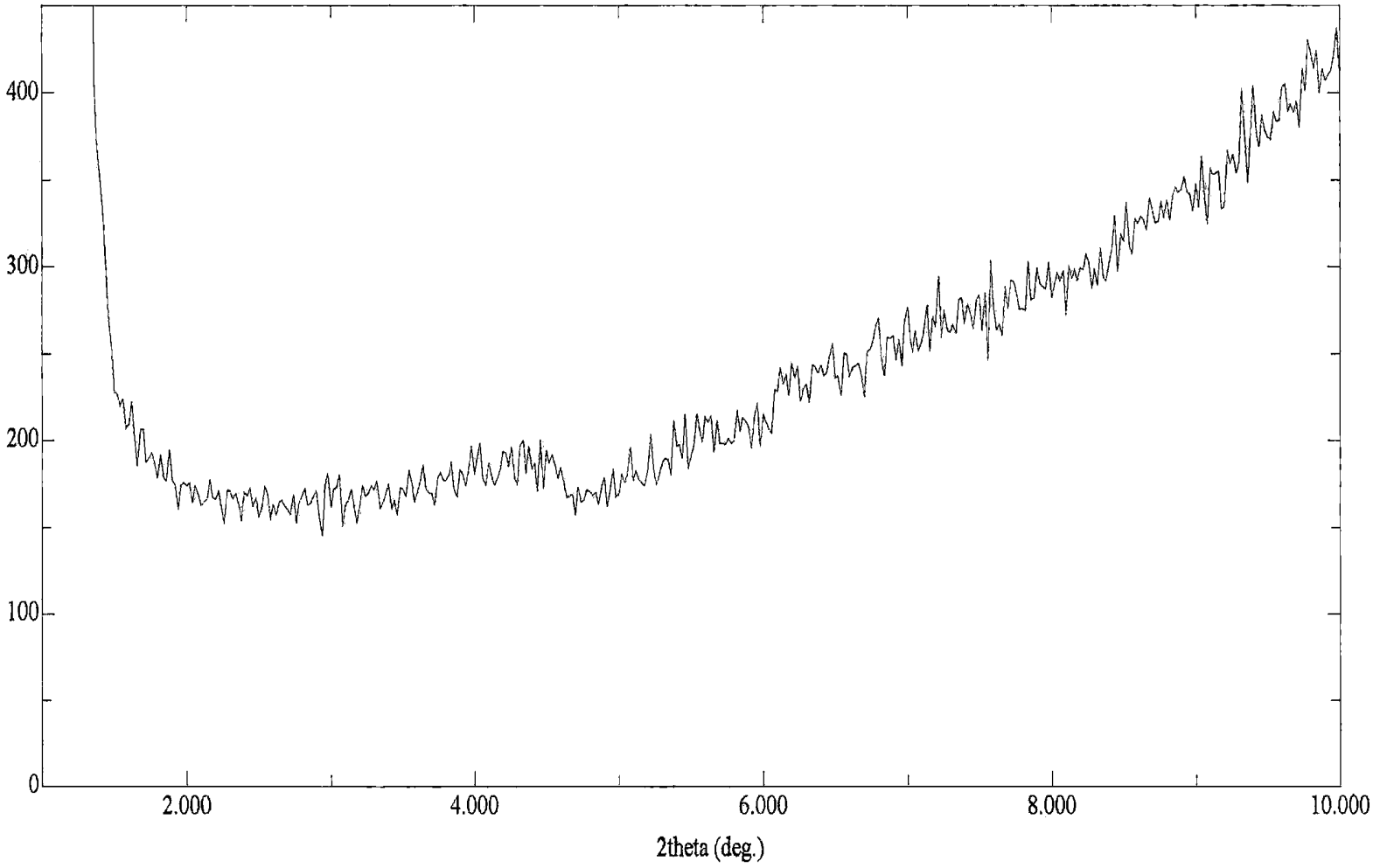

Figure C.17 XRD pattern of single extruded recycled PET

APPENDIX D

THERMO GRAVIMETRIC ANALYSIS (TGA)

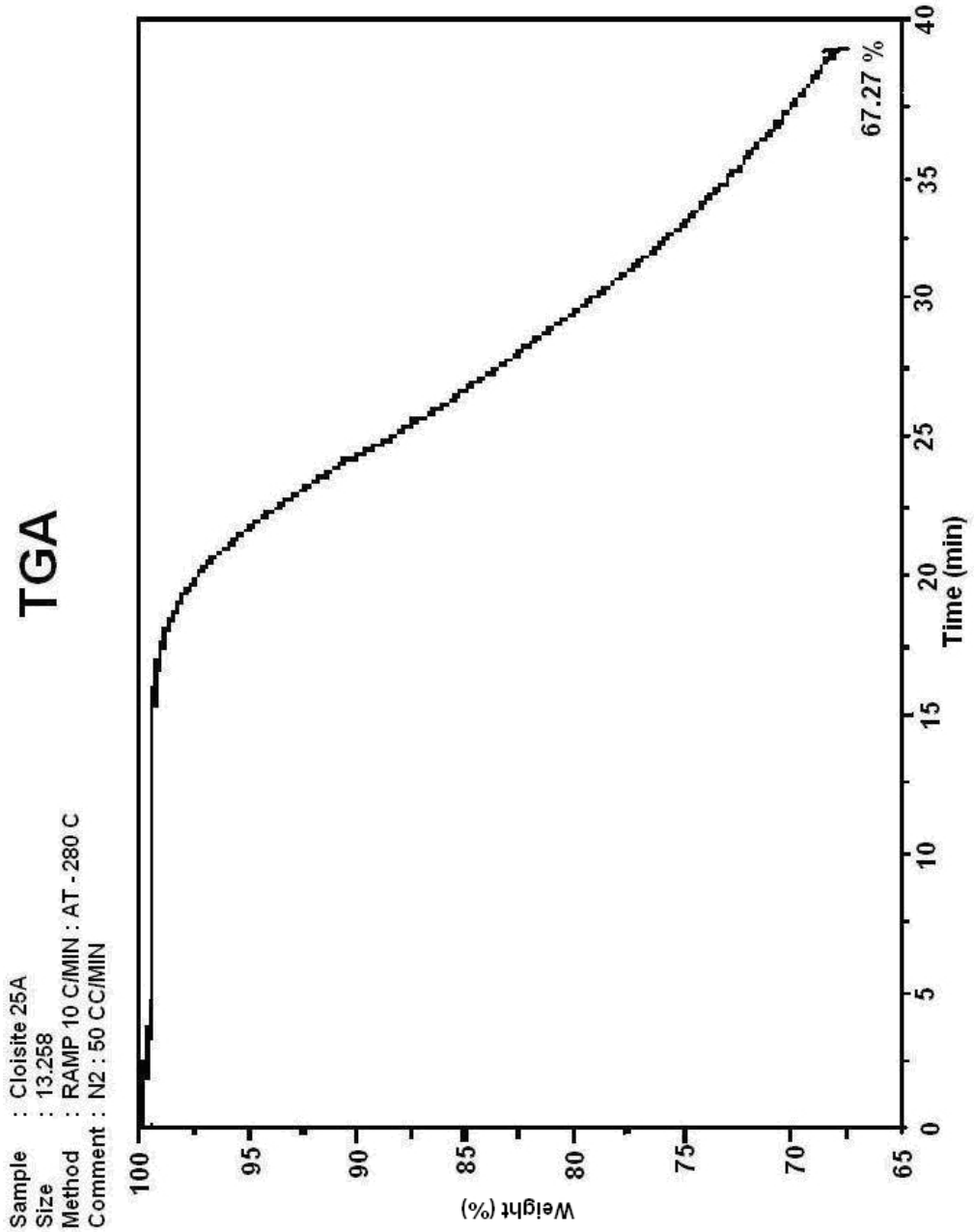

Figure D.1 TGA diagram of Cloisite 25A